The Biology of Death in *Caenorhabditis elegans*

Cassandra Coburn

Department of Genetics, Evolution and Environment,
University College London

A thesis submitted in partial fulfillment for the award of the degree of
Doctor of Philosophy
Supervisor: Professor David Gems
Secondary supervisor: Dr. Sara Mole

September 2012

I, Cassandra Coburn, confirm that the work presented in this thesis is my own. Where information has been derived from other sources, I confirm that this has been indicated in the thesis.

……

ABSTRACT

The model organism *Caenorhabditis elegans* has been extensively studied in biogerontology. A putative mechanism of ageing is oxidative damage, but this has been challenged in recent studies. One piece of supporting evidence for the role of molecular damage in *C. elegans* ageing is the presence of blue fluorescent material within intestinal lysosome related organelles, believed to be lipofuscin. This heterogenous, cross-linked aggregate of oxidatively damaged lipids and proteins that accumulates in an age-dependent fashion in post-mitotic mammalian cells. Lipofuscin can be identified by its fluorescent properties, fluorescing blue under UV light. *C. elegans* intestinal fluorescence has been equated with lipofuscin based on its similar spectral properties, and its increase in ageing populations.

This investigation initially set out to verify this assumption. Individual animals were followed *in situ* on agar pads and their *in vivo* fluorescence measured from early adulthood until after death. Intestinal blue fluorescence proved to increase not with age, but instead in a striking burst at death. Such *death fluorescence* also appeared in young worms when killed, irrespective of age or cause of death.

Using NMR-based comparative metabolomics the blue fluorophore was identified as anthranilic acid, derived from tryptophan by kynurenine pathway activity. Death fluorescence is generated within intestinal cells, typically in an anterior to posterior wave, by action of the conserved calpain-cathepsin necrotic cell death pathway, a type of cell death previously only observed during neurodegeneration. Using mutational analysis and *in vivo* fluorescent reporters, we demonstrate that this wave is propagated by calcium influx. Strikingly, inhibition of systemic necrosis delays stress-induced mortality, demonstrating its role as a driver of organismal death. This first description of the biology of death in *C. elegans* implies that the passage from life to death entails a regulated, programmed transition that is amenable to analysis.

For Fran, Noel and Seamus;
with love, and gratitude.

ACKNOWLEDGEMENTS

I am indebted to many people who have helped me throughout my PhD:

Firstly, I would like to thank my collaborators: Erik Allman and Keith Nehrke (University of Rochester), Parag Mahanti and Frank Schroeder (Cornell University), Filip Matthijssens and Bart P. Braeckman (University of Ghent), Manolis Vlachos and Nektarios Tavernarakis (University of Crete) and Zachary Pincus (Yale University). Of these, I must single out Keith, Parag, Filip, Bart and Zachary for their exceptional contributions to this project, and the fun we have had across oceans trying to figure out why the worms go blue.

I would also like to thank past and present members of the Gems lab, Daniel Ackerman, Caroline Araiz, Catherine Au, Alex Benedetto, Filipe Cabreiro, Alex Davidson, Graham Fischer, Elly Tyler, Abbie Mandel, Jennifer Tullet, Michele Riesen, Matt Sanders and Yila De La Guardia for invaluable camaraderie, friendship, support, advice and entertainment throughout my PhD. Included in this must be other past and present occupants of office 313: Sahar Emran, Iain Rogers and Jorge Ivan Castillo-Quan. I have also picked the brains of everyone in the Institute of Healthy Ageing at some stage or another, and greatly appreciate their interest in and support of my unusual project.

I gratefully acknowledge the financial support of the Biotechnology and Biosciences Research Council grant throughout my PhD. I would also like to thank my second supervisor, Dr. Sara Mole.

Seamus O'Shea has been through the highs and lows of this PhD with me. Thanks are due to him for all the late night lab vigils, hot meals, indignant Welsh mathematical interjections and a great deal of my sanity.

Finally, the largest debt of gratitude must fall to my supervisor, David Gems. It has been a pleasure to work with him, and he has been both an excellent mentor and friend over the past four years.

TABLE OF CONTENTS

FIGURES AND TABLES

1. INTRODUCTION

2. MATERIALS AND METHODS

3: ENDOGENOUS *C. ELEGANS* BLUE FLUORESCENCE INCREASES WITH DEATH, NOT AGE

4. DEATH FLUORESCENCE IS PRODUCED BY NECROTIC CELL DEATH

5. BIOCHEMICAL IDENTIFICATION OF DEATH FLUORESCENCE AS ANTHRANILIC ACID DERIVATIVES

MOVIE LEGENDS

Movies have been written onto a CD, placed on the inside back cover.

Movie 1: Death fluorescence in worms dying from old age.
Blue fluorescence in 5 class C (senescent, non-motile) wild-type worms, viewed with a DAPI filter set, over 5 hrs. The rise in fluorescence at death coincides with cessation of residual movement.

Movie 2: Death fluorescence in a young adult worms dying from injury (dessication).
Blue fluorescence in a young wild-type adult worm dying of desiccation over several hours. Note the rise and spread of death fluorescence in an anterior to posterior wave.

Movie 3: Death fluorescence in a young adult worms dying from injury (heat).
Here death has been induced more rapidly by placing a heated wire immediately adjacent to it. The fluorescence spreads down the length of the animal over the 6 mins of filming.

Movie 4: Death fluorescence does not spread in an *inx-16* mutant.
Here a young adult *inx-16* mutant adult on an agar plate is killed by placing a hot pick immediately adjacent to it. The fluorescence does not spread down the length of the animal and only fades in intensity during the six minutes of filming.

Movie 5: Spread of a wave of calcium influx during death.
Here, in two dying worms calcium levels rise first in the anterior intestine, followed by an anterior to posterior wave of increased calcium. High levels of calcium appear red.

Movie 6: Loss of acridine orange-stained puncta as death fluorescence rises.
Here the intestine of an young adult *C. elegans* is stained with the lysosomotropic dye acridine orange (AO). Initially the blue and orange puncta co-localize in intestinal cell puncta (gut granules). However, as the animal dies from desiccation on the slide, death fluorescence rises, and the orange puncta disappear. AO cannot pass through membranes when it is fluorescent, implying that gut granule membranes become permeable at death.

Movie 7: An anterior to posterior wave of cytosolic acidosis in the intestine during death.
Here a group of worms die one after the other, in each case accompanied by an anterior to posterior wave of cytosolic acidosis in the intestine. Lower pH is show in dark blue. The second and third worms from the bottom died before the start of filming.

1. INTRODUCTION

1.1 Ageing is not mandatory

"The thing that amazed me was that anything so perfect and beautiful should have matured and come forth from the interior of what, to me, was an old woman. It was like, I reflected, breaking open the old, brown, prickly husk of a chestnut and finding the lovely gleaming trophy inside."

-- Gerald Durrell, observations on birth as a child,
Birds, Beasts and Relatives (Durrell, 2004)

Birth is often described as miraculous. A miracle is defined as "*an extraordinary and welcome event that is not explicable by natural or scientific laws*". Even taking aside the fact that births happen with a monotonous regularity and so are precluded from being extraordinary, there are other reasons for discounting this statement. Great endeavor has gone into unraveling the science of birth, and we now have a good understanding of the processes of fertilization, development, growth and birth itself. The mechanics of birth are no longer miraculous. Nonetheless there is one aspect of birth which continues to elude our scientific understanding. I refer to the seemingly miraculous fact that babies are born *young*.

In itself this does not seem so impressive, but it hides a startling implication. An infant is the product of two adults' biological contributions. These adults, and their germ-line cells, are *old*. Somehow in creating new life, we manage to cheat time: we have, within us, the capacity to protect some cells from ageing.

Ageing does not appear to be an inevitability of life. Studies of the simple freshwater animals belonging to the genus *Hydra*, and the sea anemone *Urticina felina* did not find any signs of ageing (Martinez, 1998; Schmich et al., 2007). This realization allows us to ask fascinating and important questions. What purpose could ageing serve; why has it evolved? How does ageing happen to us – and could we prevent it? The burgeoning field of biogerontology is only now beginning to tackle these questions with systematic experimental rigor.

1.2 The evolution of ageing

Denham Harman has defined as ageing as "the result of progressive accumulation of changes in the body which occur with the passing of time, and which cause the increase in the probability of diseases and death of the individual," (Vina et al., 2007). Thus, ageing underlies multiple detrimental changes experienced by the elderly. In humans, these changes include loss of muscle elasticity, loss of sensory acuity and decreased motor and cognitive function (Vina et al., 2007). Decreased immune activity with age also increases both likelihood and severity of infections. Increased age also increases the likliehood of developing endogenous pathologies, such as cancer or neurodegeneration. Altogether, these increased numbers of age-related pathology increase the possibility of death.

Conseqeuently, ageing appears deleterious and non-adaptive: it is difficult, on the face of it, to see how ageing could have evolved. An organism which could mature and reproduce indefinitely would appear to have a selective advantage over one which matured and reproduced only for a finite length of time.

This conundrum initially puzzled evolutionary biologists. Weismann advanced an early evolutionary theory of ageing in 1891. Given that evolution acts through natural selection on progeny, he proposed that ageing was beneficial as it removed older, worn-out individuals from the population. This would allow their progeny greater resources and would facilitate natural selection (Kirkwood and Holliday, 1979). However, this argument is circular: it presupposes what it purports to explain, namely ageing within a population.

In 1952, Medawar proposed an alternative theory of ageing. He had the important insight that the force of natural selection would weaken with age, even if age-related morality did not exist (Kirkwood and Holliday, 1979). Even in a non-ageing population, cumulative adult mortality from extrinsic hazard will increase with time. This will lead to a decline in reproductive probability, and thus weaken the force of natural selection (Williams, 1957).

Williams built on this insight. He proposed that ageing results from the action of pleiotropic genes. If the genes conferred a beneficial effect when the organism was young, such as increased fecundity, then they would be selected for. Due to the reduced selection pressure on post-reproductive organisms, these genes would still be selected for even if they then conferred a deleterious effect on the older organism.

Williams proposed that ageing may result from these antagonistically pleiotropic genes, where ageing was the deleterious flip side of a fit, fecund youth. Consequently, Williams predicted that animals which are subject to high levels of extrinsic hazard (such as predation) should have reduced longevity, even in the absence of that extrinsic hazard (Williams, 1957).

Another theory, proposed by Kirkwood in 1977, is the disposable soma theory of ageing which posits a resource trade-off between somatic maintenance and reproduction (Kirkwood, 1977). As discussed above, selection pressure lessens with age. Somatic cells need only be maintained long enough to attain a fit reproductive maturity; after a certain duration the risk of extrinsic hazard-mediated morality increases, and outweighs the cost of maintaining replicative fidelity. However, investing resources in germ-line cells' replicative machinery lessens the possibility of damaging mutations arising in progeny and so increases their odds of survival. Consequently, this hypothesis predicts that soma are "disposable": only the minimal viable level of resources are devoted to their maintenance, consequently increasing their risk of error catastrophe and causing them to age (Kirkwood and Holliday, 1979). However, the disposable soma theory makes certain assumptions. One assumption is that mechanisms capable of tissue specific resource allocation have evolved; another is that ageing is brought about by error catastrophe, or other kinds of molecular damage.

These theories provide a theoretical framework that allows us to explain the evolution of ageing. They imply that ageing is not likely to be programmed in the sense of being selected *for*; rather ageing most probably arises from the selection of other beneficial traits.

1.3 Mechanistic theories of ageing

Inanimate objects such as cars and buildings deteriorate over time, and it is tempting to liken our own ageing to this process. However, as discussed above, organismal ageing can be understood as a non-mandatory, genetically controlled process. Consequently, biological mechanisms which cause us to age must exist. There are several proposed mechanisms of ageing, of which some are merely mechanistic, some attempt to integrate evolutionary theory and some which explain ageing only in specific organisms. Here I shall describe only proposed theories which are capable of explaining ageing in the model organism used in this thesis,

Caenorhabditis elegans; for example, I will not discuss theories of cellular senescence, as these do not apply to *C. elegans*' post-mitotic adult soma.

The molecular damage theory of ageing was originally proposed as the free radical theory of ageing by Harman in 1956. He noted that irradiation induced ageing in living beings, possibly through the creation of free radicals. Free radicals are atoms or molecules made highly reactive by the presence of at least one unpaired electron. Free radicals had been demonstrated to be present in living cells (Commoner et al., 1954) and so Harman proposed that they could react with cellular constituents, leading to damage: "in this manner, functional efficiency and reproductive ability of the cell could eventually be impaired," (Harman, 1956). This theory gained wider acceptance with the discovery of anti-oxidant enzymes and *in vivo* hydrogen peroxide (H_2O_2) (Muller et al., 2007), and changed to encompass other reactive oxygen species (ROS) capable of causing oxidative damage within cells. ROS are produced as by products from multiple biological processes, arising most notably from mitochondrial respiration. In its current form, *the oxidative damage* theory of ageing posits that ageing occurs due to an accumulation of cellular damage, caused either by an increase in ROS-mediated damage or by a decrease in cellular antioxidant defenses. This theory has been extensively tested in model organisms. Investigations have looked both for evidence that increased oxidative damage levels correlate with age and that manipulating levels of oxidative damage lead to changes in the rate of ageing (Gems and Doonan, 2009).

Many different cellular constituents can be damaged by ROS attack. Proteins, lipids and DNA can all be oxidatively damaged, and so multiple studies in a variety of organisms have examined whether these types of damage increased with age (Bokov et al., 2004). Many studies confirm that oxidative damage does increase with advanced age, irrespective of type of damage being measured. For example, a by-product of oxidative damage in DNA is 8-oxo-2-deoxyguanosine (oxo8dG). Hamilton and colleagues measured oxo8dG in different tissues of multiple rodent strains and discovered significant age-related increases in all tissues sampled (Hamilton et al., 2001). Other such examples have been seen in damaged lipids and proteins (Muller et al., 2007).

Experiments seeking to manipulate levels of oxidative damage have attempted to either increase or decrease endogenous levels of ROS in order to see if ageing is accelerated or retarded respectively. Levels of oxidative damage can be reduced by

reducing ROS levels or by increasing endogenous antioxidant defenses. One of the most widely used interventions has been the manipulation of the antioxidant enzymes superoxide dismutase (SOD) and catalase. SODs convert the ROS superoxide ($O_2^{\bullet -}$) into hydrogen peroxide (H_2O_2). H_2O_2 can subsequently be converted to water and oxygen by the enzyme catalase (Keaney et al., 2004).

Experimental manipulation of these enzymes was first carried out in *Drosophila*. Flies that had been selectively bred for their increased longevity were found to have increased SOD and catalase activity levels (Arking, 1987). Thus, there was great interest in discovering whether increasing enzyme activity levels could increase lifespan. Overexpression of *Sod1* (which encodes the cytoplasmic SOD) through the use of the constitutive β-actin promotor gave very different data: some groups reported an increase in lifespan (Sohal et al., 1995); others a decrease (Seto et al., 1990). *Sod1* null flies show an unambiguously shortened lifespan, of ~20% of wildtype (Reveillaud et al., 1994). However, a *Sod1* mutant with partially rescued wildtype *Sod1* expression of 5% had a normal lifespan (Mockett et al., 1999). As Muller and co-authors point out in their extensive 2007 review on this topic: "[it is] difficult to explain how 5% of normal *Sod1* activity (i.e. a 95% knockdown) is sufficient for completely normal lifespan, yet *Sod1* levels 150% of normal…actually result in an extension of lifespan" (Muller et al., 2007). There is similar contention between contradictory interventionist experiments with SOD and catalase in mice and worms (the latter discussed in more detail below) (Muller et al., 2007).

Another difficulty with the oxidative damage theory is the fact that mechanisms that control ROS induced damage have been identified. For example, yeast cells differentially partition carbonylated (oxidatively damaged) proteins when dividing (Liu et al., 2010), and the levels of carbonyls decrease during the differentiation of embryonic stem cells (Dang et al., 2009). Thus, if oxidative damage does cause ageing, but can be ameliorated, why have greater, more precise antioxidant defenses evolved? This can be understood in the light of the disposable soma theory, which could argue that such effective antioxidant defenses may be energetically costly. However, it may be equally well understood if one assumes that ageing does not result from oxidative damage and so the selection pressure driving the evolution of better antioxidant defenses is absent.

Thus, despite correlative data showing an increase in oxidative damage with age, the consensus of intervention studies is that the role of oxidative damage as a *cause*

of ageing has not been sufficiently demonstrated to be considered a public, or conserved, mechanism of ageing across species (Muller et al., 2007). As a consequence, other theories of ageing which do not invoke molecular damage as a causative mechanism of ageing are being considered. The *hyperfunction* or *bloated soma* theory of ageing argues that ageing does not arise from molecular damage but by quasi-programmed hyperfunction (Blagosklonny, 2006). Proposed by Blagosklonny, here a quasi-programme is defined as "an unintended continuation of the developmental programme" (Blagosklonny, 2007). Blagosklonny illustrates quasi-programme concept using an analogy between development and running a bath. The programme for running a bath which leaves your bathtub full becomes a quasi-progamme for flooding your bathroom if the water is not turned off (Blagosklonny, 2007).

The hyperfunction theory can be understood in the light of antagonistic pleiotropy. Phenotypic plasticity has evolved in response to differing environments, and, in particular, resource levels. Growth pathways such as the insulin/IGF-1 signaling (IIS) and target of rapamycin (TOR) pathways are induced by nutrient availability, and stimulate somatic growth. Thus biosynthesis rates will increase in response to nutrient availability in younger organisms but will result in hyperfunctional pathologies in later life. In contrast, low nutrient availability would be predicted not to induce these biosynthetic pathways thus reducing pathology in old age (Blagosklonny, 2008). Thus, the hyperfunction theory of ageing could also explain the mechanism by which dietary restriction extends lifespan.

There are multiple examples of age-related pathologies of excessive growth or stimulation, among which the most salient are cancer, diabetes and obesity, all of which increase in an age-dependent manner (Blagosklonny, 2006), and a recent paper has shown correlative evidence for age-related hyperfunction in *C. elegans* ageing (Figure 1.1) (Gems and de la Guardia, 2012). This theory has only been proposed recently and so much experimental work needs to be done in order to test its predictions. However, it is an exciting theory as it offers an alternative mechanism of ageing to that of molecular damage.

It is clear that the mechanisms of ageing are far from being conclusively answered and work therefore continues on model organisms. The nematode worm *C. elegans* is a widely used in genetic research, and I will now discuss its use as a model organism for ageing research.

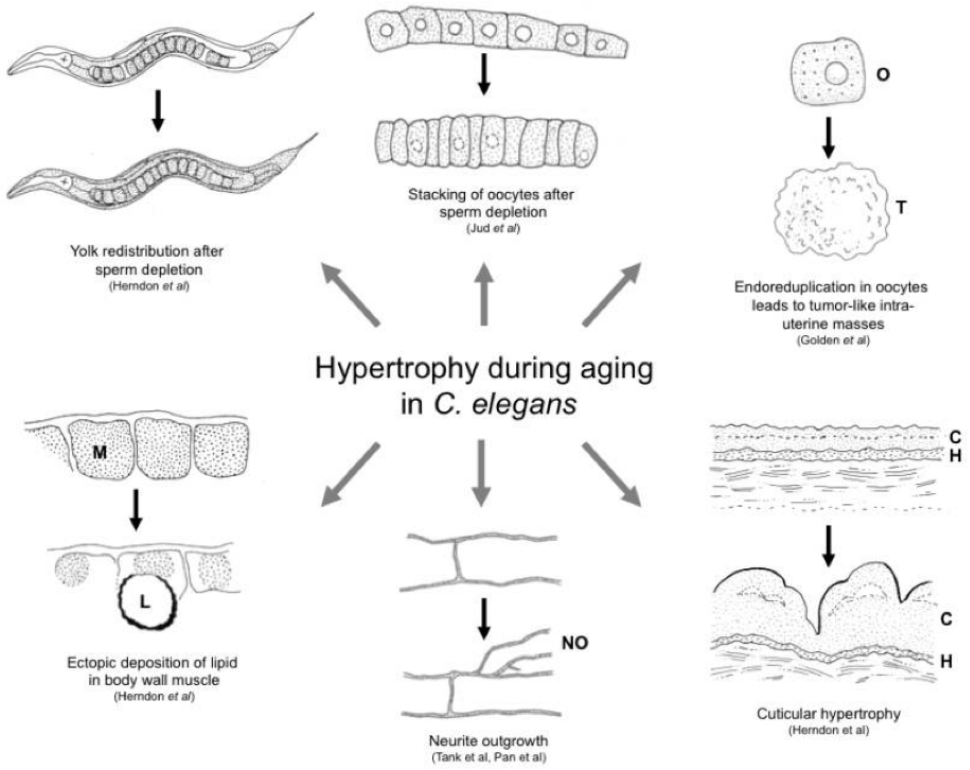

Figure 1.1: Evidence of hypertrophy during ageing in *C. elegans*. This figure shows six examples of age-dependent changes in *C. elegans* physiology which involve hypertrophy. Figure reproduced from Gems and de la Guardia, 2012.

1.4 *C. elegans* as a model organism

1.4.1 Introduction to *C. elegans*

C. elegans was first proposed as a model by Sidney Brenner in 1974 due to the ease of using it for genetic screens (Brenner, 1974). It has subsequently become one of the most widely used scientific model organisms due to its rapid lifecycle, small size and the ease of maintaining laboratory stocks. *C. elegans* was the first multicelluar organism to have its genome sequenced (1998) and now rejoices in a wealth of dedicated interactive tools to aid further discoveries, such as WormBase, WormBook and WormAtlas.

C. elegans is a small, transparent nematode worm which grows to an adult length of approximately 1.5mm (Riddle et al., 1997) (Figure 1.2). The animals are found in microbe rich habitats, such as decaying plant matter (Felix and Braendle, 2010). In the laboratory, *C. elegans* can easily be maintained on Petri dishes seeded with a bacterial lawn of *Escherichia coli* as a food source. A single unmated animal can

produce up to 350 progeny in a lifetime, surpassing even the progeny production of a bacteriophage (Riddle et al., 1997). Furthermore, stocks can be maintained almost indefinitely by freezing, both providing biological records and safeguarding against the strain divergence which comes from long laboratory cultivation (Riddle et al., 1997).

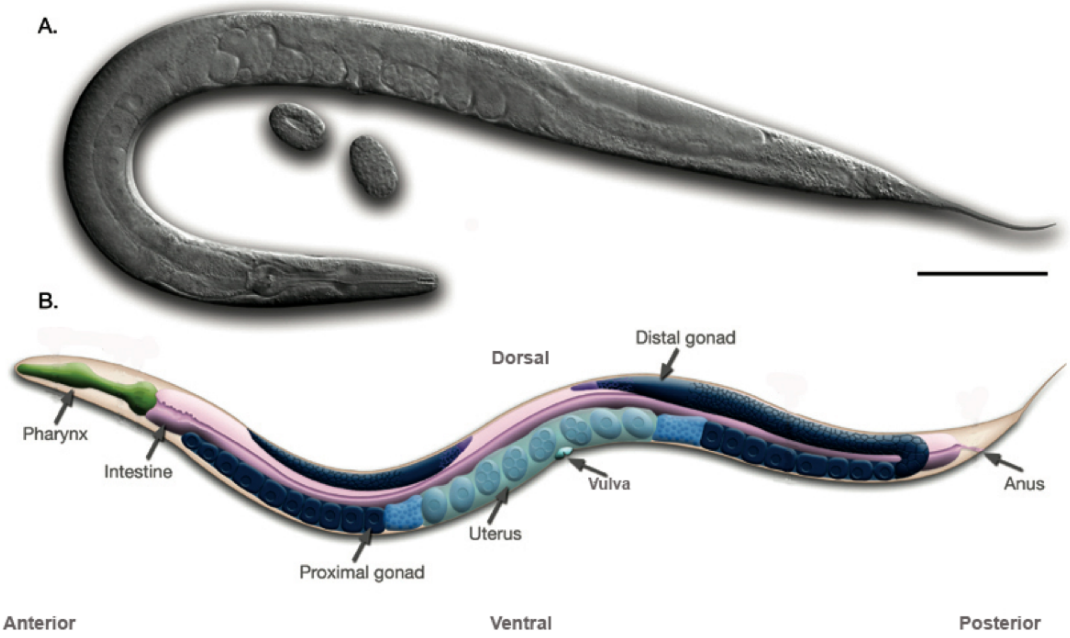

Figure 1.2: *C. elegans* hermaphrodite anatomy. (A) shows a micrograph of an adult *C. elegans* hermaphrodite using Nomarski microscopy and (B) shows a schematic drawing of the same. The scale bar is 0.1mm, images reproduced from WormAtlas (www.wormatlas.org).

C. elegans are diploid and have two sexes: male and hermaphrodite (Herman, 2005). Hermaphrodites have five pairs of autosomes and two sex chromosomes (XX), whereas males share the same autosomes but lack a sex chromosome (XO). Almost all gametes produced by hermaphrodites have a single X chromosome and thus hermaphrodites most frequently produce hermaphroditic progeny through self-fertilization (Herman, 2005). Males can spontaneously arise from hermaphroditic selfing due to X chromosome loss, but this is rare, occurring at a rate of ~0.1% (Riddle et al., 1997). Hermaphrodites mated with males produce an even sex ratio, but this is immediately disorted when hermaphrodite progeny begin to self. Consequently, unless maintained for parity, most populations' sex ratios are skewed towards a clonal

culture of hermaphrodites which provides a useful tool for the generation of isogenic populations and subsequent genetic analysis.

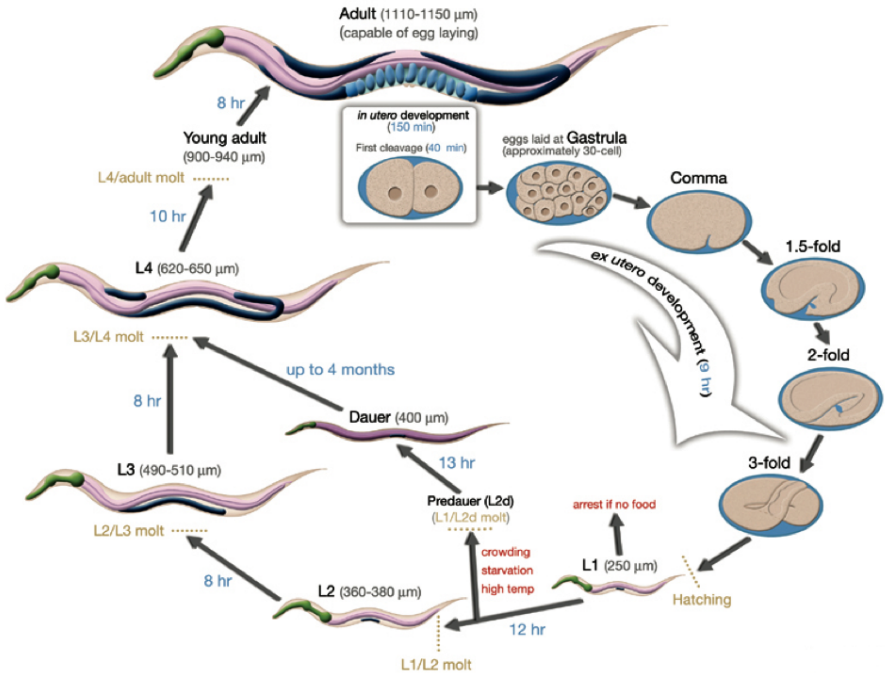

Figure 1.3: *C. elegans* lifecycle at 22°C. Developmental time shown in blue. Figure taken from WormAtlas (www.wormatlas.org).

C. elegans have a short, temperature dependent lifecycle (Figure 1.3), with a mean lifespan of 19 days when maintained at 20°C. When fully fed, the animals pass through a short developmental period with four larval cuticle molts (L1-L4, Figure 1.2) (Felix and Braendle, 2010). However, under stressful conditions, *C. elegans* larvae can undergo developmental arrest and enter an alternative, non feeding L3 stage known as 'dauer' (taken from the German, meaning 'to endure'). Strikingly, this appears to be a non-ageing state (Klass and Hirsh, 1976). When conditions improve, larvae can exit the dauer state and re-enter the developmental lifecycle, ageing normally irrespective of the duration in the dauer state (Klass and Hirsh, 1976).

1.4.2. *C. elegans* anatomy

The adult hermaphrodite *C. elegans* is comprised of 959 somatic cells, with an entirely documented developmental lineage (Sulston et al., 1983). The animals are pseudocoelomates, having a simple body structure of two concentric tubes separated by a fluid filled space; their shape is maintained by this hydrostatic pressure (Riddle et al., 1997). *C. elegans* anatomy can be subdivided into the body wall, which

comprises the cuticle, hypodermis, excretory system, neurons and muscles, and the inner system comprised of the alimentary and reproductive systems. The cuticle is a flexible and durable external surface which acts to protect the animals from environmental hazard. It also maintains the animals' body shape and enables motility by acting as an external skeleton (WormAtlas, 2002-2012). The nervous system consists of 302 cells, of which 282 neurons make up the somatic nervous system and 20 others comprise the pharyngeal nervous system (WormAtlas, 2002-2012). *C. elegans* have both striated and non-straited muscles, of which the former is used for motility and the latter for feeding. The alimentary canal, consisting of the pharynx, intestine, rectum and anus, is the main organ of *C. elegans*, and acts not only to intake, digest and excrete nutrients but also has liver-like metabolic properties (Figure 1.1).

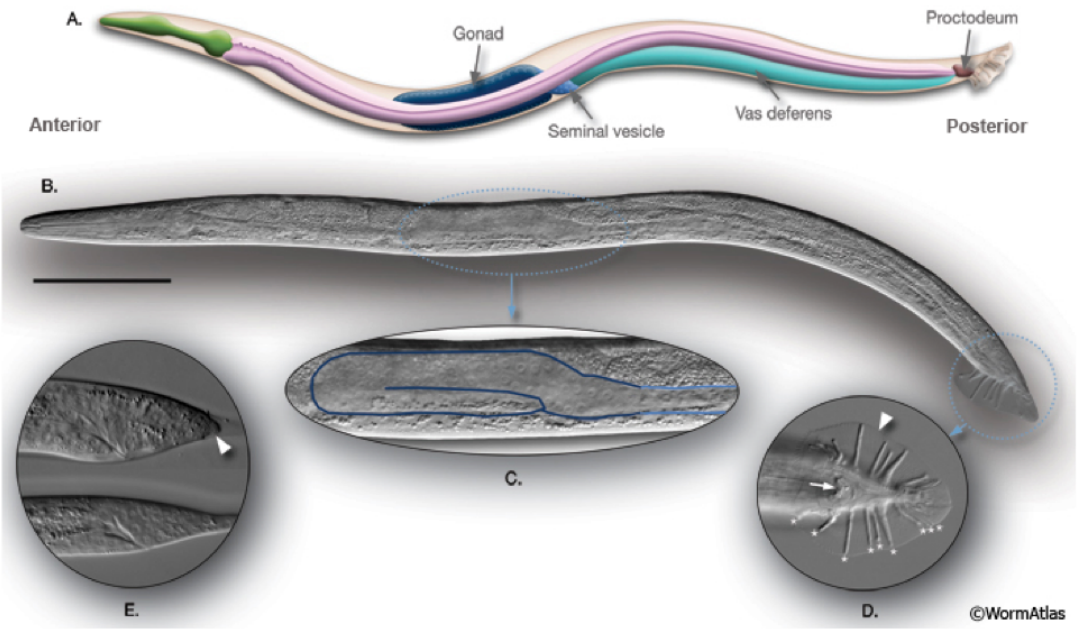

Figure 1.4: Male *C. elegans* anatomy and reproductive system. (A), schematic of male anatomy and B, micrograph of the male using Nomarski microscopy; scale bar 0.1mm. (C-E), the male reproductive system. (C) shows the male gonad, (D) the enlarged male tale, used as a copulatory apparatus, (E) the tail developing as an L3 larva. Images reproduced from WormAtlas (www.wormatlas.org).

In the hermaphrodite, the reproductive system consists of the gonad, germline and vulva. Two U shaped gonad arms pass through spermathecae and connect to the uterus. Germ cells develop into oocytes in the ovaries and are fertilized by the spermathecae en route to the uterus. Fertilized eggs are released through the vulva.

Male anatomy differs somewhat to that of the hermaphrodite. From L2 onnwards, larvae develop an altered, thicker tail which eventually develops into a copulatory apparatus. The male reproductive system consists of a single gonad arm, a seminal vesicle and vas deferens (Figure 1.4) (WormAtlas, 2002-2012).

1.4.3. *C. elegans* genetics

1.4.3.1. *C. elegans* as a genetic model organism

C. elegans was originally selected as a model partly due to the ease with which it could be genetically manipulated and studied. With the complete sequencing of *C. elegans*' ~100Mb genome in 1998 (C.S.C. et al., 1998), and its subsequent annotation, even more genetic tools are now available to the worm researcher (Hodgkin).

One of the most useful tools for genetic analysis in *C. elegans* is the ease of mutation generation; multiple different techniques work reliably in the worm, including exposure to ionizing radiation and the chemical mutagen ethyl methane sulfonate (EMS) (Hodgkin, 2005). As the animals are diploid hermaphrodites, lethal mutations can be carried in heterozygotes without killing the animal, and hermaphroditic self fertilization allows production of homozygotes even if the mutation greatly reduces reproductive fitness. The ease with which mutations can be generated and mapped has lead to the creation of a central stock center, the Caenorhabditis Genetics Center (CGC, 2012). The CGC maintains a multitude of frozen strains which can be thawed and easily mailed worldwide. Deletion mutations not yet available can be custom made by one of two consortiums in either Japan (NBR, 2012) or in Northern America (CKC, 2012).

C. elegans is entirely transparent, allowing detailed microscopy of development and the visualization of fluorescent reporter genes' expression to be observed *in vivo*. These fluorescence reporters, and other genetic material can be introduced relatively easily, e.g. by microinjection (Evans, 2005) (Figure 1.5). Microinjection uses a very fine needle to inject genetic material directly into the distal arm of the gonad (Figure 1.4). Once injected, the animal is allowed to recover and is placed alone on an plate. After self-fertilization, some of the F1 progeny of the injected animal will carry the introduced genetic material. Injected genetic material can also be integrated into the genome via irradiation, where the radiation damages the DNA and causes chromosomal breaks. The extra-chromosomal array can subsequently be integrated

into the genome via ligation using the endogenous DNA repair mechanisms (Evans, 2005).

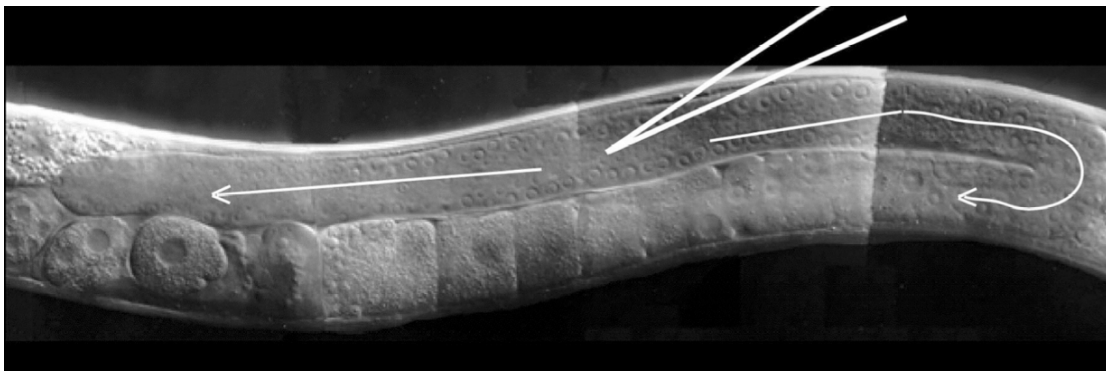

Figure 1.5: Microinjection of the *C. elegans* gonad showing optimal positioning of the needle in the distal arm of the germline. Reproduced from WormBook (Evans, 2005).

1.4.3.2. *C. elegans* genetic nomenclature

The *C. elegans* research community has developed worm-specific gene nomenclature, outlined as follows (WormBase, 2012):

A gene name consists of three or four italicized lower case letters, a hyphen and number, e.g. *unc-30*. This name can be followed by non-italicized Roman numerals to indicate which linkage group the gene is found on; here *unc-30* IV. For genes discovered by mutation-induced phenotype, the phenotype can be referenced in the gene name; here ***unc***oordinated. For those genes described by sequence similarity, the gene name will refer to the predicted genetic product, e.g. *sod-1* for ***s***uper***o***xide ***d***ismutase. Genes which have homology to genes in other species are given names which correspond, such as *rnt-1* for the *C. elegans* homolog of the Drosophila gene *runt*. Genes which have similar mutant phenotypes are given the same three letter code and a number, as seen in *unc-1* to *unc-132*.

Every *mutation (allele)* has a unique code designation of one or two italicized letters and a number, which follow the gene name, e.g. *glo-1(zu437).* The letters refer to the laboratory group which first isolated the allele, and the reference codes are registered with the CGC: for example, David Gems' group code is *wu*. The numbering arises from the lab of origin. Transgenes are also named according to lab designation but the prefixes "Ex" or "Is" are added to indicate if the transgene sits on an extrachromosomal array or is integrated into the genome respectively. The transgenes are numbered, and the gene name is contained within square brackets.

Thus an injected extrachromosomal array expressing a *rol-6(su1006)* mutation made in the Gems lab is designated *wuEx166 [rol-6(su1006)]*.

Strains are given non-italicized names consisting of two to three uppercase letters followed by a number. The letters refer to the lab where the strain originated, but are distinct from the mutation prefixes; for example the Gems lab has the strain prefix GA. The lab strain prefixes are also registered with the CGC.

C. elegans proteins are given the same letter-number designation as the gene that encodes them, but are written in non-italicized capitals to differentiate between the two. Thus the gene *daf-16* encodes the protein DAF-16.

I will use this nomenclature throughout this thesis.

1.5 The study of *C. elegans* in ageing research

As mentioned above, *C. elegans* have an alternative, non-ageing third larval stage called dauer, which they enter in to in response to stressful environments such as high temperatures, crowded conditions or low availability of food. First described in 1975 (Cassada and Russell, 1975), the genetics and biochemistry of dauer formation has provided insights into longevity regulation in *C. elegans*. Dauers are smaller and thinner than L3 larvae (Figure 1.6). They develop a specialized, thicker and re-enforced cuticle which protects the larvae from environmental hazards and desiccation. Their pharynx is remodeled, shrunken (WormAtlas, 2002-2012) and does not pump (Cassada and Russell, 1975).

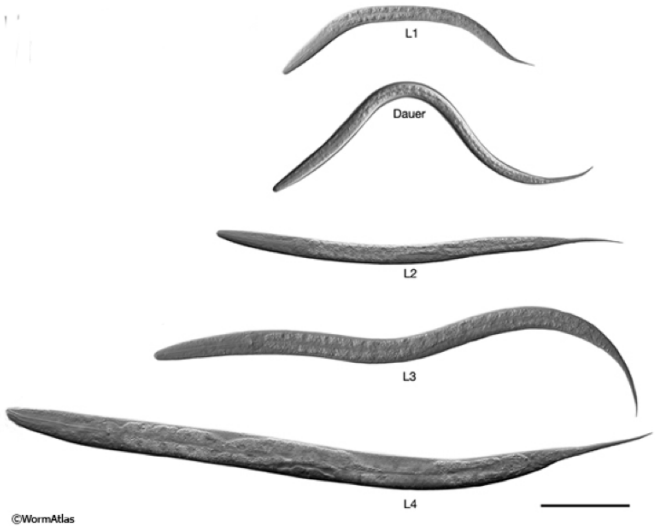

Figure 1.6: Micrographs of the larval stages of *C. elegans*. Images viewed with Nomarski microscopy, including the dauer stage, which is smaller and thinner. Scale bar is 0.1mm. Reproduced from WormAtlas (www.wormatlas.org).

36 genes controlling ***da***uer ***f***ormation (*daf* genes) have been identified to date. Mutations in Daf genes fall into two classes, constitutive (Daf-c) or defective (Daf-d), where dauers occur in normal, non-stressful environments or do not form in response to normal triggers, respectively. Some Daf-c mutants are temperature sensitive, and only form dauers at permissive temperatures. Multiple Daf genes that play important roles in determining *C. elegans* longevity have been identified, including *daf-2* and *daf-16*.

1.5.1. The insulin signaling pathway in *C. elegans*

The *daf-2* gene is a temperature dependent Daf-c mutant. In 1993, Kenyon and colleagues discovered that if *daf-2(sa189)*, *daf-2(e1370)* and *daf-2(sa193)* mutants were shifted to their non-permissive temperature at the L4 stage, the lifespan of the *daf-2* mutants increased by 230% (Kenyon et al., 1993). Moreover, the animals displayed an extended youthspan: when N2 animals were dead or immobile, *daf-2* animals still moved actively on their plates. The activity of the gene *daf-16* had been shown to be required for *daf-2* constitutive dauer formation. Thus, Kenyon and colleagues tested to see if *daf-16* mutants affected the longevity phenotype of the *daf-2* mutants. *daf-16(m26)* completely suppressed the lifespan extension of *daf-2(e1370)* mutants (Kenyon et al., 1993). These findings contributed to previous research that had tried to identify long lived mutants in *C. elegans*. A screen in 1983 by Klass had identified eight long lived strains (Klass, 1983). Of these, one was later identified to be a mutation in the gene *age-1*, later identified by Friedman and Johnson as the catalytic subunit of phosphoinositide 3-kinase (PI3K) (Friedman and Johnson, 1988).

It has subsequently been discovered that these three genes all act within the insulin/IGF-1 signalling (IIS) pathway. *daf-2* encodes an insulin/IGF-1 receptor which lies upstream of the phosphatidylinositol 3-kinase (Kenyon, 2010). *daf-16* was found to encode a forkhead transcription factor (FOXO class) (Lin et al., 1997; Ogg et al., 1997) which acts downstream of *daf-2* and *age-1* (see Figure 1.7). When the *daf-2* receptor is activated by ligand binding, it initiates a downstream signaling cascade which results in the phosphorylation of DAF-16 by AKT kinases (Paradis and Ruvkun, 1998). When phosphorylated, DAF-16 is unable to enter the nucleus (Lee et al., 2001; Lin et al., 1997) However, when either *daf-2* or *age-1* functions are impaired by mutation, DAF-16 is phosphorylated and can enter the nucleus, stimulating or inhibiting gene transcription which results in the increased longevity

described above. Thus one of the most important questions in ageing research has become: what genes are affected by *daf-16*? Current opinion points to *daf-16* being a "master regulator" of many different gene sets, including upregulation sets of genes involved in stress response, antimicrobial defense and metabolism (Murphy et al., 2003; Schuster et al., 2010).

Many other genes have been shown to be present in, or interact with, the IIS pathway, and it remains a frontier of biogerontology research in *C. elegans*. However, it is important to note that since the discovery of this pathway in *C. elegans*, homologs in other model organisms have been discovered where mutation also leads to significant lifespan increases. For example, mutations in the *Drosophila,* insulin/IGF-1 receptor InR increased lifespan by ~80% (Tatar et al., 2001), as do mutations in the downstream insulin receptor substrate *chico* (Clancy et al., 2001).

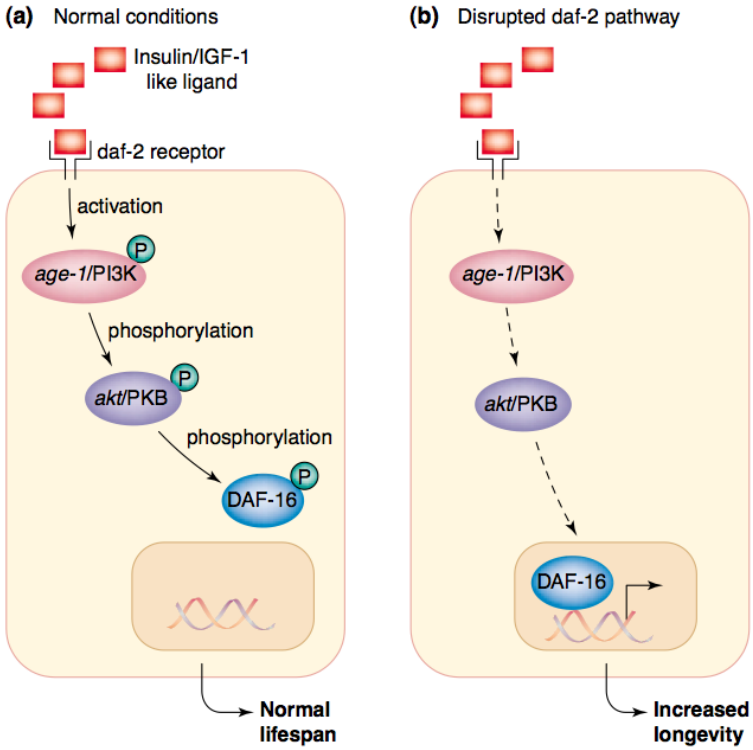

Figure 1.7: Simplified schematic showing the insulin/IGF-1 signaling pathway in *C. elegans*. Disruption of ligand binding to the DAF-2 receptor prevents DAF-16 phosphorylation and allows it to enter the nucleus, inducing upregulation of genes required for longevity. Please note: many different interactions that have been discovered are not shown for the sake of simplicity. Image reproduced from Carter et al., 2002.

In mice, which possess separate insulin and IGF-1 receptors, heterozygous knockouts of the IGF-1 receptor has been shown to extend lifespan ~30% longer than wildtype

(Holzenberger et al., 2003). Loss of the insulin receptor in adipose tissue extends the lifespan of mice by ~18% (Bluher et al., 2003). Multiple other examples of conserved ("public") mechanisms of ageing across model organisms have been discovered (Kenyon, 2005). Moreover, a study of Ashkenazi Jews demonstrated a correlation between increased longevity and mutations in the IGF1R gene, which encodes the IGF-1 receptor. These mutations were shown to lead to a partial loss of function, implying that IIS pathway alteration may increase human longevity (Suh et al., 2008).

1.5.2. Oxidative damage theory of ageing in *C. elegans*

As discussed above, it remains unclear whether ROS-mediated oxidative damage limits longevity (Muller et al., 2007). Work using *C. elegans* as a model has both supported and challenged the oxidative damage theory of ageing.

There is ample evidence consistent with the possibility that oxidative damage affects *C. elegans* lifespan. Long lived *C. elegans* IIS mutants have been shown to be resistant to oxidative stress (Larsen, 1993) and researchers have successfully used resistance to a ROS generating compound as a selective mechanism to identify long lived *C. elegans* strains (de Castro et al., 2004). A mutation in the mitochondrial respiratory chain has been shown to make mutants hypersensitive to high oxygen environs: the *mev-1(kn1)* mutation in succinate dehydrogenase cytochrome b decreases lifespan by ~35% (Ishii et al., 1998). Conversely, *C. elegans* grown in low levels of oxygen have been shown to have an increase in lifespan (Honda et al., 1993). Multiple other mutations affecting respiration have been shown to increase lifespan, but whilst it has been suggested that this effect occurs due to decreasing levels of ROS, this has not been directly examined (Kenyon, 2005).

However more recent work has challenged the role of ROS and oxidative damage in *C. elegans* ageing (Gems and Doonan, 2009; Kenyon, 2010). Firstly, evidence in *C. elegans* has emerged that high levels of ROS may in fact increase longevity. The organic compound juglone produces superoxide anion radicals . However, when *C. elegans* were exposed to 40μM juglone, it was found that exposure actually significantly *increased* their lifespan by a mean of 15 days (Heidler et al., 2010). Another experiment demonstrated that 2-deoxy-glucose, which has shown to increase longevity in *C. elegans* both stimulated the longevity increasing AMP kinase and raised ROS levels. However longevity was suppressed when the 2-deoxy-glucose was

supplemented with antioxidants, implying that increased longevity was not due to AMP kinase activity but instead from increased ROS levels (Schulz et al., 2007).

Other intervention experiments have also raised doubt about oxidative damage in *C. elegans*. As outlined above, a widely used test is the overexpression or mutation of antioxidant enzymes. Antioxidant manipulations have also been tested in *C. elegans* by using SOD and catalase mimetic compounds and mutations to increase *in vivo* antioxidant activity. Several trials, both using the EUK-8 and EUK-134 mimetics, reported contradictory results. One group found a 44% increase in mean lifespan (Lithgow et al., 2005; Melov et al., 2000) whereas four other groups found no effect on *C. elegans* lifespan (Keaney and Gems, 2003; Keaney et al., 2004; Kim et al., 2008; Uchiyama et al., 2005). Furthermore, high doses of EUK-8 and EUK-134 actually decreased longevity in a dose dependent manner (Keaney et al., 2004; Kim et al., 2008).

Genetic manipulation of endogenous antioxidants does not appear to increase longevity. Most eukaryotes possess three SOD isoforms. One is expressed in the mitochondrial matrix, another in the cystol and another in the extracellular matrix. *C. elegans* is unusual in having two isoforms in each compartment (Doonan et al., 2008). Systematically deleting or inhibiting gene expression of the mitochondrial isoforms showed no change in lifespan (Doonan et al., 2008; Yang et al., 2007). A small reduction in lifespan was seen in some studies when the cytosolic isoform was deleted or its expression knocked down (Doonan et al., 2008; Yang et al., 2007) but another study saw no change in longevity (Van Raamsdonk and Hekimi, 2010).

Thus, whilst it is possible that ROS plays a role in ageing, taken together, this and other data does not conclusively support oxidative damage as a significant cause of ageing in *C. elegans*.

1.6 Lipofuscin accumulation: evidence for a role of oxidative damage in *C. elegans* ageing?

A frequent difficulty in oxidative damage ageing research is that claims of altered oxidative damage are not always empirically demonstrated. An example is the discovery of the *mev-1(kn1)* mutation affecting the *C. elegans* succinate dehydrogenase cytochrome *b*, located in complex II of the mitochondrial respiratory chain (Ishii et al., 1998). *mev-1(kn1)* showed decreased lifespan at elevated oxygen levels and Ishii and colleagues claimed that *mev-1* "governs the rate of ageing by

modulating the cellular response to oxidative stress". However no evidence was presented demonstrating that the *mev-1(kn1)* mutation increased oxidative stress or damage (Ishii et al., 1998). Instead, both were assumed.

Other investigations into the oxidative damage theory of ageing in *C. elegans* have had similar difficulties. The oxidative damage theory predicts that oxidatively damaged cellular constituents should accumulate over time. One product of oxidative damage found in ageing postmitotic mammalian tissues is lipofuscin. This substance is a heterogenous, cross-linked aggregate of oxidatively damaged lipids and proteins that accumulates in an age-dependent fashion (Brunk and Terman, 2002a; Jung et al., 2007). Discussed in more detail in the introduction to Chapter 3, *C. elegans* contains lysosome related organelles, or "gut granules", in its intestinal cells (Chitwood 1950). These organelles contain an autofluorescent substance which has been proposed to be lipofuscin (Davis et al., 1982; Gerstbrein et al., 2005; Klass, 1977). This autofluorescent material has similar spectral properties to lipofuscin and its levels have been shown to increase in an age dependent manner in *C. elegans* cohorts (Davis et al., 1982; Garigan et al., 2002; Gerstbrein et al., 2005). Despite not being biochemically identified as lipofuscin, nor shown to increase with increased levels of oxidative damage, this pigment has been identified as lipofuscin in over 50 original research papers and used as a biomarker of ageing. Please see Appendix 1 for examples of *C. elegans* blue fluorescence being used in this manner.

Biomarkers of ageing are defined as "measureable parameters that predict individual longevity better than chronological age" (Baker and Sprott, 1988). Biomarkers of ageing are an important tool in biogerontology as they allow researchers to distinguish between interventions that affect longevity by altering the risk of death and those which actually affect the rate of ageing. In two otherwise identical populations of organisms, one may be more likely to die from extrinsic hazard than the other. The cumulative survivorship of these populations cannot distinguish between death from age and death from extrinsic hazard. In an elegant study, Mair and colleagues demonstrated how to experimentally separate these two parameters to distinguish whether dietary restriction extended lifespan through reduced risk or through altered ageing rate (Mair et al., 2003). In order to understand the mechanisms of ageing through model organism experimentation, it is important to distinguish between these two causes. A reliable biomarker of ageing would be one way of doing this.

Extrinsic hazard would not affect the expression of a valid biomarker of ageing and so experimental interventions could be assessed for their alteration of the ageing rate, not just cumulative mortality. One of the most interesting questions in *C. elegans* biogerontology is how genetically identical animals exhibit such variability in their longevity. Pincus and colleagues studied individually cultured *C. elegans* in order to understand this (Pincus et al., 2011b). They identified several biomarkers of ageing in *C. elegans* which could be used to predict a substantial degree of variation in lifespan between individuals. For example, the expression of microRNA miR-71 alone explained 47% of future longevity. Other physiological biomarkers of ageing have been identified in *C. elegans*. Amongst other traits, elderly worms show decreased motility, an increased levels of mislocalized yolk in the body cavity, reduced levels of pharyngeal pumping and a surfeit of bacteria within the intestine (Garigan et al., 2002). *C. elegans* autofluorescence has been assumed to be another biomarker of ageing, particularly because of its equation with lipofuscin, and I will discuss this problem in further detail in the introduction to Chapter 3.

1.7 Aims

C. elegans is an important model that has been extensively used in biogerontology to understand the mechanisms of ageing. As discussed above, one of the most important theories of ageing is the oxidative damage theory, and this has been tested extensively in *C. elegans*. However, despite the large amount of work done on this topic, ambiguities remain. My initial aims were to investigate the intestinal autofluorescence in *C. elegans* in order to verify its identify as the age pigment lipofuscin. This would serve two functions. Firstly, if true, it would be an important piece of evidence for the oxidative damage theory of ageing. Secondly, it would validate its use as a biomarker in ageing studies. However, earlier work done by an undergraduate summer student, Sally-Anne Edwards, in the Gems lab had suggested that levels of autofluorescence remained unchanged during life, and instead only increased at death.

As I shall demonstrate in the Chapter 3, I successfully confirmed her observations and showed that *C. elegans* emit a burst of blue fluorescence when they die. My supervisor David Gems allowed me to continue to work on this fascinating discovery, despite my showing its irrelevance to ageing. In Chapter 4, I describe how this fluorescence is generated by a type of necrotic cell death only previously observed in

neurodegeneration, and I outline how systemic necrosis contributes to *C. elegans* organismal death. In Chapter 5 we use NMR based comparative metabolomics to identify the blue fluorescent material as a product of the kynurenine pathway. Detailed background to both of these topics are given in the relevant introductions.

In order to successfully understand this phenomenon it was necessary to collaborate with other labs, as we lacked necessary expertise in several areas. Consequently, this thesis includes some results which I did not personally obtain. In all cases, data generated by others is clearly attributed as such, and I have summarized their contributions on the next page (Table 1.1). I also supervised several students over the course of my PhD and their results, where relevant, have also been included and attributed. The project swiftly outgrew both me and my PhD, but at all times I remained involved in the work being done elsewhere in the world. Only with my collaborators' help could we ever have begun to understand the biology of death in *C. elegans.*

Name	Data obtained	Page
Filipe Cabreiro	Hyperoxia oxyblot	64
Caroline Araiz	FAC oxyblot	64
	hsp-4::GFP and blue fluorescence measurements	64
Alexander Davidson	DF measurements in larvae, males and other species	68
Zachary Pincus	Independent verification of fluorescence patterns	70
Grahame Fischer	Images of curtailed DF wave in *inx-16*	93
	Acridine orange staining	97
Erik Allman and Keith Nehrke	*in vivo* calcium measurements	95-96
	in vivo pH measurements	98
Manolis Vlachos and Nektarios Tavernarakis	Some lifespan data	99
Alexandre Benedetto	Osmotic stress data	100
Parag Mahanti and Frank Schroeder	2D NMR and DANS data	116
	Identification and verification of AA derivatives	117
Filip Matthijssens and Bart Braeckman	Measurement of L-Trp changes at death	119
Abraham Mandel	TDO RNAi fluorescence measurements	120
	TDO RNAi lifespan data	121

Table 1.1: Data presented in this paper which has been contributed by others.

Data is also accredited as it appears in the text.

2. MATERIALS AND METHODS

2.1 *C. elegans* maintenance and methodology

2.1.1. Stock maintenance

Unless otherwise stated, all *C. elegans* strains were maintained on 60mm Petri dishes containing nematode growth medium (NGM), seeded with OP50 *Escherichia coli* (*E. coli*) bacteria as a food source. OP50 bacteria are uracil auxotrophs, limiting its growth on the NGM agar. Consequently, *C. elegans* strains are transferred several times a week to freshly seeded plates to avoid starvation or contamination (see below).

Depending on what type of population was required, different stock maintenance methods were used:

(i) Individual animal were transferred using a flame-sterilized thin platinum wire ('worm pick'). This is known as picking.

(ii) Large numbers of a worms were transferred by using a flame-sterilized scalpel to cut a chunk of NGM agar from an old plate, and transfer it to a freshly seeded one. This is known as chunking.

Picking is used to generate a precise population, as individual numbers and stages of worms could be precisely picked. Chunking is used to maintain a growing population of mixed stage animals. The transfer frequency depended on what experiments were being undertaken, the strains being used and the growing temperature. N2 (wild type) were sub-cultured every 3-4 days.

2.1.2. Decontamination and population synchronization

Given that NGM agar is specifically designed to provide an excellent growth environment for *E. coli* bacteria, it is unsurprising that growing populations of worms are frequently contaminated with bacterial, fungal and yeast growths. Small fungal contaminants can be excluded by chunking worms found away from the growth and then serially transferring them from new plates. However, aggressive fungal, bacterial and yeast contaminants require a different approach. Animals were treated with an alkaline hypochlorite solution which killed and dissolved the contaminated animals whilst leaving their chitin-encased eggs intact. This technique could also be used for large-scale synchronization of populations.

2.1.2.1. Alkaline hypochlorite treatment (egg prep)

The protocol for alkaline hypochlorite treatment is as follows:
First, make the alkaline hypochlorite (bleach) solution, which is 7:8 sodium hypochlorite: 4M NaOH. Then, using M9 bugger, wash gravid adults from plates and into an 1.5ml eppendorf. Allow worms to settle by gravity, then aspirate excess liquid until only 200µl remains. Add 150µl bleach solution and invert the eppendorf for no more than 4 minutes. (It is important to note that the reaction is heat-dependent, and so the eppendorf should be held only by the lid whilst inverting.) The reaction is stopped by addition of M9 to 1.5mls. Vortex and centrifuge at 6000rpm for 30 seconds. Aspirate off all but 200µl of liquid, make up to 1.5ml with M9 and re-suspend the pellet by shaking vigorously. Vortex, centrifuge and repeat twice more. After the third repetition, aspirate off most of the excess M9, and then transfer the pellet to freshly seeded plates under sterile conditions.

2.1.2.2. Egg lays

Another method for population synchronization is to use an egg lay. This is a non-invasive and non-stressful procedure. Here, several gravid worms are transferred to a fresh plate for a given amount of time to lay eggs. The number of worms transferred and their duration on the new plate depends on size of the desired final population.

2.1.3. Lifespan measurements

An animal's lifespan will most likely be influenced by its genotype and the environmental conditions. Thus to see if a given genetic manipulation alters lifespan, the environment needs to be kept as constant as possible. Animals were age synchronized via one of the two methods mentioned above, and 25 worms were placed on four seeded plates (NGM or IPTG, depending on whether RNAi was being used). Animals were then scored for viability every other day. 10µM 5-fluoro-2'-deoxyuridine (FUDR) was sometimes applied topically on this plate to stop progeny development (Gandhi et al., 1980). If so, FUDR was applied after plates had been seeded with OP50 and allowed to grow for two days. When trials used FUDR, animals were placed on FUDR seeded plates as L4s; L4 = day 0 and age was described in terms of days of adulthood.

Animals were scored for survival every other day. An animal was deemed dead if it made no movement in response to gentle prodding with a worm pick. Any animals which displayed signs of non-ageing related pathology, such as uterine rupture or internal hatching of embryos (bagging), were censored. Animals which burrowed into the agar, or dried from desiccation after climbing on the plate wall were also censored.

2.1.4. Stress assays

2.1.4.1. Thermotolerance

Animals were assessed for thermotolerance by exposing them to high temperatures and then examining their survival over time. One day prior to the beginning of the experiment, unseeded NGM plates were placed in a 35°C incubator. 40 animals per strain, 20 per plate, were then transferred to the pre-heated plates. Survival was scored every two hours, again with animals classified as dead if they failed to respond to gentle prodding. However, in this assay animals were not censored if they displayed signs of pathology, as this was deemed to be induced by the stressor.

2.1.4.2. Osmotic stress assay

Animals were assessed with resistance to osmotic stress by exposing them to increased levels of sodium chloride. Standard NGM plates were made (see section 2.5.4.) except to a final concentration of NaCl of 500mM NaCl. They were seeded with OP50 *E. coli* and synchronized one day old hermaphrodites were placed on them. These animals were scored for survival after one day. This assay was performed by Alexandre Benedetto.

2.1.5. Acridine orange staining

Animals were stained as previously described (Hermann et al., 2005; Kostich et al., 2000). 500µl of 0.5mg/ml Acridine Orange (Invitrogen, Molecular Probes) was added topically to OP50 seeded NGM plates, which were then left to dry in darkness. Young adult N2 animals were transferred to the stained plates, which were covered in tin foil to protect against light, for 1 hr. The animals were then collected, washed twice with S-buffer and left to recover on an unstained OP50 plate for 1 hr.

Fluorescence was measured via microscopy as described below, under a FITC filter ($\lambda_{ex}/\lambda_{em}$ 460-500nm/512-542nm) with a 195ms exposure time. This assay was performed by Grahame Fischer.

2.1.6. Methods of killing

Different killing assays affected the rate of death fluorescence formation and were used accordingly. Pick killing was used to observe DF dynamics in individual animals over a shorter time scale. Acute exposure to tert-butylhydroperoxide (t-BOOH) was used for individual animals to capture DF dynamics with a better temporal resolution. Freeze-thaw assays were used for cohorts of worms to determine if levels of DF were altered by genotype, and for acquisition of whole spectrum excitation/emission scans.

Pick killing: Individual animals' fluorescence was measured on NGM plates, as above. Animals were killed by application of a heated platinum wire onto the agar, adjacent to the animal.

Exposure to tert-butylhydroperoxide: Worms were exposed to 0.726M (or 7%) t-BOOH, diluted in M9, for 5 minutes. Following exposure, worms were moved to a 2% agarose pad for time lapse imaging. Worms were imaged at 100x magnification, on a Nikon Eclipse TE2000-U inverted fluorescence microscope quipped with an excitation monochromator (Polychrome IV, TILL Photonics) and a high-speed monochromatic camera (Sensi-Cam, Cooke). Fluorescence emissions were monitored at 460-nm after 4 ms excitation at 360 nm. Images were captured every 10 secs. Image capture and quantitative measurements were performed using the TILLvisION software package (TILL Photonics). Traces were plotted in Microsoft Excel. This was used by Erik Allman and Keith Nehrke for *in vivo* calcium and pH analysis.

Freeze-thaw: 60 young adult animals were individually picked into a V-shaped microtitre (Greiner) well containing 100µl of M9 buffer. 50µl of 0.2% levamisole was added to settle the worms. Fluorescence was measured in a plate reader (InfiniteM200, Tecan) using $\lambda_{ex}/\lambda_{em}$ 340/400-450nm. The microtitre plate was then placed at -80°C for 15 mins to freeze. Plates were then thawed, and fluorescence

re-measured; death fluorescence was defined as the difference between the alive and dead fluorescence readings. All data shown was based on three biological replicates.

2.2 Microscopy

2.2.1. Microscopy hardware and software

2.2.1.1. Microscopy hardware

All readings were taken using Leica DMRXA2 microscope (Leica Microsystems) and a Hamamatsu C10600 – 10B Orca R2 camera (28 MHz digital CCD camera, cooled, absorption spectra: min 300 nm, max 1050 nm; PerkinElmer). UV light was produced by a 100 W mercury lamp (HBO ebq 100 isolated; Leica Microsystems) in conjuction with a DAPI cube (Set 4900 Chroma Technology Corp, λ_{ex}: 350/50nm, λ_{em}: 460/50nm). The shutter (LEP Mac 5000 4 channel shutter driver; PerkinElmer) was connected to the bright field source. The computer controlling the system is an iMac (2.66GHz Intel Core 2 Duo, 4GB memory; Apple). The microscope is connected to the computer through an EasySync USB to RS232 cable adaptor (UC232R-10, EasySync). Multiple filter cubes were fitted to the Leica microscope to allow for the visualization of many spectra (please see Table 2.1)

Cube name	Excitation filter	Range (nm)	Emission	Range (nm)
Rhodamine	546/12	540-552	600/40	580-620
DAPI	350/50	325-375	460/50	435-485
GFP	470/40	450-490	525/50	500-550
FITC	480/40	460-500	527/30	512-542
Laser safe	440/10	435-445	475	>475
dsRed	545/30	515-575	620/60	590-650

Table 2.1: Spectral ranges of filter cubes fitted to Leica DMXRA2.

2.2.1.2. Microscopy software

The iMac runs OS X 1.5.6. (Leopard, Apple). The microscope system is automated by Volocity 5.2 for Macs (Improvision, PerkinElmer). Volocity has

four different components, which can be assembled together. Volocity Acquisition and Volocity Quantitation were used; Acquisition captures images and they can be analyzed within Quantitation without need for export.

2.2.2. Image acquisition

Using an integrated software system, multiple images could be automatically acquired and merged to create multi-channel stop motion photography films. Here I describe how to set up automatic multi-channel image acquisition, and then discuss the specific protocols used in my experiments.

2.2.2.1. Automatic image acquisition

Acquisition protocols are made up of multiple 'lightpaths'. A lightpath is a command to take an image under specific conditions, such as a specific exposure time or using a particular filter cube. Filter cubes are chosen depending on the fluorophore of interest. As blue intestinal fluorescence was the most studied fluorophore in this work, a DAPI filter cube, spectra above, was used most frequently. Image intensity depends on exposure time: longer exposure times will lead to brighter images, but will come at the sacrifice of speed of acquisition, and may potentially also lead to photobleaching by overexposure. Other options are available to increase the intensity of the signal being received: both contrast enhancement and increasing gain will boost the fluorophore signal. However this technique sharpens images by decreasing the information received; images look clearer but are less informative. Thus when measuring fluorescence levels, all artificial means of image enhancement should be avoided. Many of these options can be applied to the image after acquisition to give a clean image for display.

In order to set up a lightpath, one selects a free lightpath option (see Figure 2.1), right clicks and holds. This brings up the light path properties which has an array of options (Figure 2.2). When an option box is ticked, the light path will always take note of the settings in that option and apply them to the protocol. For example, if "exposure" is selected, the lightpath will take the current exposure time (e.g. 500 ms) as the default exposure time. Thereafter, selecting that lightpath will automatically set the exposure time to 500 ms. Shutters can also be controlled in lightpaths too. When viewing fluorescence, the brightfield shutter must be closed or the signal will be overwhelmed by intensity. Also, importantly, the fluorescence shutter must be open!

When programming lightpaths false colour can also be used to allow visualization of multiple fluorophores simultaneously. False image colouring can be selected by entering the wavelength of light emitted in the “color” option.

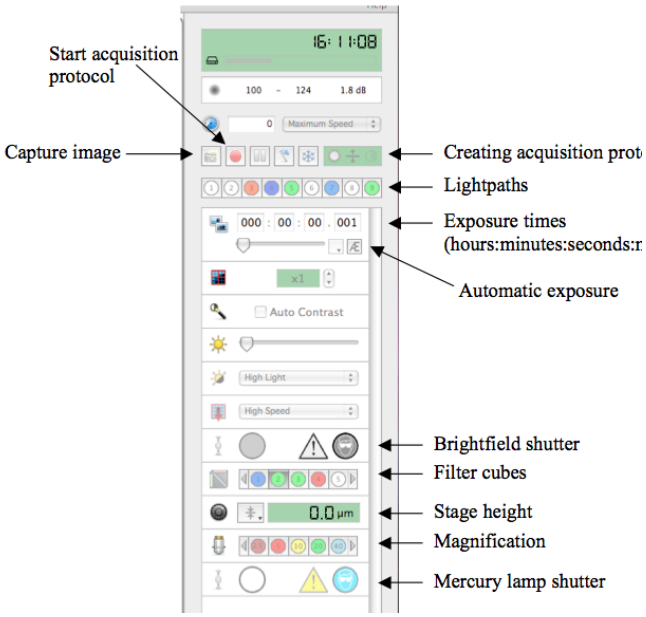

Figure 2.1: Volocity acquisition control. Volocity Acquisition software makes automatic control of multiple microscope functions possible.

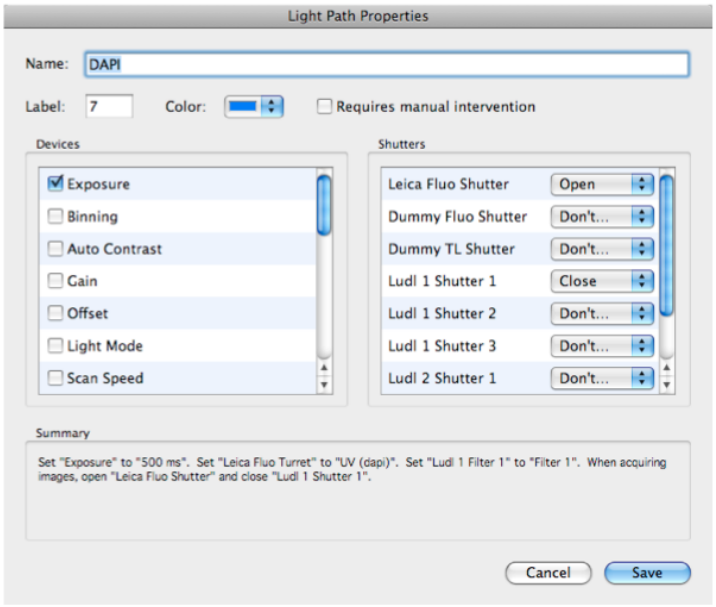

Figure 2.2: Volocity acquisition lightpath configuration. Lightpaths are configured through the selection of different modules.

Once all adjustments have been made, the lightpath must be named, described and saved. When all necessary lightpaths have been made, they can be combined by using the image acquisition set-up (Figure 2.3). This set-up has multiple further options.

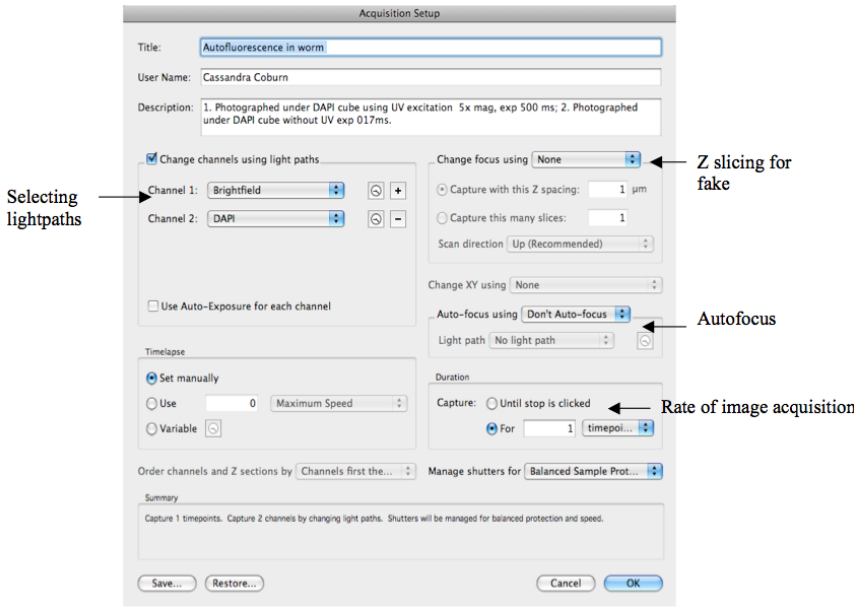

Figure 2.3: Volocity image acquisition set-up. Lightpaths can be combined with other options in order to produce complex acquisition routines, such as time-lapse photography.

The number of time points can be specified in the image acquisition set-up. Images can be acquired for one timepoint (i.e. only once), as often as possible to create stop-motion photography, or a certain number of times per unit of time, e.g. once a minute. They will be captured until told to stop or for a certain period of time.

It is also possible to specify the use of 'auto-focus' in the image acquisition set-up. Auto-focus can be used to ensure that the most important fluorophore is always in focus and is an excellent way of correcting against image shift when taking long term exposures. For example, during 24 hour imaging on NGM plates the agar slightly dries and loses volume, with the result that the initial plane of focus is set too high. Auto-focus can be used to follow the strongest fluorescent signal, thereby adjusting the focal plane.

Finally, the image acquisition set-up has the option to implement pseudo-confocal microscopy. Confocal microscopy uses point illumination so that only detail very close to the focus plane is picked up. The illumination (generally using a laser) moves up and down the sample until points over the whole sample have been picked up. These points are then computer combined, leading to a 3D-rendered object which can be digitally manipulated. Pseudo-confocal takes advantage of the microscope's automation: the microscope can be programmed to take Z slices through the sample, which is then built up into a rendered object. Z slices are pictures of focal planes, generally beginning from slightly above the sample and working through it until

slightly beneath. In the acquisition protocol one can specify how many Z slices one wants, and which lightpaths they should be taken on. This is pseudo-confocal as it is not as accurate or detailed as confocal, but does allow better resolution of points for e.g. co-localization observations.

Once all of these options have been selected, the images will all automatically be acquired in the lightpath sequence specified. The images will be merged as they are acquired. However, in the merged option, it is still possible to increase or decrease one spectra's intensity for closer examination of individual images. As each image has been acquired separately they can also be exported individually.

2.2.2.2. Life-long acquisition protocol

Preliminary trials were done in order to ascertain the best protocol for the life-long acquisition protocols. Fluorescence exposure time was difficult to determine: in order to make intensity data obtained throughout the duration of the experiment comparable, the same exposure time had to be used throughout. However, as fluorescence levels were not expected to be constant, the selected exposure time needed to be long enough to pick up low levels of fluorescence, but not so low as to cause image saturation if exposed to high levels of fluorescence.

The exposure time of 500ms was obtained by finding the auto-exposure time for several different individuals at different stages (L4, early adult, late adult). These estimates were manually adjusted to guard against over-exposure in the event of increasing fluorescence. Daily autofluorescence was measured as follows:

Animals were kept on NGM plates at all times, and cooled on ice for 10 to 15 minutes prior to imaging. Immediately before imaging each plate was wiped down with a paper towel to prevent the microscope from dripping condensation. Plates were placed under 5x magnification. 2 images were captured and merged.

> Channel 1: Brightfield. Exposure time = 158ms, Fluorescence cube = DAPI, Bright field shutter = Open, Fluorescence shutter = Closed.
> Channel 2: DAPI. Exposure time = 500ms, Fluorescence cube = DAPI, Bright field shutter = Closed, Fluorescence shutter = Open.

Shutters are managed for balanced protection and speed. When making overnight observations, measurements are taken 1 timepoint per 15 minutes. When taking images for detailed stop motion photography, measurements are taken to be as

fast as possible (i.e. acquisition of as many images as physically possible given the constraints of shutter opening speed).

2.2.3. Daily photography protocol

This protocol has also been described in Results 3.2.2. Strains were grown up under standard conditions. At the L4 stage, 30 – 40 animals were picked onto OP50 seeded NGM plates containing 15μM FuDR to prevent progeny development. Animals were scored daily on two counts: firstly, for their movement phenotype and subsequently for their fluorescence values.

Movement phenotype scoring was adapted from Herndon et al 2002, where an animal was placed into one of three movement categories depending on its movement characteristics. Preliminary trials showed that a single category could contain very different motility levels, and so three more categories were introduced to give a total of six classes:

A class: Animals spontaneously move quickly and fluidly in a clear sinusoidal pattern.

A/B class: Worms move spontaneously but do so more slowly than A, or in non-sinusoidal (uncoordinated) manner.

B class: Worms move only after gently touch with a platinum wire; movement is slow, uncoordinated or very brief.

B/C class: Worms move very slowly and briefly in an uncoordinated manner in response to manual stimulation.

C class: Worms cannot move away after touch.

Terminal C class: Worms are entirely paralyzed except for very slight head movement in response to touch.

Terminal C class animals were found to be the most likely to die within the next 24 hours, which had important implications for how their fluorescence values were measured.

Different exposure times were used when observing different spectra:

Blue fluorescence (DAPI cube): 0.5s

Green fluorescence (GFP): 1s

Red fluorescence (dsRed): 1.5s

When animals were classified as Terminal C class, they were filmed using stop motion photography for 12 – 24 hours. This allowed us to observe any changes

in fluorescence immediately prior to, during and after the animal's death. This protocol is summarized in Figure 3.7.

2.2.4. Fluorescence quantification

Levels of fluorescence were quantified in Volocity Quantitation. Merged DAPI and brightfield images were used. The brightfield outline of each worm was traced manually using an Intuos 4 graphics tablet (Wacom). The mean pixel density for the fluorescence layer of the image was then exported to Excel (Microsoft Office). The same outline was then moved away from the worm to get a background DAPI reading which was again exported to Excel. The background reading was manually subtracted from the worm reading to give the final fluorescence value, in order to discount any fluorescence variation arising from changes to ambient light or fluctuating mercury bulb intensity.

The fluorescence values were then plotted against time, where time was defined as the number of hours prior to death (0). When plotting measurements taken for stop motion photography, time was calculated in fractions of days in order to present the data on the same scale.

2.2.5. Microscope slide preparation

High magnification microscopy was required in order to visualize cellular and sub-cellular DF localization. In order to use magnifications of 20x or higher, animals were placed on glass microscope slides. A 2% agarose solution was prepared, either fresh or made molten by microwaving, and 50µl was placed on the glass slide. This was then compressed with another slide and left for several minutes to harden. The secondary slide was removed, and 2-10µl of 0.2% levamisole was dropped onto the agarose pad. Worms were picked into drop of levamisole, and a cover slip was carefully lowered over them, using tweezers to ensure careful placement. Care needed to be taken when using slides to observe DF, as if animals were left for more than ~30 min they began to die from dessciation and consequently generate death fluorescence.

2.3 RNA interference by dsRNA ingestion

RNA interference (RNAi) is the phenomenon whereby the introduction of a sequence of double stranded RNA (dsRNA) to a cell leads to targeted gene expression knockdown of the identical endogenous sequence.

2.3.1. Mechanism of action

When dsRNA is taken into a cell, it is cleaved into small interfering RNAs (siRNAs) by the enzyme Dicer. Upon being cleaved into siRNAs, they separate into single strands and bind to the RNA-induced silencing complex (RISC). Once bound, they base-pair to homologous endogenous mRNAs. An enzyme within RISC then cleaves the bound mRNA, causing it to become degraded (Montgomery, 2006): thus whilst genes continue to be expressed, their expression is knocked down (Figure 2.4). The RISC mechanism is believed to have evolved in response to retroviruses and other genetic invasions (Ketting et al., 1999). Subsequently this phenomenon has been co-opted by researchers as a convenient technique for gene function analysis, especially in *C. elegans* where an easy feeding protocol and multiple clone libraries exist.

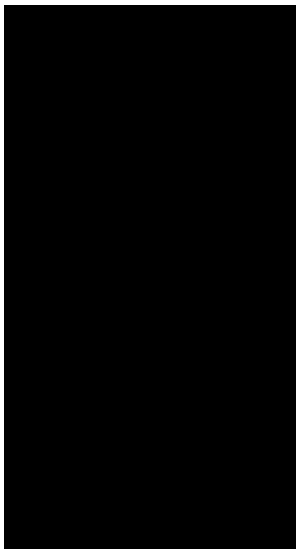

Figure 2.4: Diagram illustrating the basic mechanisms by which RNAi mediates gene expression knockdown. Illustration reproduced from www.nobelprize.org.

2.3.2. Protocol

RNAi in *C. elegans* can be induced by feeding the animals HT115 *E. coli* bacteria containing a fragment of the gene of interest cloned into the L4440 plasmid. The L4440 vector contains T7 promoters flanking the insert site, and produces T7 polymerase in response to IPTG exposure. The promoters sit in opposite orientation, allowing transcription from both ends of the fragment. T7 polymerase mediated transcription produces dsRNA of the gene of interest. HT115 bacteria carrying the empty L4440 plasmid were always used as a control in any experiment using RNAi.

In all experiments, feeding clones were already made and present in an RNAi library (The Ahringer library), kindly donated by our UCL colleague Stephen Nurrish (Kamath and Ahringer, 2003). Clones were obtained from frozen stock, and re-grown in the presence of the antibiotics ampicillin and teracycline. The plasmids were purified using the QiaSpin MINIprep kit (Qiagen) and sequenced at the Wolfson Institute for Biomedical Research, using the custom primers JJM130 and JJM131 (see section 2.5.3).

Once the sequence identity has been confirmed, HT115 bacteria are seeded onto IPTG plates and animals feed on the growing bacteria. Animals were generally raised from hatching on this bacteria, via egg lay or egg prep. The first animals raised on the RNAi are the F_1 generation; their progeny (F_2) were then used in experiments to counter any maternal rescue effects of maternal protein. If the RNAi inhibited development or growth, animals were placed on it as L4s.

2.4 Metabolomics

2.4.1 High performance liquid chromatography (HPLC)

2.4.1.1 HPLC background

In 1970 Csaba Horváth described the innovation of using high pressure to generate flow in packed columns, giving much greater resolution than previously described chromatography techniques (Waters, 2012). Now, high performance liquid chromatography (HPLC) is the most widely used chromatographic technique and is used in ~60% of separation experimentation worldwide (Lough and Wainer, 1996).

HPLC is used to isolate substances from a heterogenous compound; a typical set-up is illustrated in Figure 2.5. Compounds are separated from samples according to their relative polarities or charges. Briefly, samples are dissolved in a solvents, where the solvent depends on the sample type and compound to be isolated. When the sample is dissolved in solvent it is known as the mobile phase. The mobile phase is pumped at high pressure through a column filled of packing material (the 'stationary phase') (Figure 2.5). The packing material again will be determined by what compounds are being identified. For example, if the mobile phase is polar, the stationary phase will be non-polar. The extent of the relative attractions will determine how fast a compound moves through the column (Figure 2.6). Thus polar

compounds in a polar mobile phase will be repelled by the non-polar column and so move fast through the stationary phase. In contrast, non-polar compounds will be attracted to the stationary phase and so move slowly through it. Thus the compounds within a solvent are separated by polarity. HPLC differs from standard chromatography by the use of a pump which moves the mobile phase through the stationary phase. The pump allows the stationary phase column to be tightly packed without using a very column or losing any resolving powers as expected for non-pressurized chromatography (Waters, 2012).

Figure 2.5: Schematic of typical HPLC system set-up. Image repdroduced from http://www.waters.com/waters/nav.htm?cid=10049055&locale=en_US; accessed 22.8.2012.

Figure 2.6: Samples in HPLC are differentiated by relative attraction. Here, if the solid phase is polar, the yellow compound is the least polar of the three compounds and so moves fastest through the solid phase. Image source as in Figure 2.2.

As the compounds exit the column, moving at separate speeds, they will pass through a detector. The detector used again depends on what compounds are under scrutiny: for example, when looking at fluorescence compounds, a fluorimeter can be used to detect intensity at specific wavelengths. The intensity peaks are then plotted on a chromatagram (intensity against time the sample was eluted) (Figure 2.5). If required, peaks can be fractionated by collecting samples at specific times, and so the samples can be physically separated for further analysis.

We aimed to use HPLC as a first step to biochemically identify the death fluorescence fluorophore. In order to do this we hoped to identify the compound(s) of characteristic fluorescence present in the wild type samples that were absent or reduced in the *glo-1(zu437)* background.

2.4.1.2 Sample preparation

Whole worm sonicates were prepared in $_{d}H2O$ from large mixed stage populations grown on OP50 seeded NGM plates. Sonication was performed in repeated cycles of 1 min followed by a 30 sec pause for cooling in a 'Bioruptor' water bath sonicator (Diagenode) until samples were homogenously clouded. Samples were spun down at 4°C at 14,000rpm for 15 minutes, and the supernatant extracted. Cold 100% ethanol was added in a 1:9 sample:ethanol ratio and left at -20°C overnight. Samples were spun down again as above. The remaining supernatant was taken as the blue fluorescence sample. Samples were then evaporated in vacuum at room temperature, resuspended in 500 µL methanol, centrifuged and 1-30 µL aliquots were used for HPLC-MS analysis.

2.4.1.3. Protocol

HPLC was performed using an Agilent 1100 Series HPLC system equipped with a Varian Pursuit XRs-3-C18 column (4.6 x 250 mm, 5 µm particle diameter) connected to a Quattro II spectrometer (Micromass/Waters) A water (containing 0.1% acetic acid) – acetonitrile (also containing 0.1% acetic acid) solvent gradient was used at a flow rate of 0.7 ml/min, starting with an acetonitrile content of 5% for 15 min which was increased to 35% over a period of 20 min and subsequently to 95% over a period of 5 min and continued at 95% for 6 min (for graphical summary please see Figure 2.7). Metabolite extracts were analyzed by positive and negative electrospray ionization-MS. High resolution HPLC-MS was performed using a Waters nanoACQUITY UPLC System equipped with a Waters Acquity UPLC HSS C-18 column (2.1 x 100 mm, 1.8 µm particle diameter) connected to a Xevo G2 QTof Mass Spectrometer.

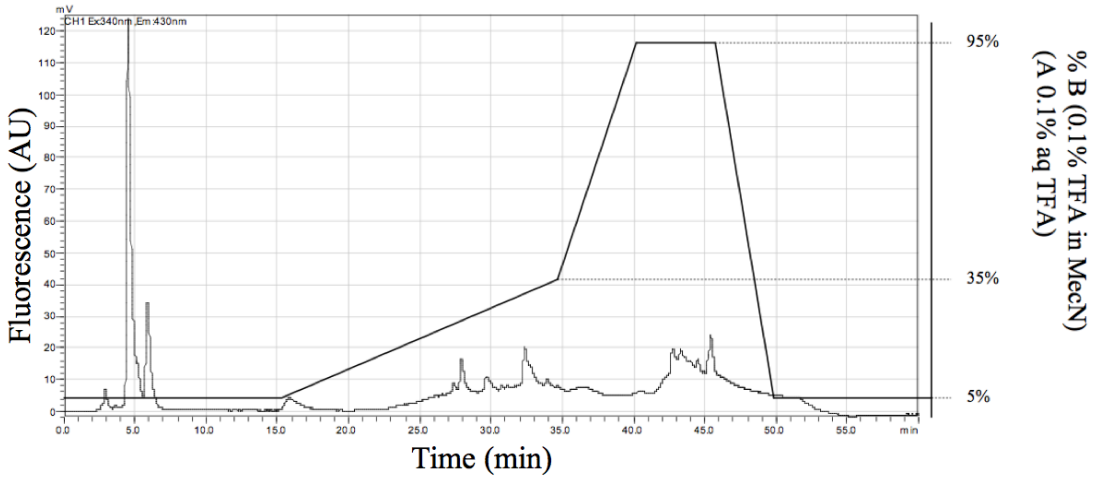

Figure 2.7: Diagram of HPLC protocol overlaid over data seen from N2 sample. The solvent front of B is shown diagrammatically to show the elution of the putative death fluorescence peaks at ~5 minutes in the polar solvent front.

2.4.2. NMR and DANS

Please note, both NMR and DANS were performed by Parag Mahanti and Frank Schroeder.

2.4.1.1. NMR and DANS background

Nuclear magnetic resonance spectroscopy (NMR) is a technique which allows molecular identification of species based on the magnetic resonance of their nuclei. Magnetic resonance arises from the quantum mechanical property of 'spin'. 'Spin' is the angular momentum specific to most nuclei (Evans, 1995). This momentum endows the nuclei with magnetic field, and so when the magnetic nuclei are exposed to a magnetic field this magnetism is converted to energy (Evans, 1995). These energies give nuclei characteristic signatures (spectra) which can be read, allowing subsequent molecular identification of the species in question. More information about the species can be obtained by using different types of magnetic field (fixed or continuous wave), or by obtaining the NMR signal as a function of frequency. Multi dimensional NMR uses magnetic pulses of different frequencies and durations in a particular order (pulse sequences) over time to extract multiple types of information from the molecular species.

DANS (**D**ifferential **A**nalysis of 2D **N**MR **S**pectra) is a two dimensional analysis of metabolomes derived from different genotypic backgrounds (Schroeder et al., 2007). Here multidimensional 2D NMR spectra are produced from the sample of

interest and a control. Using graphical analysis, the two spectra produced can be overlaid to clearly isolate signals derived from the sample of interest. This method results in silencing of signals common to both spectra, irrespective of the relative abundances of shared and unique signals. This method accelerates the identification of genome-specific compounds because it does not require extensive chromatographic fractionation. In traditional structural elucidation schemes, chromatographic fractionation is a major cause of compound loss due to degradation or decomposition, and so can significantly hamper the speed of identification (Forseth and Schroeder, 2011a). Several recent examples have demonstrated the utility of a specific type of 2D NMR spectrum (double quantum filtered correlation spectroscopy, or dqfCOSY) for compound identification via DANS (Forseth and Schroeder, 2011b). This technique has led to the successful identification of differentially expressed metabolites in *C. elegans* (Hu and Sherman, 2009; Pungaliya et al., 2009). Given that *glo-1* animals do not possess endogenous blue fluorescence, we decided to try and use DANS to identify metabolites differentially expressed between N2 and *glo-1*.

2.4.1.2. Sample preparation and protocol

N2 and *glo-1* samples were prepared as previously described to acquire the blue fluorescence containing supernatant (Section 2.4.1.2.). Samples were then evaporated in vacuum at room temperature and then the residues were dissolved in 200-600 µL of methanol-d4.

NMR spectra were recorded on a Varian INOVA 600 NMR (600 MHz for 1H, 151 MHz for 13C) and INOVA 400 NMR (400 MHz for 1H, 100 MHz for 13C) instruments. Non-gradient phase-cycled dqfCOSY spectra were acquired using the following parameters: 0.6 s acquisition time, 500-900 complex increments, 8-32 scans per increment. Gradient and non-gradient HSQC[AD], HMQC, and HMBC[AD] spectra were acquired with these parameters: 0.25 s acquisition time, 300-600 increments, 8-32 scans per increment. 1H,13C-HMBC spectra were optimized for JH,C = 6 Hz. Susceptibility-matched NMR tubes (Shigemi) were used for sample amounts smaller than 2 mg. NMR spectra were processed using Varian VNMR, MestreLabs MestReC and Mnova software packages.

2.5 Reagents

2.5.1. *C. elegans* strains used

N2 was the wild type (WT) strain in all experiments and the terms are used interchangeably. N2 was obtained from the Caenorhabditis Genetic Center (CGC). Most mutant strains were also obtained from the CGC, those that were not are acknowledged here or in the text.

Necrosis:

ZB1028 *crt-1(bz29)* V,

CB540 *unc-68(e540)* V,

JT73 *itr-1(sa73)* IV,

CB4027 *tra-3(e1107*);*eIs2137* IV,

CB189 *unc-32(e189*) III,

RB938 *vha-12(ok821*) X,

RB2035 *asp-4(ok2693*) X,

PJ1 *cad-1(j1*) II.

Apoptosis:

MT1522 *ced-3(n717*) IV,

MT4770 *ced-9(n1950*) III,

MT2547 *ced-4(n1162)* III.

Calcium measurements:

KWN190 *pha-1(e2123ts)* III, *him-5(e1490)* V;*rnyEx109* [pKT67 (P*nhx-2*::D3cpv); pCL1 (*pha-1*(+)],

KWN26 *pha-1(e2123ts)* III;*him-5(e1490)* V;rnyEx006 [pIA5nhx-2 (P*nhx-2*::pHluorin); pCL1(*pha-1*(+)],

pH measurements:

KWN385 *inx-16(ox144)* I;*pha-1(e2123ts)* III;*him-5(e1490)* V rnyEx006 [pIA5nhx-2 (P*nhx-2*::pHluorin); pCL1 (*pha-1*(+)].

Other:

BA671 *spe-9(hc88)* I,

GH10 *glo-1(zu437)* X, obtained from the Hermann lab

EG144: *inx-16(ox144)*;

GA91: *ftn-1(ok3625)* V;

GA1200 *mdl-1(tm311)* X,

GA200 *wu*Ex41[*rol-6(su1006)]*.

2.5.2. Reagents

Freezing medium

Dissolve 20 ml 1 M NaCl, 10 ml 1M KH_2PO_4 (pH 6.0), 60 ml 100% glycerol in purified H_2O, make up solution to 1 L with purified H_2O, autoclave and add 0.6 ml 0.1 M MgSO4.

Luria-Bertani (LB) buffer

Dissolve 10 g tryptone, 5 g yeast extract, 10g NaCl in purified H_2O, make up solution to 1 L with purified H_2O, adjust pH to 7.5 with NaOH and autoclave.

M9 solution

Dissolve 7 g $Na_2HPO_4.2H_2O$, 3 g KH_2PO_4, 5 g NaCl, 0.25 g $MgSO_4.7H_2O$ in purified H_2O, make solution up to 1 L with purified H_2O, and autoclave for sterility.

Nematode growth media (NGM)

Dissolve 3 g NaCl, 20 g agar and 2.5 g peptone in H_2O, make up solution to 1 L with purified H_2O and autoclave. Then add 1 ml 1 M Ca Cl_2, 1 ml 1 M $MgSO_4$, 1 ml 5 mg/ml cholesterol (in ethanol) and 25 ml 1M KH_2PO_4.

NGM Isopropyl-ß-D-1-thiogalactopyranoside (IPTG) agar

Dissolve 3 g NaCl, 20 g agar and 2.5 g peptone in H_2O, make up solution to 1 L with purified H_2O and autoclave. Then add 1 ml 1 M $CaCl_2$, 1 ml 1 M MgSO4, 1 ml 5 mg/ml cholesterol, 25 ml 1M KH_2PO_4, 400 µl 50 mg/ml carbenicillin and 1 ml 1M IPTG.

OP50 growth solution

Dissolve 5 g tryptone, 2.5 g yeast extract in H_2O, make up solution to 1 L with purified H_2O and autoclave.

Phosphate Buffered Saline (PBS)

Dilute 10 x PBS (100 ml + 900 ml purified H_2O) and add 1 ml Tween-20.

2.5.3. Primers

These primers were used to identify RNAi cultures by sequencing in a pL4440 vector (see section 2.3), and were originally generated by Josh McElwee (past Gems lab member).

JJM130	GGGAAGGGCGATCGGTGCGGGCC
JJM131	GCGCAGCGAGTCAGTGAGCGAGG

3. ENDOGENOUS *C. ELEGANS* BLUE FLUORESCENCE INCREASES WITH DEATH, NOT AGE

3.1 Introduction to *C. elegans* autofluorescence

C. elegans contains autofluorescent puncta within its intestinal cells (Clokey and Jacobson, 1986; Hermann et al., 2005) which have been likened to lipofuscin-containing lysosomes. Here I introduce the age pigment lipofuscin, *C. elegans* inetsinal autofluorescence, and discuss why the two have been equated. I then examine potential problems with this equation, and how I aim to test it.

3.1.1. Lipofuscin in mammalian cells

Post-mitotic mammalian cells, such as neurons and muscle fibres, accumulate a yellow-brown, autofluorescent pigment with increasing age (Brunk and Terman, 2002a). This pigment was first discovered in 1842 by Hannover, and it was dubbed *lipofuscin* by Hueck in 1912 (derived from the Greek *lipo* for fat and the Latin *fuscus* for dark) (Brunk and Terman, 2002a). Despite being described in the 1800's, lipofuscin's formation and composition have only been the subject of investigation relatively recently.

Lipofuscin is defined as a heterogenous, cross-linked aggregate of oxidatively damaged lipids and proteins that accumulates in an age-dependent fashion in post-mitotic mammalian cells (Brunk and Terman, 2002b; Jung et al., 2007; Terman and Brunk, 1998). Damaged cytosolic proteins and lipids are predominantly degraded by the proteasome (Coux et al., 1996). However, proteins and lipids that have been severely oxidatively damaged are highly reactive, and so are more likely to form intra- and intermolecular cross links causing aggregation (lipofuscin) (Jung et al., 2007). The ability of the proteasome to degrade damaged molecules appears to be greatly compromised by this cross-linkage, and there is evidence to suggest that lipofuscin can inhibit the proteosome (Friguet and Szweda, 1997; Shringarpure et al., 2000). Consequently, lipofuscin is taken up into the lysosomes by autophagy (Kurz et al., 2007). However, as a consequence of the extensive cross-linkage within lipofuscin it is not degradable by proteolytic lysosomal enzymes (Brunk et al., 1992). Therefore lipofuscin accumulates within lysosomes and the cytosol. In dividing cells, lipofuscin concentration can be diluted through division, but in post-mitotic cells lipofuscin accumulates with age (Brunk and Terman, 2002a). Lipofuscin levels have been found

to correlate negatively with the age of post mitotic cells, and consequently are frequently used as a biomarker of ageing (Sitte et al., 2000; Taylor and Davies, 1987). Lipofuscin generated in a non-age-dependent manner is known as 'ceroid', and is implicated in multiple juvenile diseases (Mole, 2011).

Lipofuscin composition is dependent on the cell type of origin, and so is highly variable, preventing the development of an antibody (Jung et al., 2007). Consequently lipofuscin is therefore most readily identified by its endogenous autofluorescence, although there is disagreement about its exact spectral signature. Lipofuscin excited by UV light *in vitro* emits blue fluorescence, most likely reflecting Schiff base formation between carbonyl and amino groups (Chio and Tappel, 1969; Fletcher et al., 1973). Schiff bases are functional groups with a carbon-nitrogen double bond attached to a hydrocarbon or aromatic ring group (Davis et al., 1982). However UV excitation of lipofuscin *in vivo* gives a peak at 540 – 640nm, or orange-yellow fluorescence (Eldred et al., 1982). Blue fluorescence has also been observed *in vivo*, but it has been suggested that this may be due to instrumental bias (Eldred et al., 1982). Moreover, multiple excitatory wavelengths produce a variety of fluorescent emissions depending on filter type (Brunk and Terman, 2002a). These discrepancies in reported spectra may well be due to the heterogeneous nature of the material, but it does compromise accurate identification of lipofuscin in model organisms such as the nematode *C. elegans*.

3.1.2. *C. elegans* contain autofluorescent lysosome-related organelles (LROs)

The *Rhabditidae* family of nematode worms, of which *C. elegans* is a member, contain cytoplasmic 'rhabditin granules' within their gut cells (Chitwood and Chitwood, 1950) (Figure 3.1). These granules are formed early in *C. elegans* development, being first visible in the embryo at four to six hours after fertilization (Laufer et al., 1980). These granules are denser than the surrounding tissue and so cause light to be refracted, or bent, around them, making them appear bright under polarized microscopy (Nill, 2006). They also contain autofluorescent material, of which the predominant spectral signature is held to be UV-excited blue fluorescence $\lambda_{ex}/\lambda_{em}$ 340/430nm (but see below) (Gerstbrein et al., 2005). These autofluorescent, granules are thought to correspond to *C. elegans* intestine-specific lysosome related organelles (LROs) (Hermann et al., 2005).

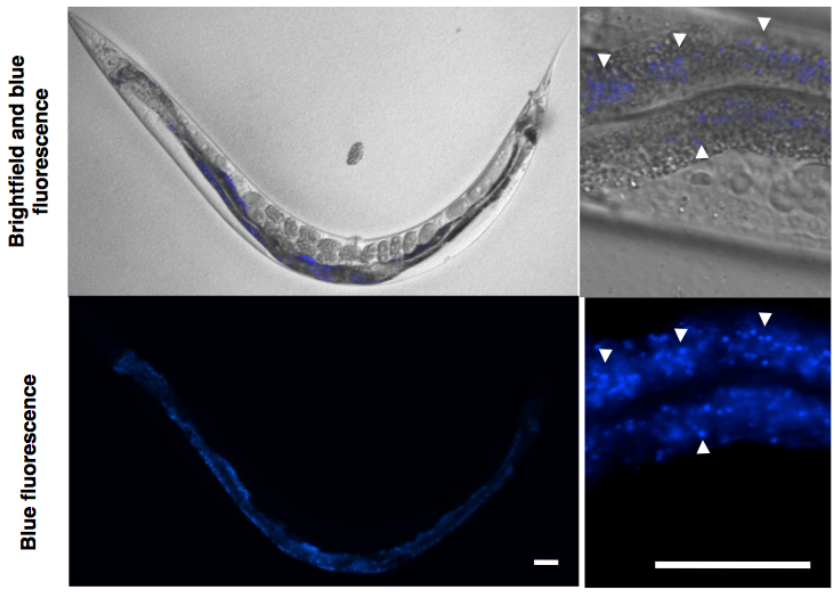

Figure 3.1: *C. elegans* contain punctate blue fluorescence in their intestinal cells (white arrow heads show puncta). Bar = 50μm.

The exact nature of lysosomes in *C. elegans* is somewhat unclear. In 1987, Clokey and Jacobson proposed that the autofluorescent puncta were lysosome-like organelles, as they were acidic (demonstrated by staining with the lysosomotropic dye acridine orange) and were capable of endocytosis (Clokey and Jacobson, 1986). Mammalian cells contain a structurally distinct family of lysosome associated membrane proteins (LAMPs), which are found in endosomal-lysosomal compartments (Kostich et al., 2000). The closest *C. elegans* homolog is encoded by *lmp-1*, which contains the consensus lysosomal targeting motif on the C-terminus found on all mammalian LAMPs (Kostich et al., 2000). LMP-1 antibodies stain granules within *C. elegans* intestinal cells in a similar pattern to that observed for autofluorescent, acidic granules. However, co-localization of the two patterns was not demonstrated (Kostich et al., 2000).

In 2005, a class of mutant was discovered which lacked these autofluorescent puncta. These Glo mutants (Gut granule LOss) did not show staining with either of the lysomotropic dyes acridine orange or Lysotracker red (Figure 3.2) (Hermann et al., 2005). However, LMP-1::GFP puncta were still present in *glo-1* mutant animals, potentially indicating that LMP-1 associated granules are in a different class to the autofluorescent puncta. *glo-1* encodes a putative Rab GTPase, whose protein sequence is very similar to those of *Drosophila* and *Dictyostelium* Rabs (45 and 47% conserved identity respectively) (Hermann et al., 2005).

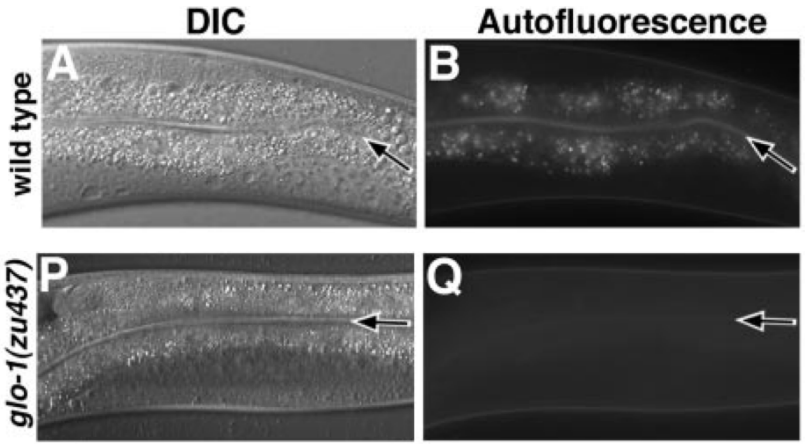

Figure 3.2: Glo mutants lack intestinal autofluorescence (image reproduced from Hermann et al 2005).

These Rabs have been implicated in biogenesis of the specialized lysosome-like pigment-containing organelle melanosomes (Hermann et al., 2005). Thus, it has been suggested that the autofluorecent puncta observed in *C. elegans* intestinal cells might be melanosomes (Raposo and Marks, 2007). However, an alternative explanation – widely accepted in the ageing field - may be that the gut granules contain autofluorescent lipofuscin.

3.1.3. Equation of *C. elegans* autofluorescence and lipofuscin

C. elegans intestinal autofluorescent material was initially characterized through *in vitro* aqueous and chloroform-methanol extraction, showing a spectral signature of $\lambda_{ex}/\lambda_{em}$ 320-365/450-480nm (Davis et al., 1982; Klass, 1977).

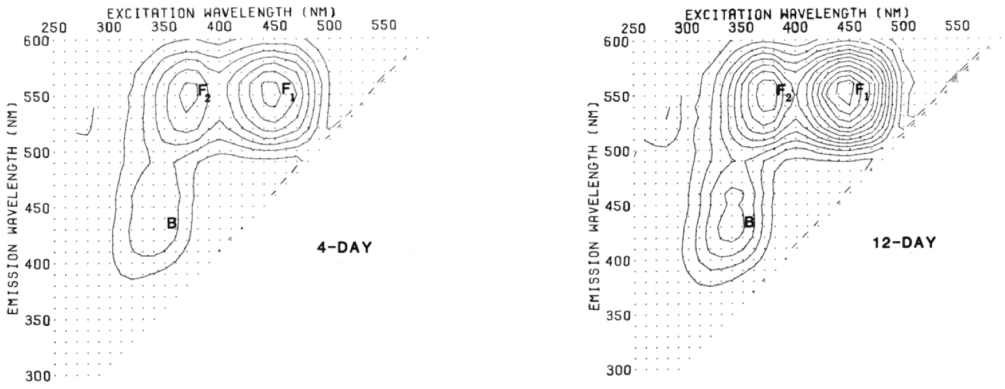

Figure 3.3*: C. elegans* blue fluorescence increases with age in vitro. Figures show blue fluorescence contained in aqueous extractions (marked "B") taken from cohorts of 4 and 12 day old wildtype worms. Figure reproduced from Davis et al, 1982.

This blue fluorescent pigment was shown to increase in older samples, and, based on spectral similarities to the Schiff bases found within lipofuscin, it was suggested that the material could represent *C. elegans* lipofuscin (Figure 3.3) (Davis et al., 1982; Klass, 1977). However, it was also noted that both reduced NAD and anthranilic acid have similar blue spectral signatures, and thus that further analysis would be required to confirm the biochemical composition of the autofluorescence (Davis et al., 1982).

Subsequent studies examined *C. elegans* autofluorescence *in vivo* in ageing animals. These studies followed the fluorescence levels of either individual or populations of animals, and investigated a variety of fluorescent signatures. Observation of wild type worm populations on day 2, 5 and 10 of adulthood identified an age-related increase in UV-excited *green* fluorescence (525nm bandpass filter), whose appearance was delayed in long lived *daf-2* animals (Garigan et al., 2002). Another study also examined the spectral signature of a population of animals *in vivo*. Gerstbrein and colleagues scanned a large excitation/emission range, but only found significant age-related increases in UV-excited *blue* fluorescence, with an excitation maximum of 430nm (Figure 3.4) (Gerstbrein et al., 2005). Finally, an *in vivo* study monitoring individual animals found significant age related increases in levels of *red* fluorescence ($\lambda_{ex}/\lambda_{em}$515-573/590-650) (Pincus et al., 2011a).

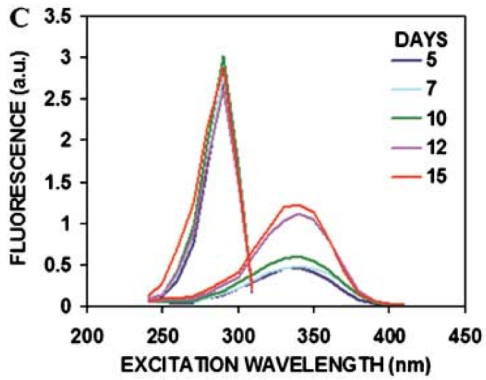

Figure 3.4: *C. elegans* blue fluorescence increases with age *in vivo*. The levels of fluorescence attributed to the amino acid tryptophan residues (left) remains constant, as compared to the blue fluorescence (right) which is shown increasing with age in cohorts of animals. Figure reproduced from Gerstbrein et al 2005.

Thus, these data suggest that autofluorescence in *C. elegans* increases in an age-dependent manner. On the basis of these studies, and those mentioned above showing autofluorescent puncta to be acidic lysosome-like organelles, it is now

widely held that *C. elegans* autofluorescence is lipofuscin (Adachi et al., 1998; Fisher and Lithgow, 2006; Fujii et al., 1998; Ishii et al., 1998; Masse et al., 2008). Thus, despite there being no direct evidence that *C.* elegans autofluorescence is lipofuscin, a literature search revealed over 50 papers (please see Appendix 1) citing one or more of the above papers as evidence that *C. elegans* autofluorescence being lipofuscin.

3.1.4. Challenges to the assumption that *C. elegans* autofluorescence is lipofuscin

The assumption that *C. elegans* autofluorescence is equivalent to lipofuscin has not been verified. One difficulty is that cohort studies do not take into account heterogeneity in fluorescence levels between individual worms[1]. This issue was raised by a previous study (Gerstbrein et al., 2005), as follows. Aging worms can be classed according to their degree of motility: class A animals move normally, class B animals move more slowly, and class C animals do not move away when touched, and are near to death (Herndon et al., 2002). Notably, blue fluorescence levels did not different between class A and B, and only increased in class C worms (Figure 3.5) (Gerstbrein et al., 2005).

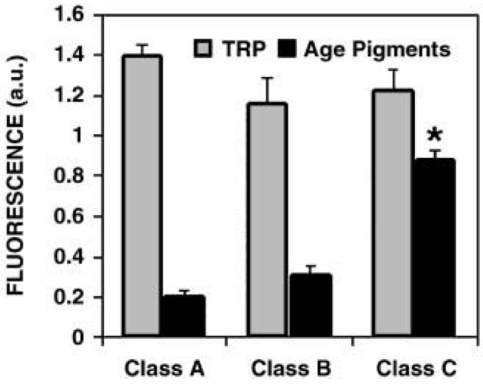

Figure 3.5: *In vivo* measurements of *C. elegans* cohorts show that blue fluorescence only increases significantly when animals are "C" stage, or close to death, rather than increasing gradually with age. Figure taken from Gerstbrein et al 2005.

This suggests that blue fluorescence levels in worms increase only as they approach death. Average fluorescence levels from cohorts could therefore mask individual heterogeneity (Figure 3.6). Another difficulty regarding the assumption of autofluorescence as lipofuscin is the lack of tested predictions. Mammalian lipofuscin is a product of oxidative damage (Brunk and Terman, 2002a). When human foreskin

[1] Please note that we began this investigation prior to the publication of the 2011 Pincus et al study which individual animals were used.

fibroblast cultures were exposed to 40% normobaric hyperoxia (40% O_2) they accumulated significantly more lipofuscin than those under atmospheric conditions (Terman and Brunk, 1998). One attempt to test this in *C. elegans* yielded somewhat inconclusive data, which implied that increased oxidative damage leads to increased autofluorescence levels, but did not demonstrate a significant effect (Hosokawa et al., 1994).

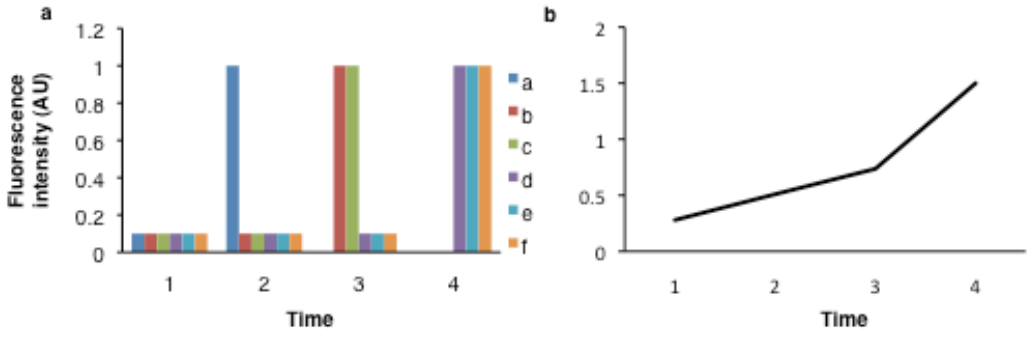

Figure 3.6: Cohort fluorescence levels may mask population heterogeneity. (a) Individuals a-f are plotted showing changing intensity peaks through time. Individual a shows peak intensity at time 2, and then no more fluorescence, whereas individual f shows steady fluorescence until peak intensity at time 4. However, as shown in (b), when cumulative population data is presented, the illusions of fluorescence gradually increasing over time appears.

Finally, the existence of single gene mutations that entirely abrogate (Glo) or alter (Flu) intestinal autofluorescence argues against it resulting from cumulative oxidative damage (Hermann et al., 2005). The Flu class of mutants contain single gene mutations which alter the spectral signature of the intestinal autofluorescence; for example, the mutation *flu-1* results in purple-blue fluorescence in response to UV excitation and *flu-2* animals show green (Siddiqui and Von Ehrenstein, 1980). For more detail, please see Chapter 5.

Taken together, these issues challenge the assumption that *C. elegans* autofluorescence is equivalent to mammalian lipofuscin. As outlined in the introduction, a valid biomarker of biological ageing would be a useful tool in biogerontology. Biomarkers of ageing are better than mortality as a measure of ageing, as morality is influenced by both extrinsic hazards as well as intrinsic risks of death. It is therefore important to rigorously test this assumption before its use in research. Consequently, the initial aims of this project were to test some of the predictions generated by the hypothesis that *C. elegans* autofluorescence could be

lipofuscin. Firstly, if the autofluorescence is lipofuscin, then increasing oxidative damage levels should increase autofluorescence. Secondly, individual animals should show gradually increasing levels of autofluorescence with age.

3.2 Results

3.2.1. Creating a microscopy system capable of monitoring individual animals over time

As outlined above, in order to avoid artefacts caused by looking at aggregate fluorescence data in population cohorts, it was necessary to follow individual animals as they age. Preliminary data obtained by Sally-Anne Edwards indicated that there was no increase in fluorescence during life, but instead showed an increased fluorescence at death. The preliminary data for this study was acquired in a slow, manual manner. Images were collected on a Leica DMXRA2 microscope. Brightfield and fluorescence filters were manually moved into position, their respective light sources were manually turned on and off and two images were taken separately, and manually overlaid. The autofluorescence was then analysed on OpenLab software (Improvision) by drawing an outline of the worm on the bright field image, and then superimposing that outline onto the fluorescent image. This value was measured, and a subsequent value was taken from the background in order to normalize the data. The final fluorescence value was then calculated as the mean pixel density measured from the fluorescent image.

This method was sufficient to observe that the increase in autofluorescence was correlated with death (see below). In order to determine the dynamics of fluorescence increase at death, it was necessary to upgrade to a system capable of time-lapse image capture. Thus, the microscope system required upgrading to one that was capable of automatic control. The new system was upgraded as follows:

- The computer controlling the microscope was upgraded to a new iMac computer (Apple) which was capable of supporting updated software, and had greater processing power, giving faster control.
- OpenLab was upgraded to Volocity (Improvision) which made it possible to create automatic acquisition protocols known as ‘lightpaths’ (please see Section 2.2) that were capable of controlling the microscope automatically from the computer.

• A bright field shutter was acquired. This shutter fits over the bright field bulb, allowing computer control of illumination. This in turn allows acquisition of multiple images almost simultaneously, and so makes time-lapse photography possible. Previously only manual control of bright field illumination was possible.

• A new DAPI filter cube was acquired. The previous filter cube produced very faint fluorescence; when removed, it was found to be covered with a dark residue that could not be cleaned off. The replacement filter cube (detailed in Section 2.2.2.1.) required lower exposure times for brighter images, further increasing the overall efficiency of the system.

This new system made possible the creation of automated programmes, capable of controlling most of the aspects of microscopy hardware. The system is integrated with control software, which can automatically alter aspects of image acquisition. In order to examine large numbers of individual animals on a daily basis (see below), fast throughput was especially important. That the new system increased speed and reproducibility of image acquisition can be seen in the time taken in acquiring a merged brightfield and epifluorescent image: ~5 seconds under the old system, 0.6 seconds for the new. Thus we were confident that this setup would be sufficient to accurately observe small changes in *C. elegans* autofluorescence over time.

3.2.2. Developing a protocol to monitor individual animals over time

Previous studies looking at *C. elegans* autofluorescence *in vivo* monitored age-matched cohorts of animals (Garigan et al., 2002; Gerstbrein et al., 2005), a method which, as discussed previously, may generate misleading data. At the time of experimentation, there was no protocol for following individual animals in this way, and so we had to develop one. This protocol is outlined briefly here, and discussed in more depth in Materials and Methods.

Strains were grown up under standard conditions. At the L4 stage, 30 – 40 animals were picked onto OP50 seeded NGM plates containing 15μM FuDR to prevent progeny development. Animals were scored daily on two counts: firstly, for their movement phenotype and subsequently for their fluorescence values.

Movement phenotype scoring was adapted from Herndon et al 2002, where an animal was placed into one of three movement categories depending on its agility.

Preliminary trials showed that a single category could contain very different motility levels, and so three more categories were introduced to give a total of six classes:

A class: Animals move quickly and fluidly in a clear sinusoidal pattern, without the need for manual stimulation.

A/B class: Worms move without manual stimulation but do so more slowly than A, or in non-sinusoidal (uncoordinated) manner.

B class: Worms are manually stimulated to move by touching gently with a platinum wire; movement is slow, uncoordinated or very brief.

B/C class: Worms move very slowly and briefly in an uncoordinated manner in response to manual stimulation.

C class: Worms cannot move away from manual stimulation.

Terminal C class: Worms are entirely paralyzed except for very slight head movement in response to manual stimulation.

Terminal C class animals were found to be the most likely to die within the next 24 hours, which had important implications for how their fluorescence values were measured.

Animals' fluorescence values were determined by fluorescent microscopy. In order to measure the same animal's fluorescence values daily, it was necessary to do so without harming them. As such, animals remained *in situ* on NGM plates, and were not mounted onto glass slides. They were placed on ice for 10 – 15 minutes in order to induce stillness for the measurements.

Animals were initially measured only for their blue fluorescence levels, characterized by Gerstbrein et al at approximately $\lambda_{ex}/\lambda_{em}$ 340/430nm. A DAPI filter set was used for these readings. Preliminary trials established an exposure time of 500ms as being sufficient to see intestinal fluorescence, and this was held constant throughout the trial to make all data points comparable.

Daily observations acquired two images in quick succession: brightfield and then blue fluorescence. These two images were automatically overlaid, and the brightfield outline of the animal was traced by hand using a graphics tablet, thus supplying the mean fluorescence pixel density for the animal. The worm outline was moved to right of the worm image and a background pixel density reading was taken. The final fluorescent value was obtained by subtracting the background from the outline reading. Plotting these pixel densities over time showed each animal's lifelong fluorescence readings.

When animals were classified as Terminal C class, they were filmed using stop motion photography for 12 – 24 hours. This allowed us to observe any changes in fluorescence immediately prior to, during and after the animal's death. This protocol is summarized in Figure 3.7.

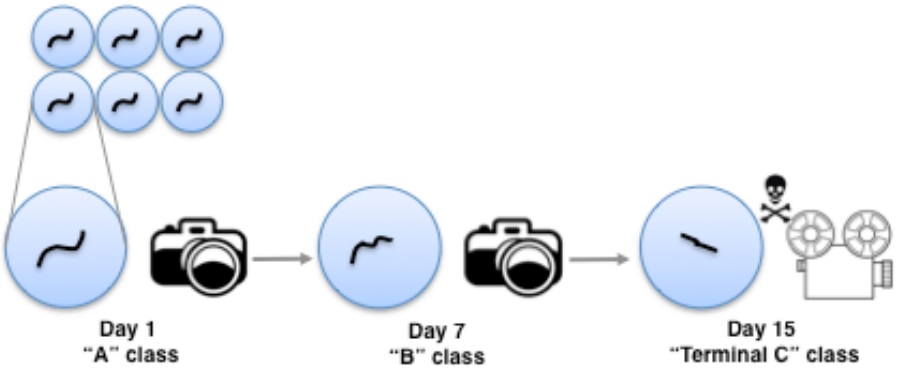

Figure 3.7: Schematic illustrating protocol for observing individual animal fluorescence over time. Animals are individually plated and photographed in situ until they reach the "Terminal C" stage of mobility. They are then filmed until after death.

3.2.3. Blue fluorescence does not increase with increased oxidative damage

To probe whether the blue fluorescent material in *C. elegans* LROs is lipofuscin, we asked whether oxidative stress increases fluorescence levels. First, we subjected young adult *C. elegans* to normobaric hyperoxia (90% partial pressure O_2), and measured levels of protein oxidation, and blue fluorescence. Protein oxidation was measured via oxyblot, which detects protein carbonyls that have been formed through oxidative damage, and has previously been used in *C. elegans* (Van Raamsdonk and Hekimi, 2010; Yang et al., 2007). Blue fluorescence levels were measured using the microscopy set-up described above. This work was carried out in collaboration with Filipe Cabreiro and Caroline Araiz.

Hyperoxia resulted in a 29% increase in oxidative damage (protein carbonyl levels) relative to normoxia controls, but did not increase blue fluorescence (Figure 3.8). By contrast, in mammalian cells, 40% O2 significantly increased lipofuscin levels (Terman and Brunk, 1998). We then exposed animals to 15mM ferric ammonium citrate (FAC), which have been shown to increase oxidative damage in *C. elegans* (Valentini et al., 2012). Again, this treatment significantly increased levels of protein damage, but blue fluorescence levels showed no significant changes (Figure 3.9).

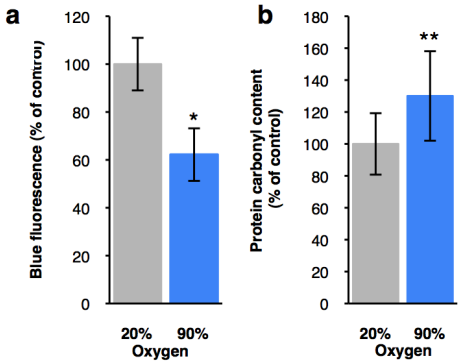

Figure 3.8: Exposure to hyperoxia increases levels of protein carbonyls, but not blue fluorescence. (a) Blue fluorescence levels do not increase under hyperoxia. (b) Quantified oxyblots show that hyperoxia (90% oxygen) increases protein carbonyl levels compared to atmospheric levels (20% oxygen). Graphs show mean of 3 biological replicates, ± SEM. Asterisks indicate significant differences, where * $p < 0.05$ and ** $p < 0.01$, Student's t test.

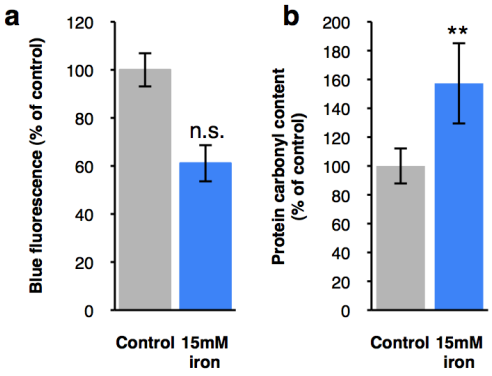

Figure 3.9: Exposure to free iron (FAC) increases levels of protein carbonyls, but not blue fluorescence. (a) Blue fluorescence levels do not increase after exposure to 15mM FAC. (b) Quantified oxyblots show that 15mM FAC increases protein carbonyl levels compared to control. Graphs show mean of 3 biological replicates, ± SEM, Student's t test.

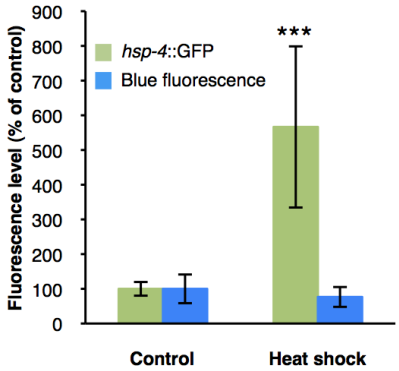

Figure 3.10: Blue fluorescence does not increase with heat-shock induced increased unfolded protein response (UPR) activity, as indicated by increased levels of hsp-4::GFP. Graphs show mean of 3 biological replicates ± SEM, Student's t test.

Finally, we attempted to measure a different type of damage. Increased expression of *hsp-4*::GFP is a marker for the unfolded protein response, symptomatic of protein damage (Urano et al., 2002). Heat shock significantly increased levels of *hsp-4*::GFP expression but again blue fluorescence levels showed no increase (Figure 3.10). These results imply that *C. elegans* intestinal fluorescence is not the product of oxidative damage, and so may not be lipofuscin.

3.2.4. Blue fluorescence increases with death, not age

In mammalian cells, lipofuscin is not degradable by proteolytic enzymes, and so accumulates in the lysosomes with age. Thus if *C. elegans* intestinal fluorescence is lipofuscin, it should increase gradually with age. As outlined above, previous studies have described increased mean fluorescence levels with age in *C. elegans* cohorts (Garigan et al., 2002; Gerstbrein et al., 2005) but there is concern that population heterogeneity may mask individuals' fluorescence levels. To test this, the fluorescence levels of individually cultured, wild-type *C. elegans in situ* on NGM agar plates were examined at intervals throughout life (DAPI filter; $\lambda_{ex}/\lambda_{em}$ 350/460nm). The fluorescence levels of animals identified as Terminal C were measured during the subsequent 12–24 hrs using time-lapse photography in order to capture fluorescence changes during death.

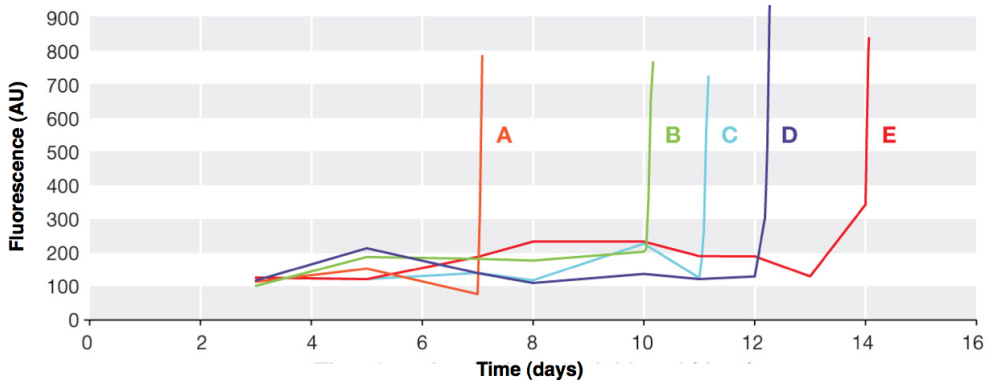

Figure 3.11: Blue fluorescence increases death, not age. Graph showing individual worm's levels of blue fluorescence viewed *in situ* on NGM plates; there is no change during life but then a large, significant increase in fluorescence at death (for individuals a – e, days 7, 10, 11, 12 and 14 respectively).

Over the course of adulthood until a short time prior to death, blue fluorescence levels in individual animals did not increase significantly (Figure 3.11).

However, a striking and rapid increase in fluorescence levels occurred in class C animals, which coincided with complete cessation of movement (i.e. with death) (Figure 3.12, Movie 1; for movies please see DVD appendix inside back cover). This burst of fluorescence entailed an average increase in fluorescence of ~400% above basal levels (Figure 3.12). This fluorescence developed very quickly as the animals approached death, typically starting to rise two hours prior to the cessation of movement, and then fading during the first six hours after death (Figure 3.12, Figure 3.13).

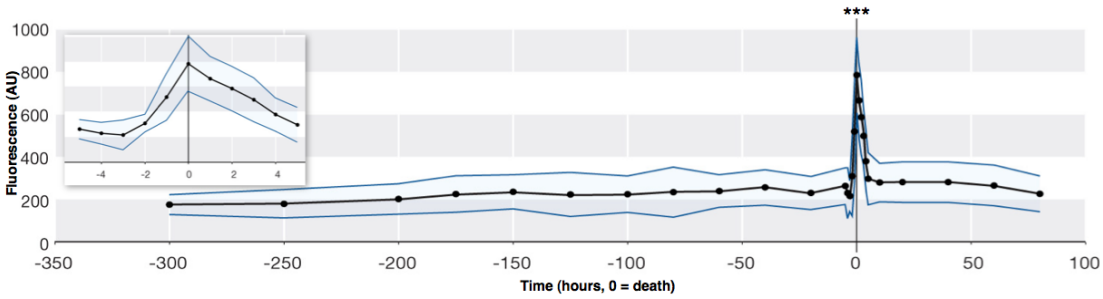

Figure 3.12: Blue fluorescence increases with death, not age. Mean levels of fluorescence normalized to time of death of 47 individual animals. Time 0 = time of death. Shaded area ± SD. The burst of fluorescence has a duration of approximately six hours from beginning until fading (see inset).

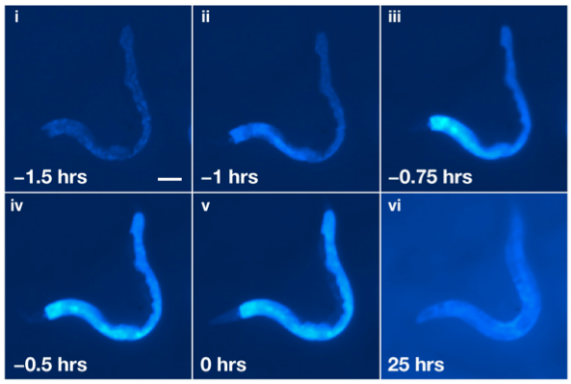

Figure 3.13: Representative image showing fluorescence change during death from old age. Time is hours, where 0 marks a complete cessation of movement, defined as death. The fluorescence is initially punctate (i), then increases in intensity in the anterior intestine (ii-iii), engulfs the intestine (v) and finally fades in a diffuse distribution (vi).

The fluorescence also showed a marked alteration in its distribution. Living animals show punctate gut granule fluorescence (Figure 3.1, Figure 3.13 i). However, as death approached, fluorescence engulfed entire cells one after another, until the whole intestine glowed emitted a bright blue glow (Figure 3.13 i - iv, Movie 1).

Thereafter, fluorescence spread to other tissues in the animal, except the pharynx and gonad. After death, the fluorescence intensity returned to pre-death levels, but did not regain its punctate distribution (Figure 3.13 v). Taken together with our earlier result showing that increased oxidative damaged does not increase blue fluorescence levels, our data strongly argues against *C. elegans* blue fluorescence being lipofuscin. It suggests that earlier results could reflect error resulting from summing data from population cohorts. Finally, it suggests that increased levels of blue fluorescence may serve as a novel biomarker of death in *C. elegans*.

3.2.5. A burst of blue fluorescence marks death in *C. elegans* and other nematodes, irrespective of age or cause

In order to investigate whether increased levels of blue fluorescence act as a universal biomarker of death in *C. elegans*, we examined fluorescence changes in young animals dying from injury. Young adult animals were killed with a hot pick, by freeze-thaw, dessication or immersion in acetic acid (pH3) (please see section 2.1.6). Significant increases in blue fluorescence were observed in each case (Figure 3.14, Movies 2 and 3).

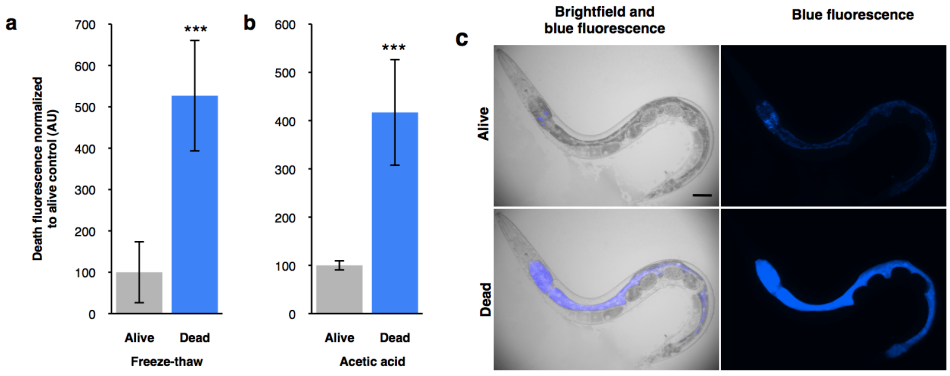

Figure 3.14: Blue fluorescence increases when young adult hermaphrodites die from injury. (a) Young adults generate death fluorescence when killed by exposure to acetic acid or freeze-thaw stress, as measured in a plate reader; please see section 2.1.6 for methodology. Graphs show percentage increase in fluorescence at death, normalized to living fluorescence ± SD, Student's t-test. (c) Representative image of young adult hermaphrodite killed by application of a hot pick to adjacent agar.

We then tested to see if males and L4 hermaphrodite larvae generated a burst of fluorescence at death. Significant increases in blue fluorescence were also observed when adult males and L4 hermaphrodite larvae were killed by heat (Figure 3.15). A

burst of blue fluorescence was also observed after heat killing in two other nematode species, *Caenorhabditis briggsae* and *Pristionchus pacificus* (Figure 3.15), and so may be widespread among nematode species (this data obtained by my student, Alexander Davidson).

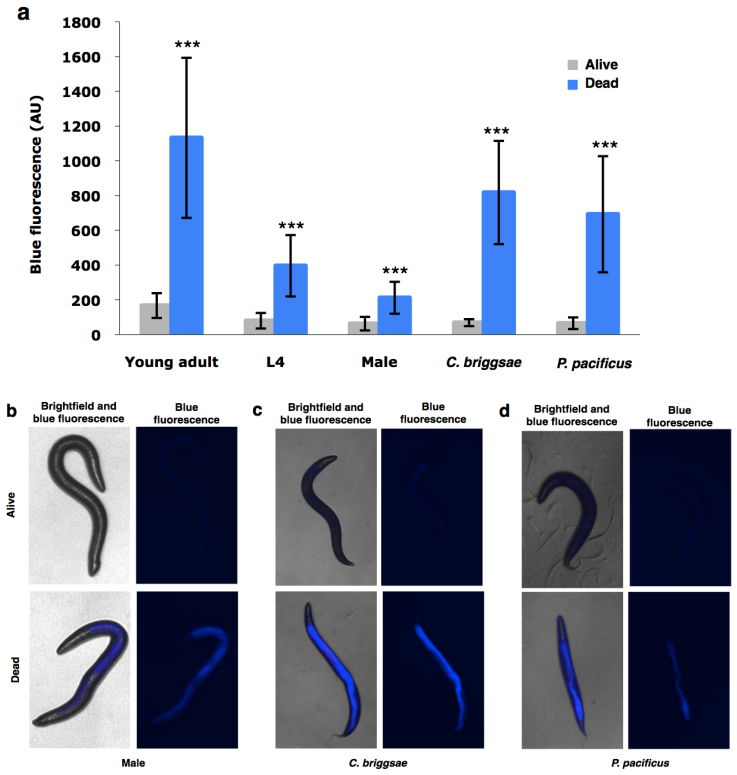

Figure 3.15: Blue fluorescence increases at death in *C. elegans* and other species. Blue fluorescence increases when L4 larvae and young adult males die from injury. (a) L4 larvae and young adult male *C. elegans* show death fluorescence when they die, as do *C. briggsae* and *P. pacificus*. Graphs show living and dead fluorescence, ± SD, Student's T test. (b-d) Representative images of a dead young male *C. elegans* (b), *C. briggsae* (c) and *P. pacificus* (d) killed by exposure to heat.

Thus, bursts of fluorescence accompany death whether caused by old age or mortal injury in *C. elegans* and other nematodes. This being so, this death-associated burst of blue fluorescence will hereafter be referred to as *death fluorescence*.

The discovery of death fluorescence confirms that blue fluorescence within *C. elegans* intestinal cells is unlikely to be lipofuscin. Previous reports of increases with age can most likely be attributed to population heterogeneity masking the effect of individuals' death fluorescence increases. Whether lipofuscin exists in *C. elegans* therefore remains an open question. However, the discovery of death fluorescence

provides a novel endogenous marker of death in *C. elegans* which could be useful, e.g. for lifespan measurements.

3.2.6. Red and green fluorescence increase with both age and death

As detailed above, multiple different fluorescent signatures have been described in *C. elegans* (Garigan et al., 2002; Gerstbrein et al., 2005; Pincus et al., 2011a). We were interested to see whether or not the reported increases in these spectra would be reproducible in individuals. Individuals were observed daily as previously described, but three fluorescent images were taken, using the DAPI, GFP (green, $\lambda_{ex}/\lambda_{em}$ 470/525nm) and dsRed ($\lambda_{ex}/\lambda_{em}$ 545/620nm) filters to examine green and red fluorescence levels along with blue. Green and red fluorescence in *C. elegans* appear much dimmer than blue fluorescence using mercury bulb illumination. Consequently, longer exposure times were required to visualize the fluorescence well enough to detect changes. This was problematic, as excessive exposure to UV light both harms the animal and can cause photobleaching of fluorescence. Preliminary experimentation found that 1 and 3 second exposure times for green and red fluorescence respectively was sufficient to visualize the fluorescence.

Levels of red and green fluorescence were both extremely low, with a high degree of variation. Both did not appear to show any increase in life, and appeared to increase only after death; not prior to death, as seen in death fluorescence (Figure 3.16). However the levels of fluorescence seen were so low, it was not possible to draw confident conclusions about the nature of red and green fluorescence in *C. elegans*.

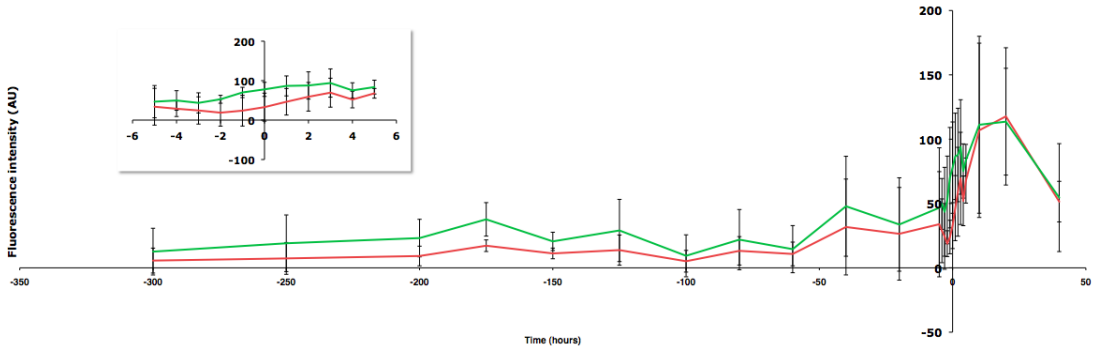

Figure 3.16: Red and green fluorescence increase only after death. Red and green fluorescence in *C. elegans* appear to increase only after death, and not during life, or prior to death in the manner of blue fluorescence.

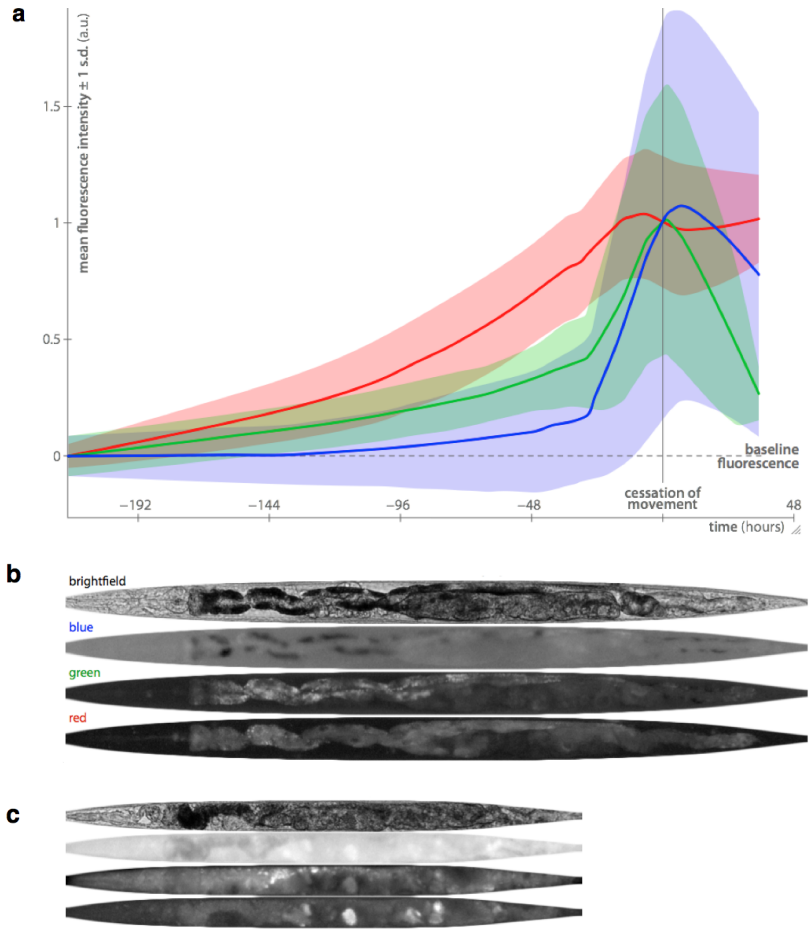

Figure 3.17: Independent experimentation showing that blue fluorescence increases at death, whereas green and red fluorescence increase with age. (a) Average levels of fluorescence normalized to time of death, viewed under red, blue and green filter sets, showing different rates of fluorescence increase with time. n = 43 individual animals. Shaded area = ± 1 standard deviation. Each plot is scaled on separate arbitrary units as absolute-terms comparisons are not possible. Note that rates of fluorescence accumulation and spatial distribution of the blue, red and green fluorescence differ, consistent with the presence of distinct fluorophores. (b and c) Typical prior to death and during death images of an animal in each fluorescence band, showing altered spatial distribution of the fluorescence. Data and figure from Zachary Pincus, Yale University.

Consequently we repeated the experiments using a more sensitive fluorescence detection system. This data was obtained by Zachary Pincus (Yale University), using the methodology as described (Pincus et al., 2011a). Fluorescence was measured using DAPI (blue, $\lambda_{ex}/\lambda_{em}$ 350/460nm), GFP (green, $\lambda_{ex}/\lambda_{em}$ 470/525nm) and TRITC (red, $\lambda_{ex}/\lambda_{em}$ 546/600nm) filter sets. Blue fluorescence measurements allowed verification that blue fluorescence does not increase prior to death (Figure 3.17).

Again, no significant age-increase in blue fluorescence was seen (though weak but non-significant increases were seen late in life) (Table 3.1). Green and red fluorescence did increase significantly with age (Table 3.1), and all three forms of fluorescence increased during death (Figure 3.17, Table 3.1).

Student's t test p value	Blue	Green	Red
Is the pre-death slope significantly greater than 0?	0.0768	2.86e-14	2.35e-27
Do pre- and post-death slopes differ significantly?	5.93e-12	5.94e-13	1.56e-06
Do pre- and peak death fluorescence maxima differ significantly?	1.02e-13	3.36e-19	1.82e-16

Table 3.1 Multiple types of fluorescence increase with death in *C. elegans*. Both green and red fluorescence increase significantly with age, but blue fluorescence does not. Table also shows a significant increase in all types of fluorescence at death, with peak death fluorescence significantly higher than at any time seen during life.

These results confirm that the increase in the blue fluorescence in *C. elegans* in aging population cohorts is predominantly a function not of aging but of death. The fact that red and green fluorescence increase with both age and death suggest that *C. elegans* may contain multiple fluorophores. However, it does show that red or green intestinal fluorescence could be used as markers of ageing in *C. elegans*, provided that death-related increases were controlled for by studying individuals, not populations.

3.2.7. Living fluorescence increases gradually with time in slide-mounted animals

Based on population heterogeneity, it is easy to understand how *in vivo* measurements of population cohorts could mask death fluorescence and show instead a gradual increase in blue fluorescence with age. However, another possibility is that in worms mounted on microscope slides, there is an age-related increase in blue fluorescence. To test this, we measured the levels of fluorescence in living animals on slides in age-matched cohorts at days 2, 5, 7, 9 and 15 of adulthood.

In order to see if increased duration mounted on slides leads to brighter fluorescence, the animals were measured immediately after being placed on slides and subsequently 20 minutes later (Figure 3.18). We found that initial measurements of fluorescence in living animals mounted on slides significantly increased in intensity with age from day 7 of adulthood. However we found that leaving animals on slides

did not increase fluorescence. These findings suggest the possibility that mounting worms onto slides damages them, and such damage leads to DF development. One possible cause of stress is physical pressure of the cover slip.

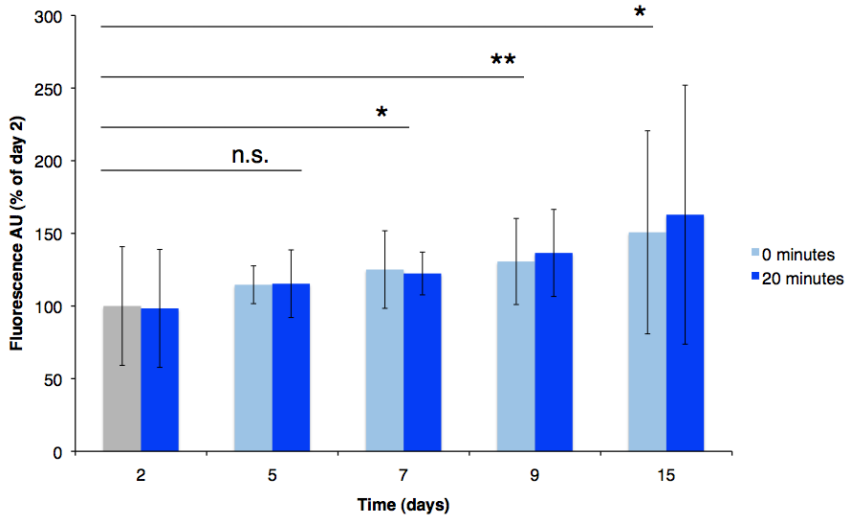

Figure 3.18: Blue fluorescence does increase with age in slide-mounted animals. There is a significant increase over time in fluorescence measured immediately after mounting. Remaining on slides for a further 20 minutes does not increase fluorescence. All values are normalized to 0 minutes, day 2 (shown in grey). Data mean of 27 individual animals, ±S.D, student's t test.

3.2.8. Death fluorescence spreads in a characteristic pattern

As death fluorescence (DF) is generated as a result of death, examining its spatiotemporal spread may reveal the dynamics of death in *C. elegans*. We examined time-lapse films of worms dying of old age to further characterize the origins of DF. 63% of animals showed significantly higher fluorescence in the anterior intestine for the start or entire duration of the burst, with a secondary focal point occurring near the vulva. Fluorescence levels increased with time, and in 69% of animals, the anterior and central intestine showed the greatest increase over the time observed. Mean data show an anterior-posterior wave of fluorescence spreading down the length of the intestine (Figure 3.19). This fluorescent wave occurred irrespective of the time scale of the burst, which varied between 2-6 hours. Our observations suggest that the origin of DF occurs in the anterior intestine. To probe this, we attempted to generate a posterior to anterior wave by placing a hot wire adjacent to either the tail or the head of young adults. In those with a hot pick applied to the head, the fluorescence rose in the anterior intestine and spread as expected (Figure 3.20). Those with a hot pick

applied to the tail showed an initial rise in fluorescence intensity, but this was restricted to the posterior 25% of the intestine (Figure 3.20). This intensity neither spread nor faded within 15 minutes of observation. Furthermore, these animals remained alive when assayed 24 hours later.

These observations imply that the wave of fluorescence can only be initiated in the anterior intestine, and must travel from anterior to posterior. Given that DF consistently originates in the anterior intestine, this area may represent an organismal weak point in *C. elegans*, where a local crisis in homeostasis can lead to organismal death.

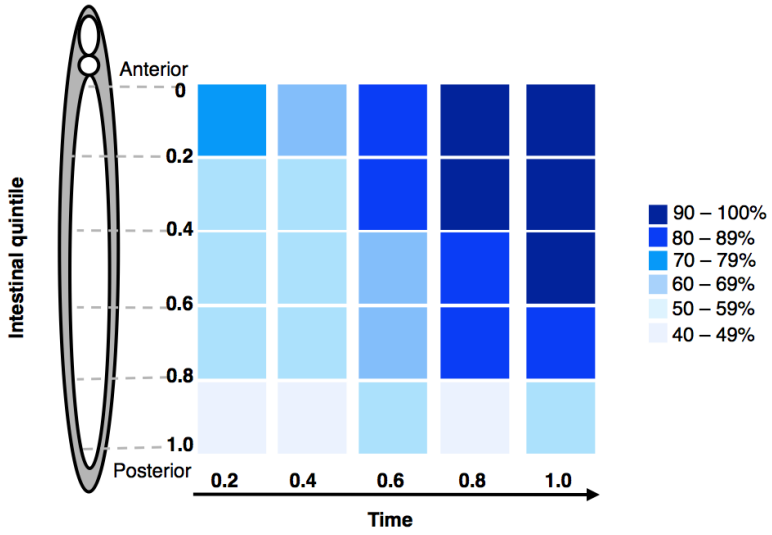

Figure 3.19: Fluorescence increases in an anterior to posterior wave. Figure shows mean fluorescence intensity (values normalized to highest value in each individual) at 5 points along the intestinal length of animals dying from age, n = 29. As time of DF spread varies between animals, the duration of each observation was divided into 5 equal points for measurement.

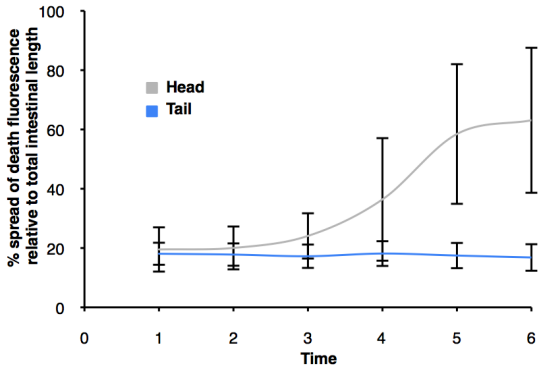

Figure 3.20: DF spreads only when anterior cells are killed. Applying a hot pick directly adjacent to anterior, but not posterior, intestinal cells leads to a spread of DF.

3.3 Discussion

3.3.1 Lipofuscin and the oxidative damage theory of ageing in *C. elegans*

C. elegans is widely used to study ageing. In recent years the idea that molecular damage is a cause of ageing in C. elegans has come into question (Gems and de la Guardia, 2012; Van Raamsdonk and Hekimi, 2010). As detailed above, blue intestinal fluorescence in *C. elegans* has been thought to be equivalent to mammalian lipofuscin. It has thus been taken as another piece of evidence in favour of the oxidative damage theory of ageing. However, this equation was based predominately on spectral similarities, and potentially misleading cohort studies (Gerstbrein et al., 2005; Klass, 1977). In these respects, the equation of intestinal fluorescence with lipofuscin somewhat resembles the correlative data showing increasing ROS levels with age; both theories have encountered difficulties when experimental manipulation tested their predictions.

We tested the prediction that manipulating levels of oxidative damage should alter the level of intestinal fluorescence in *C. elegans,* and found that it had no effect. We thereafter showed that blue fluorescence increases only with death, and not with age – and that a rise in fluorescence can be induced by killing young adult animals. It therefore seems very unlikely that this fluorescent material is lipofuscin; indeed, Chapter 5 discusses the biochemical identification of the fluorophore, and it is not lipofuscin.

This finding does not disprove the existence of lipofuscin in *C. elegans*, but its existence is an open question. We confirmed previous findings showing that both red and green fluorescence increase with age, but also show that both also increase with death. Without detailed molecular analysis it is impossible to ascertain if these species arise anew with death, or just increases their rate of formation. It is possible, therefore, that one of these species may be lipofuscin. However, as our work demonstrates, this hypothesis should be tested, biochemically if possible, before being equated with lipofuscin. Until then, our findings remove a significant piece of evidence for the role of molecular damage in *C. elegans* ageing.

3.3.2. The loss of a biomarker of ageing

As outlined in the introduction, biomarkers of ageing are important research tools for gerontologists. An accurate biomarker of ageing will respond to

experimental intervention, confirming that any alteration in lifespan is due to the manipulation of ageing and not due to altered risk of death. Lipofuscin has been shown to be a valid biomarker of ageing, as it increases in senescent post-mitotic mammalian cells It has now been shown that *C. elegans* blue fluorescence is unlikely to be lipofuscin. Moreover, our data shows that blue fluorescence cannot be used as a biomarker of ageing *in situ*, as it increases at death and not with age (although see below with reference to mounted animals).

Blue fluorescence was largely thought to be a valid biomarker of ageing based on cohort studies. As demonstrated above, these can give false conclusions if population heterogeneity is not taken into account, and, the false impression that fluorescence gradually increases with age. Longitudinal study of individual worms reveals the death-related increase. By contrast, red fluorescence does rise with age (Pincus et al., 2011a). Red fluorescence however does also increase with death, albeit to a smaller extent than blue fluorescence. Therefore red fluorescence could be used as a biomarker of ageing, but only using individually cultivated worms.

However, population heterogeneity cannot explain other results showing that blue fluorescence increases with age. Studies observing age-matched cohorts of slide-mounted worms (Garigan et al., 2002) or biochemical isolates of blue fluorescence increasing in an age-dependent manner (Davis et al., 1982; Houthoofd et al., 2002; Klass, 1977). Findings presented here show that worms mounted on microscope pads show age-dependent increases in blue fluorescence. An experiment is currently being run (September 2012) by Abraham Mandel to further test this finding. An animal's fluorescence is measured *in situ* on NGM plates and subsequently re-measured after mounting onto a microscope slide. This experiment will hopefully confirm whether slide mounting does lead to increased generation of DF. As animals age they become frailer. We suggest that as a result, older animals are more vulnerable to the mechanical stress caused by mounting, and so generate increased fluorescence.

Another observation that requires explanation is that extracts from older worm cohorts show higher levels of fluorescence than those from younger animals (Davis et al., 1982; Houthoofd et al., 2002; Klass, 1977). One might expect that killing young and old worm cohorts would result in similar levels of death fluorescence. One possibility is that this reflects the importance of the development of death fluorescence. Data presented in Chapter 4 demonstrates that the formation of DF is an active, enzymatic process probably requiring ATP. Potentially this is because older

cohorts of animals have a greater proportion of dying individuals. All *in vitro* measurements of blue fluorescence used samples of worms which had been snap frozen using liquid nitrogen (Davis et al., 1982; Houthoofd et al., 2002; Klass, 1977). We suggest that snap freezing prevented the further development of DF; hence the higher levels of DF in extracts of old worms. One way of testing this theory would be to snap freeze two samples from the same age matched cohort of animals. One could then be thawed at an ambient temperature and incubated. Both samples should then be homogenized and blue fluorescence levels measured. Here, thawing and incubation should allow development of death fluorescence and greater levels of blue fluorescence in the extracts.

3.2.3 The gain of a biomarker of death

C. elegans is widely used to study ageing. Most ageing studies are conducted by seeing if genetic or environmental manipulation alters the animals' lifespan. Measuring lifespan in *C. elegans* is time consuming. Animals are assessed by their mobility: in early life, they move spontaneously, but as they age manual stimulation is needed to trigger movement. There has been some attempt to automate this process through the use of *C. elegans* microfluidic devices which rely on the uptake of the vital dye, Sytox green (Gill et al., 2003; Rohde et al., 2007). Both methods can be problematic. Manual stimulation is tedious, time consuming and subject to bias. Automation relies on dye uptake, which may be unreliable and uneven, affecting reliability.

Death fluorescence could be used as an endogenous biomarker of death. Microfluidic devices used in conjunction with a UV emitting light source and camera could effectively monitor large populations of individual worms from birth to death. This automation could provide multiple benefits. Firstly, as the animals would be tracked individually, it would guard against false conclusions borne of aggregate cohort data. Secondly, having individual data may findings which would be obscured from cohort measurements. Most importantly, it could hugely free up one of the most valuable resources of any *C. elegans* researcher: time. A collaboration between a member of the Institute for Healthy Ageing, Eugene Schuster and David Holmes, London Centre for Nanotechnology, is currently underway to build a prototype model of this automated system, using death fluorescence as a biomarker of death, and will hopefully be complete by the end of 2012.

3.2.4. Trying to understand death fluorescence

The discovery of death fluorescence may have answered multiple questions about the nature of lipofuscin and fluorescence in *C. elegans*, but stimulated many more. The most pressing questions, addressed in the following two chapters, were: "what is death fluorescence?" and "how is it generated at death?". Thus the project became devoted to attempting to answer these questions. In so doing, my investigations became more a study of death than of ageing. I am grateful to my supervisor, David Gems, for allowing me to pursue these fascinating tangents.

4. DEATH FLUORESCENCE IS PRODUCED BY NECROTIC CELL DEATH

4.1 Introduction to necrosis

The idea of necrotic cell death as a programmed, or quasi-progammed, cascade is a recent one, and not yet universally accepted. Here I discuss the definition of necrotic cell death, outline how it has become to be understood as a conserved cascade, and explain the implications these findings have for the understanding of death of *C. elegans*.

4.1.1. Cell death classification

Cell death was first classified into two distinct types in 1972: controlled (apoptotic) or uncontrolled (necrotic) (Kerr et al., 1972). The name *apoptosis* was coined to describe cells that died in response to physiological stimuli. It was taken from the Greek word describing the way in which leaves fall from trees, emphasizing it as a non-catastrophic form of cell loss (Kerr et al., 1972). Apoptosis was described in contrast to necrosis: a more widely observed type of cell death which appeared "to be invariably caused by noxious stimuli, and is probably the result of an irreversible disturbance of cellular homoeostatic mechanisms" (Kerr et al., 1972).

This categorization was based on morphological differences between types of cell death. Scattered apoptotic cells were shown to condense into small spherical cytoplasmic fragments (apoptotic bodies), and were then degraded by phagocytosis. Necrotic cells did not condense, retained their original shape, and were not degraded. Thus, apoptosis appeared as a physiologically controlled means of cell death, and necrosis remained characterized solely by its absence of apoptotic-like features (Kerr et al., 1972).

As a consequence of these categorizations, much work was done on the mechanisms of apoptotic cell death. Necrotic cell death was more commonly regarded as "an accidental uncontrolled form of cell death" (Kroemer et al., 2009). However, evidence is now accumulating that suggests necrosis may be biochemically regulated in a manner similar to apoptosis.

In 2009, The Nomenclature Committee on Cell Death (NCCD) published its second set of recommendations for cell death nomenclature (Kroemer et al., 2009). Apoptosis has multiple characteristic morphological and biochemical features which can be used for identification, such as chromatin condensation, reduction in cell

volume, nuclear fragmentation, phagocytic engulfment, and activation of the Bcl-2 and caspase protein families (Kroemer et al., 2009). Necrosis was defined as exhibiting cytoplasmic and organelle swelling, plasma membrane rupture, and a localized inflammatory response (Kroemer et al., 2009). However, the committee noted that this definition was predominantly a "negative" definition of apoptosis: necrosis was mainly defined by the absence of apoptotic hallmarks.

Aside from the lack of necrosis-specific biochemical and morphological hallmarks, cell death classification is made more complex due to multiple examples of cells showing partial or mixed characteristics (Kroemer et al., 2009; Zong and Thompson, 2006). For example, it was found that caspase inhibition during interdigital cell death in mice did not prevent the cells from dying. Instead, the dead cells exhibited necrosis-like features, but showed no phagocytosis or inflammatory response (Chautan et al., 1999). Compounding the difficulty in identification, certain physiological stimuli appear to induce either apoptosis or necrosis, depending on the severity of the insult (Zong and Thompson, 2006). For example, human promonocytic cells (cell arising from monocytes) were treated with either 0.2mM or 2mM concentrations of hydrogen peroxide. Both concentrations proved cytotoxic, but those treated with the lower dose entered apoptosis whereas those treated with the higher dose entered necrosis (Troyano et al., 2003).

Nonetheless, there is now a growing body of literature suggesting that necrosis may also be a type of programmed cell death (Golstein and Kroemer, 2007; Luke and Silverman, 2011; McCall, 2010; Zong and Thompson, 2006). The mechanisms by which necrosis operates are not fully understood. However, examples in the literature frequently describe similar hallmarks, despite often originating from different tissues and organisms. Consequently, it is possible to sketch a general picture of necrosis. From this, it is clear is that similar mechanisms of cell death can be repeatedly seen in multiple dissimilar examples, strongly supporting the idea of necrosis as a programmed mechanism of cell death.

4.1.2. Calcium is required for necrosis

Calcium (Ca^{2+}) has long been associated with cytotoxicity, dating back to observations of calcium deposits in necrotic tissue in 1965 (Sattler and Tymianski, 2000). The mechanisms by which raised intracellular calcium levels lead to cell death are not fully understood, but it is increasingly recognized to be a major component of

necrotic cell death (Mattson, 2007; Mattson and Magnus, 2006; Yamashima et al., 1996; Zong and Thompson, 2006). Multiple insults can trigger raised intracellular calcium levels. In mammalian neuronal models, the most commonly studied model system, calcium induced cytotoxicity has been documented in response to excessive glutamate stimulation (excitoxicity) (Fryer et al., 1999), ischemia (Xiong et al., 2004) and anoxia (Aarts et al., 2003).

Intracellular Ca^{2+} homeostasis is required for normal cell function. Under normal conditions, extracellular Ca^{2+} concentration is ~1.2mM, and intracellular Ca^{2+} concentration is ~0.1μM (Zong and Thompson, 2006). Increasing intracellular calcium levels can lead to necrotic cell death.

Most intracellular Ca^{2+} is stored within the endoplasmic reticulum (ER). Thus Ca^{2+} can enter the cell both from the extracellular matrix and from the ER stores. Extracellular Ca^{2+} can cross into a cell via multiple receptors. In neurons, neurotransmitter receptors that act by binding excitatory amino acids such as α-amino-3-hydroxy-5-methylisoxazole-4-propionate (AMPA) and N-methyl-D-aspartate (NMDA) to their receptor channels, or by indirectly activating voltage-dependent Ca^{2+} channels (VDCCs) cause a rise in intracellular [Ca^{2+}] from extracellular sources (Mattson, 2007). When increase in intracellular calcium mediated by these excitatory neurotransmitters leads to neuronal death it is known as excitotoxic cell death.

In non-neuronal cells, there three types of receptors control extracellular Ca^{2+}influx:

- VDCCs, as above, control Ca^{2+} flow via proton gradient potentials across the plasma membrane.
- Entry channels, which are activated by ER Ca^{2+} release
- Acid sensing ion channels (ASICs) which are epithelial sodium channels (Zong and Thompson, 2006).

In all cells, calcium elimination is maintained by a Na^{+}/ Ca^{2+} exchanger and a plasma membrane Ca^{2+} pump (Ca^{2+}-ATPase) (Zong and Thompson, 2006).

Multiple receptor channels control the ER Ca^{2+} stores. The sarco(endo)plasmic reticulum Ca^{2+}-ATPase (SERCA) controls Ca^{2+} uptake from the cytosol. ER Ca^{2+} release is controlled by the inositol triphosphate (IP3), phosphatidyl-inositol bisphosphate (PIP2) and ryanodine receptor channels. In neurons, glutamate receptors coupled to the GTP-binding proteing Gq11 stimulates IP3 channel opening,

and so glutamate binding further increases intracellular [Ca^{2+}] and raises the risk of excitotoxic death (Mattson, 2007). Furthermore, release of Ca^{2+} by the ER leads to an increase in active transport of extracellular Ca^{2+} into the cell (Zong and Thompson, 2006), creating a positive feedback loop.

That calcium influx leads to cytotoxicity and cell death has been well documented. For example, inhibition or genetic manipulation of gap junction protein subunits in mammalian neurons greatly reduces the extent of neurodegeneration in the brain after exposure to ischemia (Wang et al., 2010; Wang et al., 2012). Gap junctions allow direct cell-to-cell transmission of calcium; thus these data implies that calcium influx can lead directly to cell death. However, the mechanisms which underlie this cytotoxicity are less well understood. Experiments examining the basis of calcium-associated neurotoxicity have shown that, contrary to early theory, calcium influx in and of itself is not necessarily toxic (Tymianski et al., 1993). Instead toxicity appears to be a function mediated by the specific receptor(s) leading to the influx. For example, levels of calcium within the cytosol that lead to cytotoxicity when mediated by the NMDA receptor were not toxic when mediated by VDCCs (Tymianski et al., 1993). This implies that toxicity is instead a function of a post-synaptic specific receptor-associated process (Sattler and Tymianski, 2000), and so under a degree of cellular control, rather than simply being catastrophically toxic. The calpain-cathepsin hypothesis, which has been comprehensively tested in mammalian neurons by Yamashima and colleagues, provides an explanation of these toxicity mechanisms (Yamashima, 2004).

4.1.3. The calpain-cathepsin hypothesis

The calpain-cathepsin cascade (Figure 4.1) was first characterized in mammalian CA1 hippocampal neurons that died from exposure to ischemia (Yamashima et al., 1996). Ischemia-mediated neurodegeneration in CA1 hippocampal neurons had long puzzled researchers. CA1 hippocampal neurons were exceptionally sensitive to ischemia, but when exposed to ischemic shock, survived for 2 to 3 days before suddenly dying (Kirino and Sano, 1984). Glutamate had been shown to accumulate after transient ischemia, and so it was thought that glutamate-bound NMDA receptors induced the Ca^{2+} influx that led to cell death. However, it was subsequently shown that NMDA receptors were present in all hippocampal neurons (Moriyoshi et al., 1991): Ca^{2+} influx into the CA1 cells could not be the sole

mechanism of toxicity. Experimentation then demonstrated that ischemia triggers increased intracellular levels of Ca^{2+} via IP3 and PIP2-mediated Ca^{2+} release from the ER stores in CA1 neurons (Ishida et al., 1992). Thus, this release of Ca^{2+} was thought to act as a second messenger, triggering other interactions which eventually led to cell death (Henzi and MacDermott, 1992).

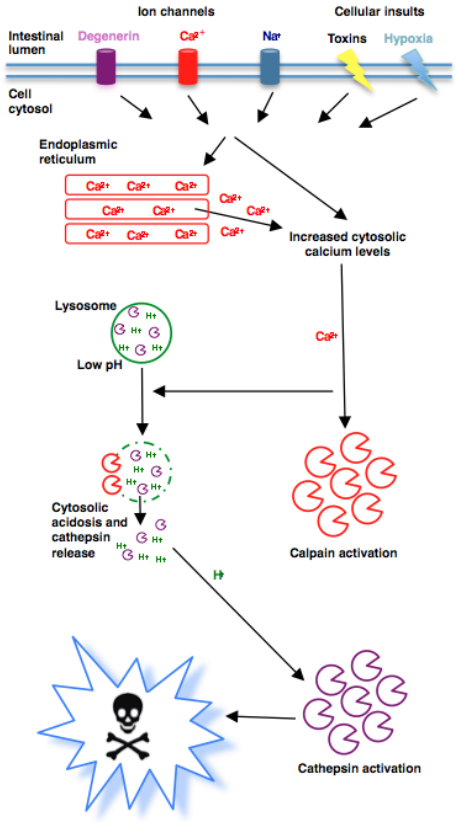

Figure 4.1: Schematic of the calpain-cathepsin hypothesis.

The first major interaction to be discovered was the activation of the calcium-dependent cysteine proteases, calpains. Calpains are a family of cytoplasmic proteases with both ubiquitous and tissue specific forms. They have multiple substrates, including cytoskeletal and membrane proteins, which they act on in a non-reversible manner (Saido et al., 1994). There are two ubiquitous forms, μ- and m-calpains, named after the molarity of Ca^{2+} required for their activation (Saido et al., 1994). The high levels of Ca^{2+} required for activation *in vitro* was surprising; even μ-calpains required more than 10^{-6} M Ca^{2+} for activation, significantly higher than cytosolic Ca^{2+} concentrations (~10^{-7} M). However, when cells are exposed to ischemia, IP3 and PIP2-mediated release of Ca^{2+} is thought to raise the cytosolic concentrations sufficiently high for activation of μ-calpains (Yamashima et al., 1996). Antibody

studies of the proteolyzed μ-calpain substrate fodrin revealed that the proteases were activated in response to ischemia (Saido et al., 1994).

Yamashima and co-workers then developed antibodies which responded to activate or inactive forms of μ-calpain (1996). The hippocampus of primates exposed to 20 minutes of ischemia were removed and Western blots were performed. In CA1 hippocampal neurons, μ-calpain was shown to be activated, whereas in all other hippocampal neurons it remain in its inactive state (the converse being true when the cells were probed with an antibody specific to calpains). Immunoelectron microscopy was used to confirm this result in CA1 cells exposed to hypoxia-hypoglycaemia *in vitro*. This technique also revealed that post-ischemia, activated μ-calpain localized specifically to lysosomal membranes, causing lysosomal membrane disruption (Yamashima et al., 1996). These findings recapitulated previously discovered but overlooked results showing lyosomal lysis in both gerbils and rat ischemic death, suggesting a conserved mechanism of action (Yamashima et al., 1996).

Disruption of the lysosomal membrane could lead to lysosomal lysis and the subsequent spilling of lysosomal contents into the cytosol. Lysosomes' main function is degradative (Repnik et al., 2012), and so they contain a multitude of destructive enzymes, including cathepsins proteases (Yamashima and Oikawa, 2009). Yamashima and colleagues noted that cathepsin B, a cysteine cathepsin, was found to be significantly increased in aged rat neurons. They assumed that common mechanisms may underlie both age-related neurodegeneration and injury induced neurodegeneration (Yamashima et al., 1996). Consequently they examined what role, if any, lysosomal lysis and cathepsin release may play in cell death.

Yamashima and co-workers discovered that cathepsin B activity levels increased steadily in primate hippocampi after exposure to ischemia (Yamashima et al., 1996). They also found that inhibition of cathepsin B with the specific inhibitor CA-074 was sufficient to inhibit CA1 neuronal death. Subsequent studies have shown that inhibition of multiple cathepsins is sufficient to ameliorate cell death in many different models, e.g. Bivik et al., 2007; Hwang et al., 2008; Johansson et al., 2003. Lysosomal cathepsins have very broad specificities, as would be expected from primarily degradative enzymes, and are low pH dependent (Repnik et al., 2012). Release of lysosomal contents would most likey lead to cellular acidosis, allowing lysosomal cathepsin activity within the cytosol, consequently causing widespread degradation (Repnik et al., 2012).

Thus, the calpain-cathepsin hypothesis outlines a deadly cascade. Calcium influx and release from the ER leads to the activation of calcium-dependent calpains. These calpains act preferentially upon the lysosomal membrane, causing to lysosomal membrane permeabilization, which in turn leads to cytosolic acidosis and the destructive release of lysosomal cathepsin proteases (Figure 4.1). This model was initially identified and tested in the CA1 subset of hippocampal neurons, but has been shown to be conserved in multiple other types of neurodegeneration – including in *C. elegans'* mechanosensory neurons.

4.1.4. Necrosis in *C. elegans*

Necrosis has been studied in *C. elegans* models of neurodegeneration. Multiple gain-of-function mutations in *C. elegans* neuronal ion channels have been found to replicate excitotoxic, necrosis-like neuronal death (Chalfie and Wolinsky, 1990; Driscoll and Chalfie, 1991). Of these, the best studied is mutant degenerin Na^+ channel MEC-4(d). MEC-4 encodes a subunit of the mechanosensory channel within *C. elegans* touch neurons (Hong and Driscoll 1994). The mutation *mec-4(u231* or *d)* leads to substitutions near the MEC-4 channel pore of amino acids with large side chains (Adams et al., 1998). These substitutions cause a change in the channel conformation, leading to it becoming constitutively open and causing excess ion influx which leads to cytotoxicity (Adams et al., 1998; Hong and Driscoll, 1994). *mec-4(d)* cell death does not require the cell's apoptotic machinery for execution, making it a distinct form of cell death (Chung et al., 2000). As *mec-4(d)* generated cell death is mediated by ion influx and leads to cell swelling it has been classified as necrotic cell death (Xu et al., 2001).

An initial screen for mechanisms of *mec-4(d)* induced toxicity employed *mec-4(d)* expressed ectopically in the ventral cord neurons under control of the *unc-8* promoter (Xu et al., 2001). This screen identified multiple genes whose mutation ameliorated *mec-4(d)* induced neuron death via control of ER Ca^{2+} storage and release. Mutations in *crt-1,* a calreticulin homolog, *unc-68*, a ryanodine receptor, and *itr-3*, an IP3 homolog, all protected neurons against necrotic death (Xu et al., 2001). These findings clearly have strong similarities with the Yamashima and colleagues' discoveries of ER calcium-mediated mammalian neuron toxicity as discussed above.

A subsequent study also looked for genes which inhibited *mec-4(d)* induced neurodegeneration (Syntichaki et al., 2002). Here, *C. elegans* mutations in multiple

different proteases were specifically examined based on the similarities to the necrosis cascade outlined above. Syntichaki and colleagues discovered mutations in genes encoding calcium regulated calpain homologs *clp-1* and *tra-3,* and the cathepsin homologs *asp-3* and *asp-4* (Syntichaki 2002). These findings recapitulated prior developments in the understanding of mammalian neurotoxicity.

The same group then published data showing that vacuolar H^+-ATPases (V-ATPases) were required for *mec-4(d)* neurodegeneration (Syntichaki et al., 2005). RNAi-mediated knockdown of *vha-2, vha-10* and *vha-12* gene expression all suppressed neurodegeneration, as did mutations in *spe-5, unc-32* and *vha-12*. All of the affected genes encoded components of the V-ATPase (Syntichaki et al., 2005). The V-ATPase is required for lysosomal acidosis. Consequently, this data demonstrates that acidified lysosomes are required for necrotic cell death in *C. elegans*. By examining double mutants with mutations in both ER calcium release as well as in the V-ATPase, they also showed that acidosis is required downstream of raised cytosolic calcium levels in order to lead to cell death. Thus, this data supports the calpain-cathepsin cascade hypothesis and demonstrates a high degree of conservation across species.

The majority of work studying necrosis has been in neuronal cell death, in both mammalian and *C. elegans* models. However, there is *C. elegans* data suggesting that necrosis is not solely a mechanism of neurodegeneration. In 2007, Luke and colleagues discovered a mutation in *spr-6* (**S**erine **PR**otease inhibitors), which encodes an extracellular serpin. Serpins are a family of proteins which act to regulate proteolytic enzymes (Luke et al., 2007). Worms carrying the *srp-6* mutation displayed the previously undiscovered phenotype Osl (**O**smotic **S**tress **L**ethal). When both adult and larval *srp-6* mutants were exposed to water, they died violently in under a minute (Figure 4.2) (Luke et al., 2007). Microscopic examination of the corpses revealed that their cells had lost plasma membrane integrity, and appeared expanded and rounded, as would be expected in necrotic cells. Consequently, the authors examined whether mutations in components of the necrotic cascade could protect against *srp-6* mediated Osl death. Double mutants contained *srp-6* and any mutation protecting against necrosis, e.g. calpain mutation *clp-5* protected against Osl (Luke et al., 2007). Interestingly, *srp-6*; *glo-1* double mutants were also protected against Osl, further confirming that gut granules are indeed lysosome like organelles, and demonstrating their contribution to necrosis.

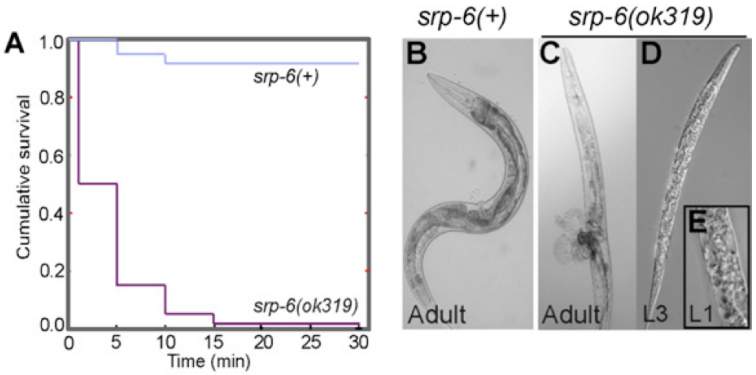

Figure 4.2: *srp-6* animals die when exposed to water. (A) shows survival of *srp-6(+)* and *srp-6(ok319)* animals after 30 minutes exposure to water; (B) shows representative images of the same. Image reproduced from Luke 2007.

These findings are of particular interest. Firstly they add to the body of proof that the necrotic calpain-cathepsin cascade exists and is conserved in *C. elegans*. Far more importantly, they imply that this cascade is not solely confined to the neurons and instead may contribute to organismal death. As described in the following results section, we confirm these conclusions and demonstrate that necrosis does indeed contribute to organismal death in *C. elegans*.

4.2 Results

4.2.1. Death fluorescence requires low pH or energy for generation

After the discovery of death fluorescence, we were interested in determining how it is generated at death. When young animals were being tested for DF generation, it was noted that worms killed with CH_3COOH (pH 3) showed much higher levels of DF than other methods of killing. Consequently, we tested to see if DF generation was pH dependent. A range of pH solutions (pH 3 to pH 11) were made using either CH_3COOH, NaOH or M9 salt solution (pH 7). The worms were placed in these solutions in a microtitre well, and left to acclimatize for ten minutes to ensure that the solution pH did not kill them. The animals were then killed by freeze-thaw (Please see section 2.1.6.), and the DF measured by plate reader. In initial trials, sodium azide was added to anaesthetize the animals. Once anaesthetized, animals sank to the bottom of the well, giving a clearer signal for the plate reader. Previous trials using non-anaesthetized animals had generated a ~500% increase in fluorescence at death (c.f. Figure 3.15). However, unexpectedly, anaesthetized

animals only generated comparable levels of DF when incubated in pH 3 or 4 (Figure 4.3), seemingly contradictory data.

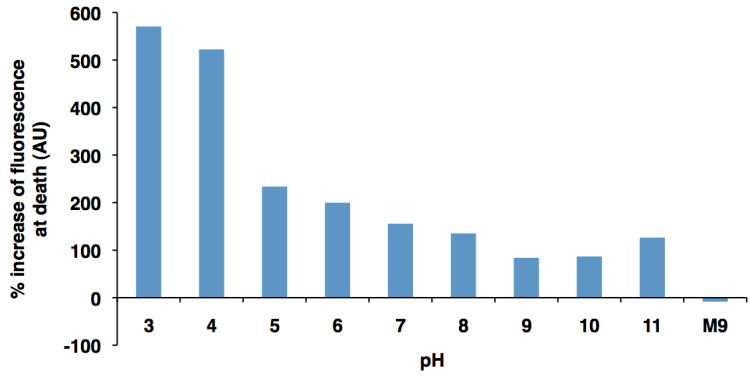

Figure 4.3: Death fluorescence of animals in a pH range killed by freeze-thaw, using sodium azide as an anaesthetic. Previously, when no sodium azide was used, animals showed ~500% increase in fluorescence at death (death fluorescence), see Figure 3.15. Here only animals killed at low-pH killed exhibit similar levels of death fluorescence.

Animals were then incubated for longer, thus sinking to the bottom of the well by gravity without the need for sodium azide anaesthetization. They were again killed by freeze-thaw. Using this protocol DF was seen at all pH values (Figure 4.4).

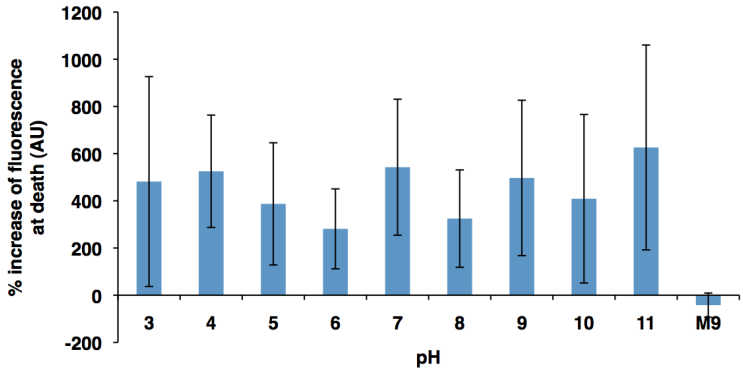

Figure 4.4: DF is generated at all pH values when animals are killed without sodium azide anaesthetization. Data is mean of three biological replicates, error bars are ± SD.

These findings show that sodium azide blocks DF generation , except at low pH. Sodium azide inhibits complex IV in the mitochondrial electron transport chain (Biswas et al., 1997). Thus, sodium azide inhibits respiration and ATP generation.

Taken together these results imply two things. Firstly, that the generation of DF is an energetically costly process, which could imply that its formation is enzymatic. However, even when respiration was inhibited, DF was still generated if animals were incubated in low pH solutions. This result suggests that the process

leading to DF formation involves acidosis, and that generation of acidosis requires energy.

An alternative possibility is that the DF fluorophore is brighter at low PH. To test this we asked whether altering the pH of a solution after DF generation affected its intensity**.** Aliquots of pH 3 or 11 were added to killed animals in M9 solution, and the change in fluorescence measured by plate reader. Both lowered fluorescence by similar amounts, presumably by diluting the solution, (Figure 4.5). Thus, acidity is required in order to generate DF.

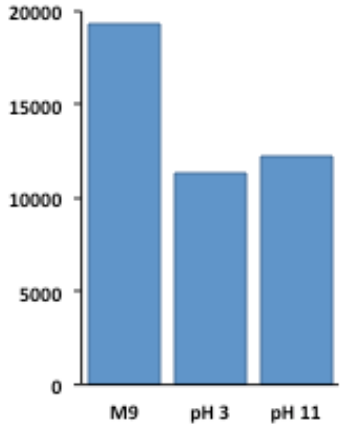

Figure 4.5: Addition of CH_3COOH (pH 3) or NaOH (pH 11) to an M9 solution containing DF-generating dead animals lowered fluorescence by similar amounts, indicating a dilution effect.

Thus our data implies that the development of DF is an energetically costly process which requires acidosis: i.e. an active process occurring during organismal death. The calpain-cathepsin hypothesis of necrosis, discussed above, is an enzymatic cascade which generates acidosis via lysosomal lysis and leads to cell death. We hypothesized that this conserved cascade, which has been shown to occur in *C. elegans*, may be involved in the generation of death fluorescence.

4.2.2. Death fluorescence is reduced in necrosis mutants

To investigate whether the necrosis cascade is required for the generation of death fluorescence, we used mutants to test whether inhibition of components of the necrosis pathway (Figure 4.1) suppresses DF. 60 young adult animals were picked into a microtitre well containing M9 salt solution, and were anaethetized with 0.2 % levamisole (which does not suppress DF development). Their living fluorescence was measured in a plate reader at ex/em $\lambda_{340}/\lambda_{400\text{-}450}$nm. The animals were then killed by

freeze thaw, and their death fluorescence measured at the same wavelengths. The living fluorescence was then subtracted from the death fluorescence to get the final value. Each experiment had an N2 control, and strains were tested one at a time to minimize any stress caused by prolonged M9 immersion.

We first tested the effect of inhibiting Ca^{2+} release from endoplasmic reticulum (ER) stores. Mutations in the ryanodine and inositol-1,4,5-triphosphate receptors, and the ER Ca^{2+} binding protein calreticulin all suppress *mec-4*(d)-induced necrotic cell death in *C. elegans*, and the necrosis-dependent hypo-osmotic stress lethal (Osl) phenotype induced by *srp-6* RNAi (Luke et al., 2007; Xu et al., 2001). Each mutation, *unc-68(e540)*, *itr-1(sa73)* and *crt-1(bz29)*, respectively, greatly and significantly reduced DF (Figure 4.6).

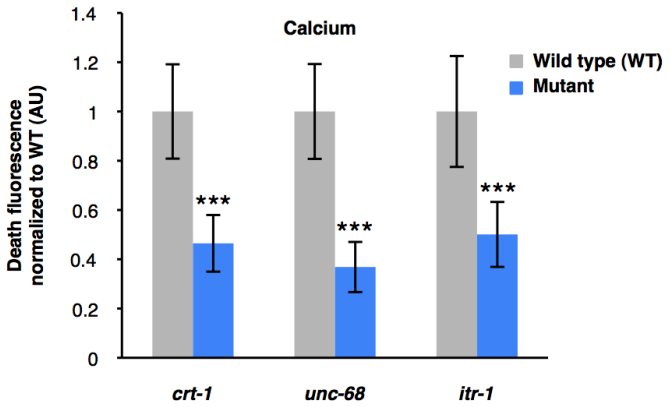

Figure 4.6: Inhibition of mechanisms of intracellular calcium influx reduces DF. Graphs show relative increase of fluorescence at death of 60 young adult animals of each strain, killed by freeze-thaw. Data of *crt-1* and *unc-68* are mean ± SD of three biological replicates, *itr-1* is mean of four replicates, ***$p < 0.001$, student's t-test.

During cellular necrosis, increased intracellular Ca^{2+} concentration can activate calpains (Ca^{2+} dependent cysteine proteases). The calpain TRA-3 is required for neuronal necrotic cell death in *C. elegans* (Syntichaki et al., 2002), and we found that the *tra-3(e1107)* mutation reduced DF levels (Figure 4.7).

The necrosis cascade (Figure 4.1) requires lysosomal lysis for cytosolic acidification and release of aspartyl proteases (cathepsins). In *C. elegans*, the vacuolar proton-translocating ATPase (V-ATPase), which mediates lysosomal acidification, is required for neuronal death in larvae (Syntichaki et al., 2005). We therefore tested two V-ATPase mutants, *vha-12(ok821)* and *unc-32(e189)*. Both mutations block *mec-*

4(d)–induced neurodegeneration (Syntichaki et al., 2005), and both also reduced DF (Figure 4.7).

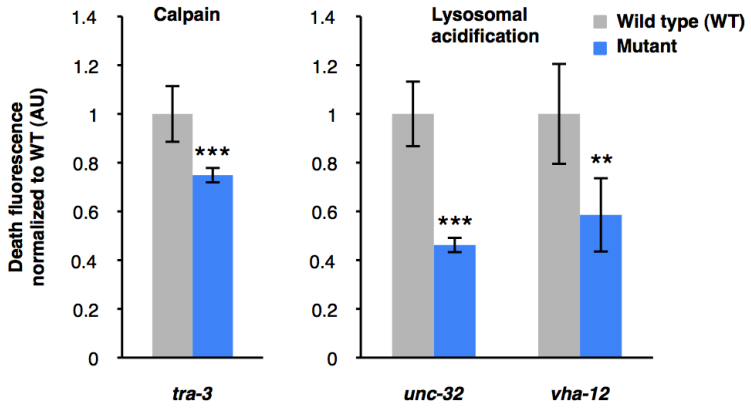

Figure 4.7: Inhibition of calpains and lysosomal acidification reduces DF. Graphs show relative increase of fluorescence at death of 60 young adult animals of each strain, killed by freeze-thaw. Data are mean ± SD of three biological replicates., ** $p < 0.01$, student's t-test.

Finally, we asked whether aspartyl proteases (cathepsins) promote DF. *cad-1(j1)* mutant animals have 10-20% of wild type cathepsin D activity (Jacobson et al., 1988), and *cad-1* is required for *mec-4(d)*–induced neurodegeneration (Syntichaki and Tavernarakis, 2002). *asp-4* encodes an aspartyl protease which is required for neuronal necrotic cell death (Syntichaki et al., 2005). Again, both *cad-1(j1)* and *asp-4(ok2693)* greatly reduced DF (Figure 4.8).

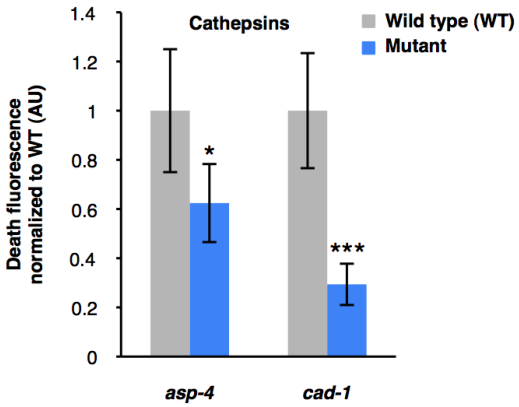

Figure 4.8: Inhibition of cathepsins reduces DF. Graphs show relative increase of fluorescence at death of 60 young adult animals of each strain, killed by freeze-thaw. Data are mean ± SD of three biological replicates, * $p < 0.05$, student's t-test.

These findings strongly suggest that the necrotic cascade promotes the formation of DF at death. We were interested to see whether DF could be generated

by necrosis alone, or if other mechanisms of cell death, such as apoptosis, also promoted its formation. *ced-3*, *ced-4* and *ced-9* are required for apoptosis in *C. elegans* (Ellis et al., 1991). To test whether apoptotic cell death machinery contributes to DF, we examined dying *ced-3(n717)*, *ced-4(n1162)* and *ced-9(n1950)* mutants. *ced-9* mutants showed no decrease in DF, *ced-4* mutants only a slight decrease and *ced-3* actually showed an increase in DF (Figure S4A) (Figure 4.9).

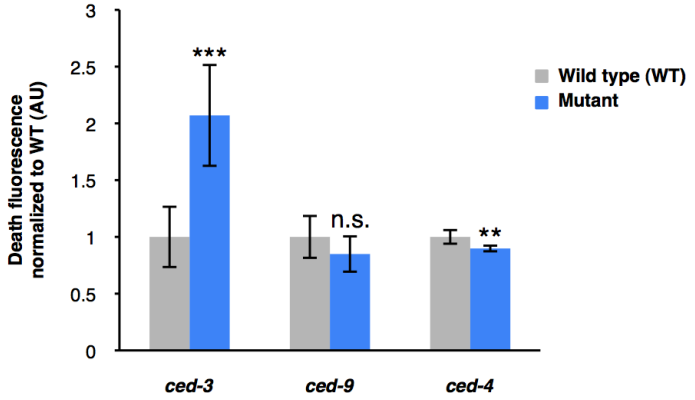

Figure 4.9: Inhibition of apoptosis does not generally reduce DF. Graphs show relative increase of fluorescence at death of 60 young adult animals of each strain, killed by freeze-thaw. Data are mean ± SD of three biological replicates.

In order to confirm that lowered DF is indeed a function of impaired necrosis and does not simply result from mutation, we tested a random selection of other mutants. Mutations in the genes *ftn-1*, *mdl-1* and *rol-6* (ferritin, the MAD-like transcription factor and a cuticular collagen, respectively) were tested, but showed wild-type levels of DF (Figure 4.10).

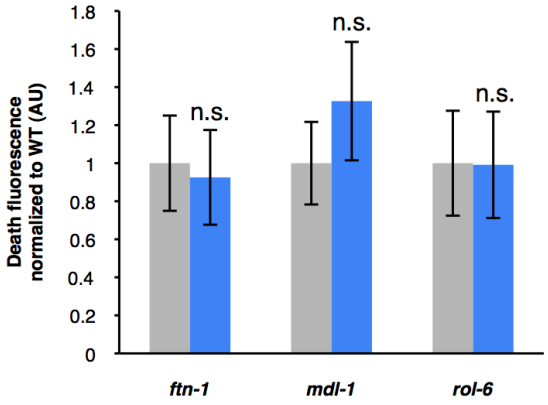

Figure 4.10: Diverse non-necrosis associated mutations do not reduce DF (negative control). Graphs show relative increase of fluorescence at death of 60 young adult animals of each strain, killed by freeze-thaw. Data are mean ± SD of three biological replicates.

4.2.3. Death fluorescence propagation requires calcium signalling

As discussed above, necrosis is heavily dependent on calcium for initiation and for propagation (Wang et al., 2010; Yamashima and Oikawa, 2009). Given that death fluorescence results from necrosis, we were curious to see if the characteristic spread of death fluorescence is calcium-dependent.

4.2.3.1. *inx-16* mutants have aberrant DF patterns

Gap junctions are channels that form between cells, allowing direct cell-to-cell contact and so diffusion of ions and molecules between cells (Bennett and Zukin, 2004). The conserved protein family which make up gap junction components are known as "pannexins", and the invertebrate proteins are known as "innexins" (Peters et al., 2007). In *C. elegans*, gap junctions exist between intestinal cells. *inx-16* encodes an intestinal innexin subunit; Figure 4.11 shows its GFP tagged intestinal expression pattern.

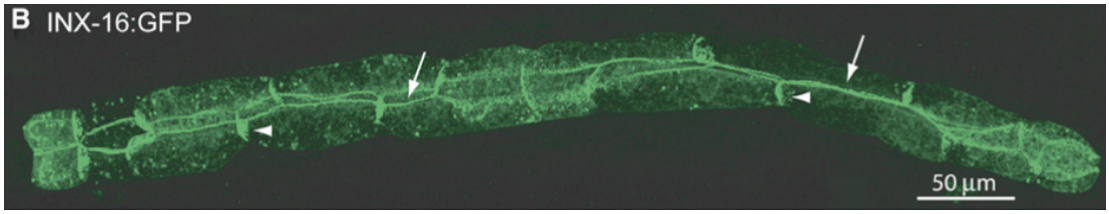

Figure 4.11: Expression of a functional translational fusion protein INX-16:GFP. Note the distribution of GFP at cell-to-cell contacts within the intestine. Image reproduced from Peters et al 2007.

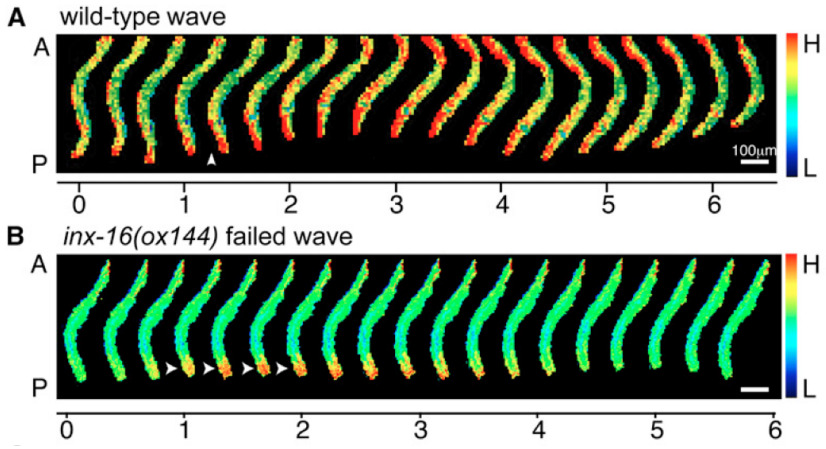

Figure 4.12: *inx-16(ok144)* disrupts the calcium propagated defection wave. (A) shows a wild-type calcium defection wave, and (B) a failed calcium defecation wave in an inx-16(ox144) mutant background. Images reproduced from Peters et al 2007.

In *C. elegans*, defecation is controlled by means of rhythmic Ca^{2+} propagation through the intestine (Figure 4.12 A). The mutation *inx-16(eg144)* was shown to disrupt this propagation, leading to a failed Ca^{2+} wave and constipation (Figure 4.12 B).

We were struck by the similarity of these waves of Ca^{2+} propagation to the systemic spread of death fluorescence. Neuronal death from ischemia had been shown to be inhibited when gap junctions are genetically or chemically inhibited (Wang et al., 2010; Wang et al., 2012). Consequently, if DF spread via Ca^{2+} propagation, we hypothesized that we might observe a curtailed DF wave in *inx-16* mutants.

We measured *inx-16* mutants' DF in the plate reader and found that the mutation dramatically reduced DF levels; mutants showed only ~10% of the DF in N2 animals (Figure 4.13a). We then attempted to see if the wave of DF failed to propagate in these animals (this data obtained by my student, Graham Fischer). The different strains were blinded to protect against bias and then killed on an agar plate using a hot pick. The subsequent wave of DF was then monitored by microscopy. We found that *inx-16* animals developed increased DF in their anterior intestine; however, it did not spread past that point nor did it increase in intensity (Figure 4.13b, Movies 3 and 4).

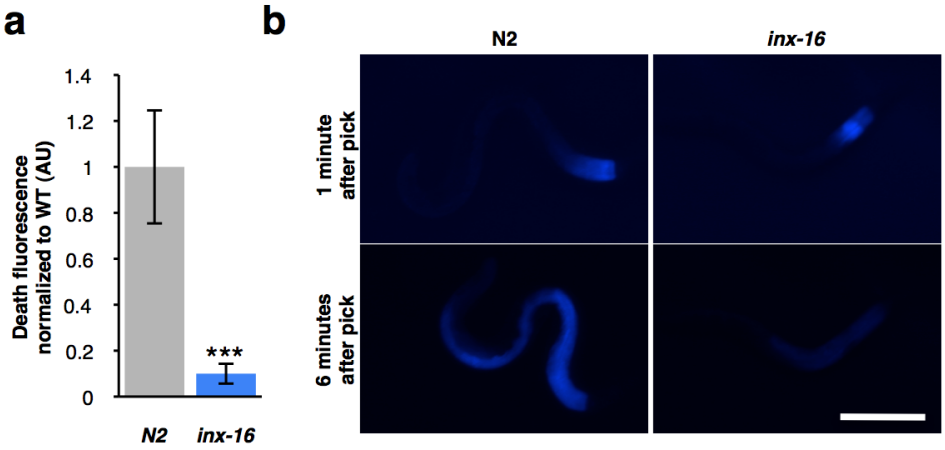

Figure 4.13: *inx-16(ox144)* mutants show decreased death fluorescence.
(a) *inx-16(ox144)* mutants show reduced death fluorescence compared to N2. Data are mean ± SD of three biological replicates, normalized to N2. (b) representative image of *inx-16* and N2 animals at one and six minutes after placing a hot pick near the anterior intestine. inx-16 mutants display reduced fluorescence which does not spread.

This finding was very exciting. Firstly, it confirmed that DF does indeed require Ca^{2+} propagation via gap junctions to spread. Secondly, it demonstrated that a mechanism, which had only previously been documented in ischemic neurons, facilitated the spread of necrosis through an organism. Given that DF occurs in all types of death studied, both age and injury induced, it suggests that a cascade of necrosis may contribute to organismal death in *C. elegans*.

4.2.3.2. *In vivo* calcium measurements

In order to verify that a wave of Ca^{2+} influx is required for the wave of DF seen as animals die, we collaborated with Keith Nehrke and Erik Allman from the University of Rochester. They had developed a microscopy set up which allowed intestinal calcium levels to be visualized *in vivo* and in real-time using individual, living, mobile animals (Miesenbock et al., 1998; Nehrke, 2003). All data referring to visualized calcium was obtained by Keith and Erik.

Transgenic worms expressing the Ca^{2+}-sensitive fluorescent reporter *d3cpv* within intestinal cells were killed by acute exposure to 0.5M tert-butylhydroperoxide (t-BOOH). This method of killing was employed to give the best time course resolution required for in vivo Ca^{2+} and pH imaging (see below). During death, changes in Ca^{2+} levels were determined through single excitation (λ_{435}), dual emission ($\lambda_{480}/\lambda_{535}$) fluorescence ratio imaging. As the animals died, there was a marked increase in intestinal Ca^{2+} levels (Figure 4.14). Comparison of Ca^{2+} fluorescence levels in the anterior and posterior ends of the intestine show that the rise in Ca^{2+} originates in the anterior intestine and only occurs in the posterior intestine after a time lag (Figure 4.14, Movie 5). This is consistent with an anterior to posterior wave of Ca^{2+} influx during death, as observed in DF propagation.

Next we asked if this rise in Ca^{2+} levels precedes or follows DF. Mosaic animals that express the construct within a subset of the intestinal cells allow for simultaneous visualization of DF and changing Ca^{2+} levels. Cells that express the Ca^{2+} indicator display a clear calcium signal that occurs due to fluorescence resonance energy transfer (FRET) between the donor and acceptor fluorophore. Adjacent cells lacking the indicator display an increase in the acceptor (λ_{530}) emissions, which does not correspond to a decrease in the donor (λ_{470}) emissions, and as such is not caused by FRET. Using wild-type animals as negative controls, they

confirmed that DF can be visualized at an ex/em of $\lambda_{435}/\lambda_{530}$, and concluded that fluorescence arising in adjacent, non-indicator containing cells must be DF.

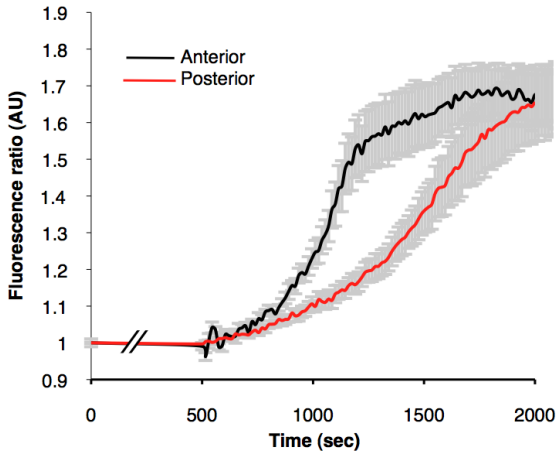

Figure 4.14: Measurements of in vivo Ca^{2+} levels using the Pnhx-2::d3cpv Ca^{2+} reporter show a rise in Ca^{2+} levels in C. elegans at death. $Ca^{2+}$was measured in anterior and posterior regions of interest (ROIs). An anterior to posterior wave of Ca^{2+}increase is demonstrated as the lag in calcium appearance in the anterior ROI (black) compared to the posterior ROI (red). Data is mean of 27 individual animals, error bars ± SD.

This fluorescence rise lagged behind the appearance of the Ca2+ peak, indicating that the wave of Ca2+ precedes that of death fluorescence (Figure 4.15).

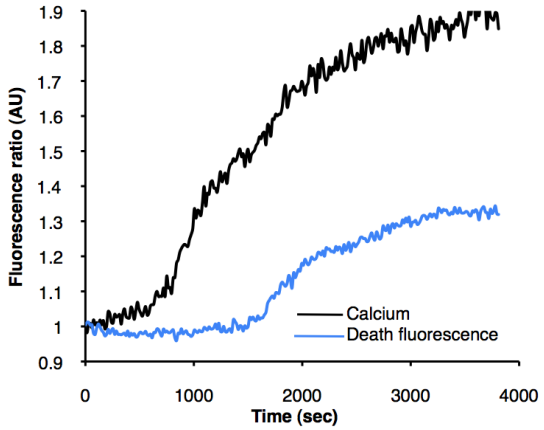

Figure 4.15: Animals expressing the Pnhx-2::d3cpv Ca^{2+} reporter mosaically demonstrate that a rise in Ca^{2+}levels precedes DF. Calcium trace taken from intestinal anterior; DF measured in adjacent, non-reporter expressing cells. Data shown is representative trace.

Finally Ca^{2+} was measured in the *inx-16(ox144)* mutants as they died (Figure 4.16). As was observed for DF, there was an increase in Ca^{2+} levels in the anterior intestine that was not propagated to the posterior intestine. Thus, Ca^{2+} signalling is

required for, and precedes, the spread of DF. This implies that during death an anterior to posterior wave of Ca^{2+} influx drives a wave of necrosis that leads to death fluorescence, confirming our previous results.

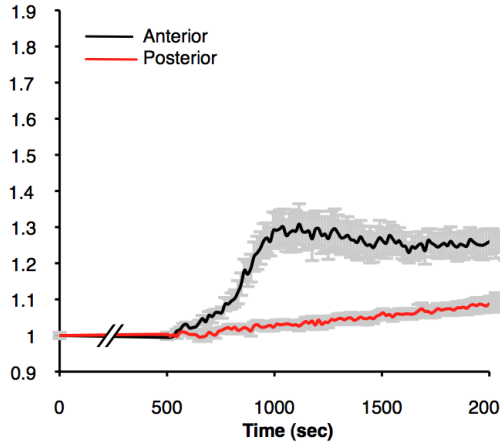

Figure 4.16: The spread of both Ca^{2+} and DF is curtailed in an *inx-16(ox144)* mutant background. The d3cpv Ca^{2+}reporter expressed in an *inx-16* background confirms that calcium begins to rise in an anterior intestine ROI at death, but does not spread to the posterior intestine ROI, a pattern previously observed with DF. Data is mean of 12 individual animals, error bars ± SD.

4.2.4. Death fluorescence occurs concurrently with low pH spread

The calpain-cathepsin model predicts that calpain-induced lysosomal lysis will lead to cytoplasmic acidosis and the release and activation of cathepsins. We therefore were interested to see if these features also accompanied DF.

4.2.4.1. Acridine orange staining

If death fluorescence is generated by necrotic cell death, then it should be accompanied by lysosomal lysis. To test this, we stained worms with the lysosomotropic dye acridine orange (AO), which stains *C. elegans* LROs (Jacobson et al., 1988). AO can pass freely through plasma membranes in its unprotonated form. In acidic environments, it becomes protonated and fluoresces orange when excited with UV light. Once protonated AO can no longer pass through membranes and so is confined inside the organelle. We reasoned that if LROs lyse during DF generation, we should see altered AO distribution (this data obtained by Grahame Fischer).

Wild-type worms stained with AO showed punctate orange fluorescence within intestinal cells, which co-localized with blue fluorescence (Figure 4.18), as previously observed (Clokey and Jacobson, 1986). Stained animals were then killed

with a hot platinum pick. This resulted in a loss of punctate AO staining, which coincided with DF (Figure 4.17, Movie 6). Once protonated, AO cannot leave a membrane-bound organelle, and so this result suggests that loss of lysosomal membrane integrity coincides with DF. The calpain-cathepsin cascade requires lysosomal lysis for the release of cathepsins and cytoplasmic acidosis: consequently, this result adds to the evidence that DF is generated by this necrotic cascade. However, insufficiently many animals were successfully stained to quantitatively measure this effect and so this data can only be treated as anecdotal. More data would be required in order to demonstrate the occurrence of lysosomal lysis at death.

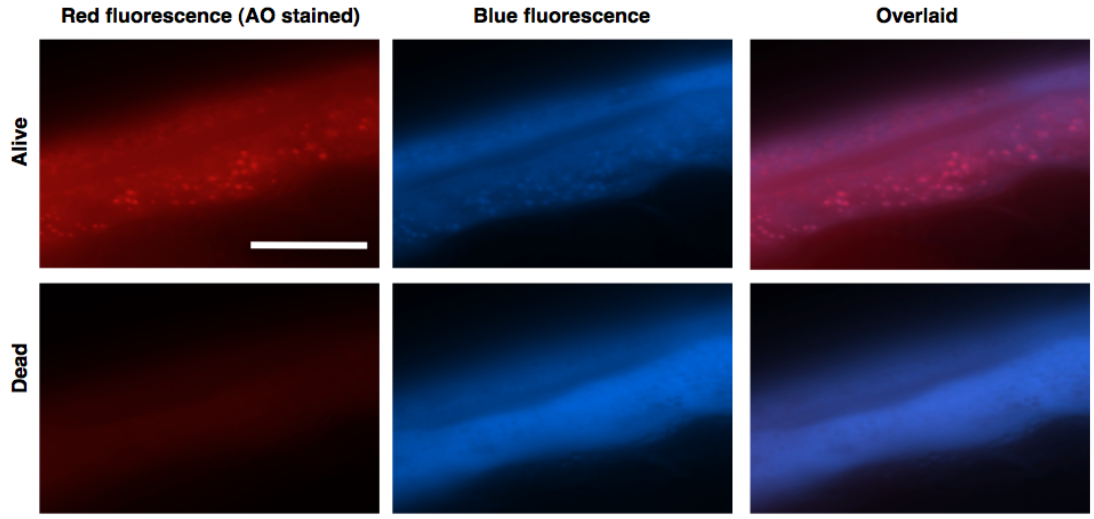

Figure 4.17: AO become diffuse at death. Initially, AO co-localizes with blue fluorescent LRO within the intestine in a living wild type young adult. However, AO staining becomes diffuse with death. As protonated (fluorescent) AO cannot cross membranes, this indicates that the lysosomal membranes become permeable as DF is generated.

4.2.4.2. *In vivo* pH measurements

According to our working model, cytosolic acidosis is part of the necrotic cascade leading to the generation of DF. We therefore asked whether a decrease in cytosolic pH (cytosolic acidosis) accompanies DF. For this, we used a pH-sensitive reporter, P*nhx-2*::pHluorin (Miesenbock et al., 1998; Nehrke, 2003) which indicates intracellular intestinal pH in vivo. This work was again carried out by Keith Nehrke and Erik Allman. In live animals, the intestinal cytosol was at approximately pH 7.4 (Figure 4.18). Upon killing, the pH dropped to 6.6 (Figure 4.18, Movie 7).

We also examined the organismal dynamics of this death-associated cytosolic acidosis. Comparison of region of interests (ROIs) in the anterior and posterior

intestine revealed a lag in the appearance of low pH in the posterior intestine (Figure 4.19). This supports the view that during death, intestinal cytosolic acidosis occurs in an anterior to posterior wave. This is the same propagation pattern observed in both calcium spread and DF. The findings that both lysosomal lysis and cytosolic acidosis occur in intestinal cells at death provide further evidence that death fluorescence is generated by the necrotic pathway.

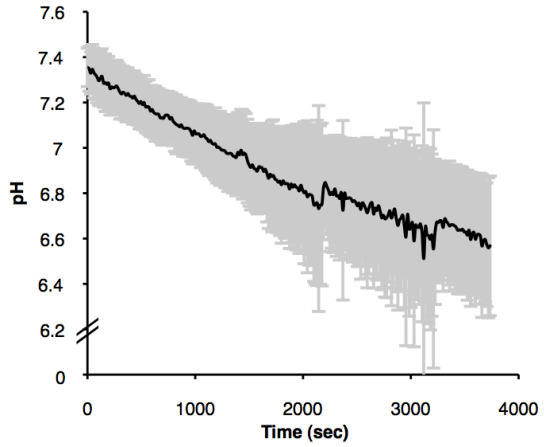

Figure 4.18: Acidosis occurs as animals die. Measurement of pH *in vivo* using an intestinal P*nhx-2*::pHluorin reporter during death shows a drop of pH from ~7.35 to ~6.6. pH was measured in an anterior intestine ROI and death was induced using t-BOOH exposure. Data mean of 18 individual animals, error bars ± SD.

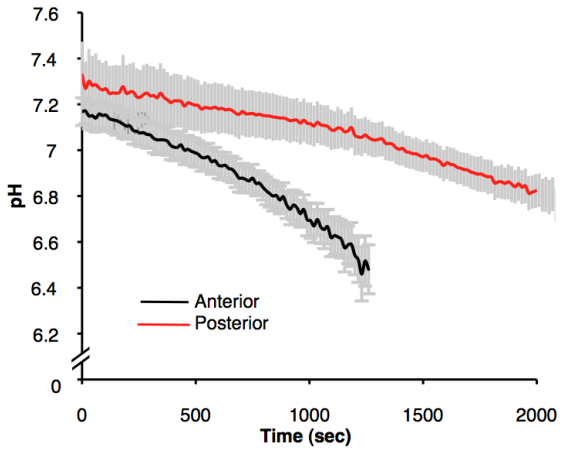

Figure 4.19: Death induced acidosis spreads in an anterior to posterior wave . Measurement of pH *in vivo* using an intestinal P*nhx-2*::pHluorin reporter during death shows that pH drops from anterior to posterior during death. pH was measured in an anterior and posterior intestinal ROIs and death was induced using t-BOOH exposure. Data mean of 18 individual animals, error bars ± SD.

4.2.5. Necrosis mutants are not long lived, but are stress resistant

Our data strongly implies that death fluorescence requires the activity of the necrotic cell death pathway for generation at death. Inhibiting components of this pathway via mutation leads to a decrease in the levels of death fluorescence generated. It also implies the occurrence of a cascade of necrotic cell death. An interesting possibility is that this cascade actually contributes to organismal death. To test this, we asked whether inhibiting necrosis postponed death, leading to increased longevity. In collaboration with the Tavernarakis lab in Crete University, we measured the lifespans of multiple strains carrying necrosis mutations. All strains were backcrossed a minimum of three times to guard against genetic background effects. However, we found that most necrosis mutants had either wild-type longevity, or were short lived (Figure 4.20).

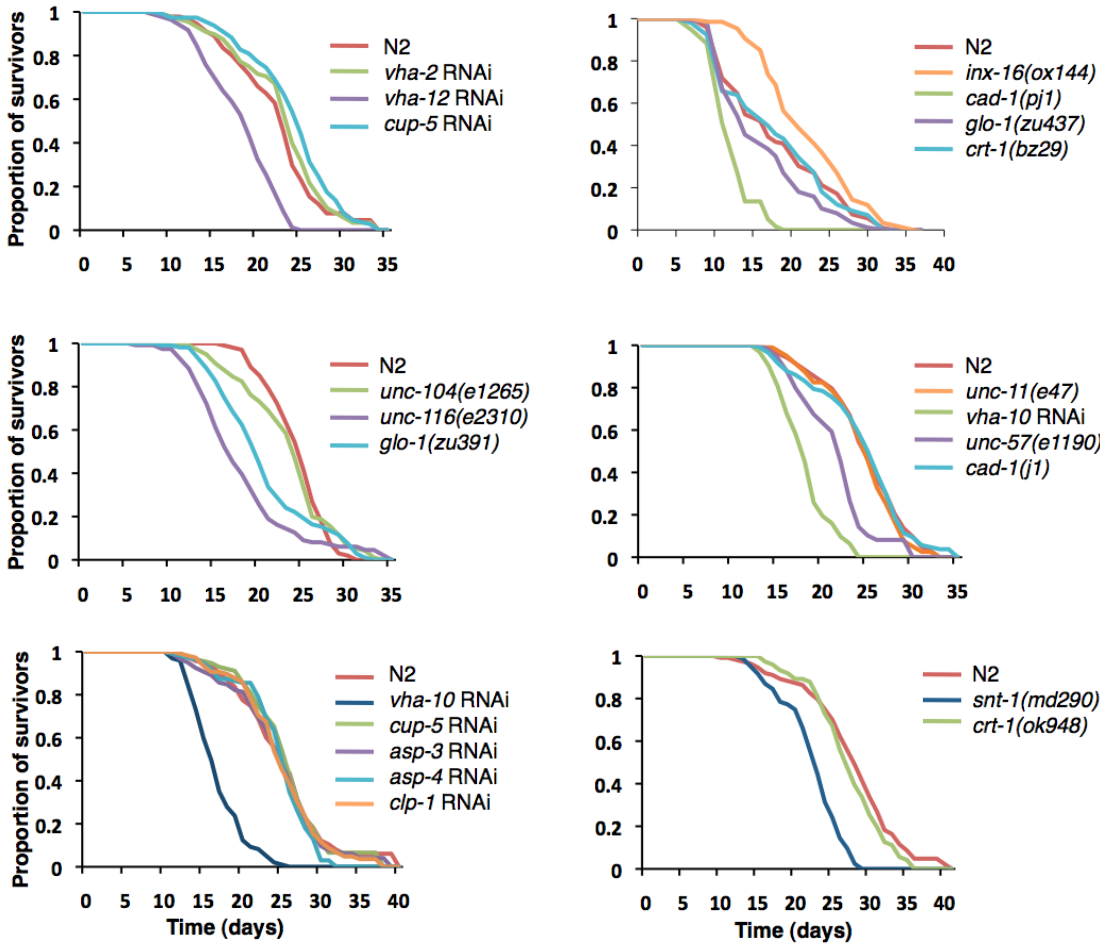

Figure 4.20: Necrosis mutants have normal or shortened lifespans. Lifespans carried out at 20°C, on OP50 NGM seeded plates for mutants and HT115 IPTG seeded plates for RNAi-mediated knockdown. Data is mean of two to three biological replicates, with a minimum of 100 worms per replicate per strain.

The sole exception is *inx-16(ox144)* which showed a 22% increase in mean lifespan. However, these mutants are very slow growing and have a starved appearance, suggesting that this strain may experience dietary restriction. Thus their increased longevity may be attributable to this, rather than reduced necrotic pathway activity.

This result was initially puzzling to us, as we had expected to observe that a decrease in necrotic pathway activity would confer some degree of protection against death. However, aging causes death by a number of processes acting in parallel, likely including systemic necrosis (given that it destroys a major organ within *C. elegans*). Here there are potential parallels in human aging: estimations of the likely upper limits of human longevity have calculated that removal of a major age-related disease (e.g. cardiovascular disease, cancer) would cause only small increases in lifespan (Olshansky et al., 1990). This is because multiple pathologies act in parallel to increase age-related mortality.

Next, we tested whether reduced necrotic pathway activity protected against stress induced death. Animals were killed using lethal thermal and osmotic stress, the latter assay being performed by Alexandre Benedetto. We found that necrosis mutants were significantly more resistant to death induced by theses stressors than wild type animals (Figure 4.21, Table 4.1). Furthermore, it was previously shown that necrosis mutants are resistant to death induced by bacterial pathogens than wild type (Wong et al., 2007). Taken together, these data provide clear evidence that necrosis does accelerate stress or injury induced organismal death in *C. elegans*.

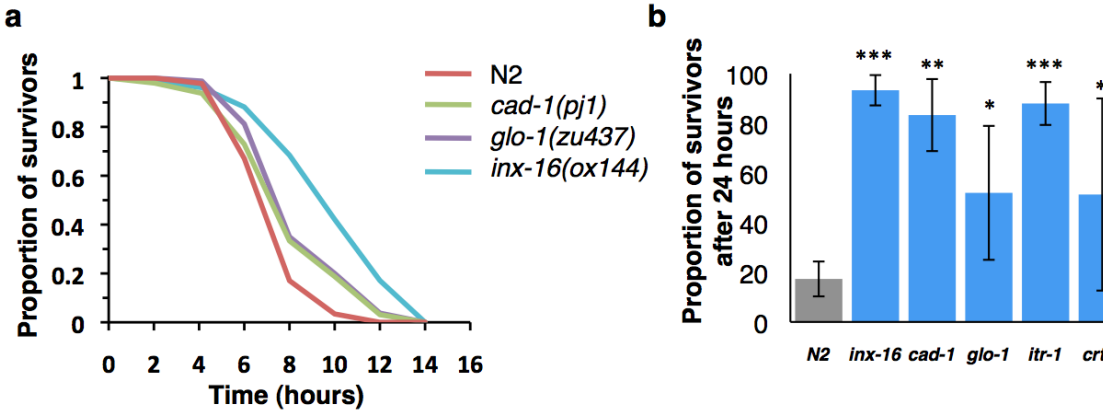

Figure 4.21: Necrosis mutants are significantly more stress resistant than WT.
Necrosis mutants are significantly more resistant to thermal (a) and osmotic (b) stress than N2. Data mean of three biological repeats, 40 animals per replicate; (b) error bars ± SD.

Strain	Mean survival time (hours)	% N2 mean survival time	*p* vs N2
N2 (control)	7.7	-	-
glo-1	8.7	113%	<0.0001
inx-16	10.2	132.4%	<0.0001
cad-1	8.4	109%	<0.001

Table 4.1: Necrosis mutants are significantly more thermotolerant than N2, log-rank.

4.3 Discussion

3.3.1. DF requires the necrotic cascade for generation

Necrosis is increasingly acknowledged as a form of programmed cell death (Yamashima, 2012). The mechanisms of necrotic cell death are yet to be fully elucidated, but extensive work in model systems supports a testable theory in the calpain-cathepsin hypothesis (Yamashima and Oikawa, 2009). Originally discovered in mammalian ischemia models, the calpain-cathepsin cascade was discovered to be conserved in *C. elegans* neurodegeneration (Driscoll and Chalfie, 1991; Syntichaki et al., 2005; Syntichaki et al., 2002; Xu et al., 2001). More recently, it has been shown that these elements are required for organismal death in the *srp-6*-dependent Osl phenotype (Luke et al., 2007). We have now shown that a functional necrotic cascade is also required for the generation of death fluorescence. When aspects of this cascade are inhibited, death fluorescence is significantly reduced.

Another hallmark of this cascade is lysosomal lysis, leading to cytosolic acidosis and the release of cathepsins. Using AO staining and *in vivo* pH measurement, we showed that lysosome lysis causes cytosolic acidosis concurrently with the appearance of DF. Finally, Ca^{2+} has been extensively documented to cause necrotic cell death in many different model systems. Using *in vivo* Ca^{2+} reporters and genetic manipulation of intestinal gap junctions, we demonstrated that DF requires Ca^{2+} propagation to spread in this its characteristic anterior-posterior wave (Figure 3.23). Taking all of these results into account, we can conclude that death fluorescence requires the necrotic calpain-cathepsin cascade for generation.

This result has several interesting implications. Firstly, it is the second example of necrosis being involved in whole organism death, as originally hinted at

by Luke and colleagues (2007). Secondly, DF allows us to visually examine the spatiotemporal dynamics of death in *C. elegans*. Finally, it adds to the growing body of evidence that necrosis can be considered as a programmed (or quasi programmed, see below) cascade of cell death.

3.3.2. Systemic necrosis contributes to organismal death in *C. elegans*

As discussed above, necrosis has predominantly been studied in neuronal models. Whilst being an excellent model system, this means of study has the disadvantage of specificity: neuronal mechanisms may not be conserved in other tissues or across species. Notably, the calpain-cathepsin model has been shown to hold across different species in neuronal cell death. Results presented here imply that the means of initiation and propagation of necrotic cell death is conserved in a manner which contributes to *organismal* death.

Wang and colleagues demonstrated that the extent of ischemia-induced neuronal cell death could be ameliorated via genetic and biochemical inhibition of gap junctions (Wang et al., 2010; Wang et al., 2012). We have shown that genetic knockout of intestinal gap junction subunit INX-16 also inhibits the spread of DF. *inx-16* animals were consistently most resistant to stress-induced death, strongly suggesting that inhibition of Ca^{2+} influx gives the best protection against necrosis, as would be predicted from multiple models of necrotic cell death.

These data also imply that systemic necrosis is a mechanism of organismal death in *C. elegans*. In humans, organismal death often occurs in a cascade of systemic failures resulting from an initial crisis, such as a stroke or heart failure. It was previously unknown whether equivalent death-inducing crises occur in *C. elegans*. The existence of DF makes it possible to visualize the spatio-temporal dynamics of death, thereby providing information about its initiation and propagation.

DF typically originates in the int1 quartet of anterior intestinal cells. From here the wave of DF is propagated backwards down the intestine. Similarly, the increase in calcium level and drop in pH show an anterior to posterior pattern of change during death. This pattern implies that the int1 cells play a pivotal role in initiating organismal death. The reason for the special vulnerability of the int1 cells remains unclear. One possibility is that these cells are more susceptible to increased Ca^{2+} levels or a signal that increases Ca^{2+} levels. This is supported by the observations

that the Ca^{2+}-mediated defecation cycle also appears to be initiated in the anterior intestine (Nehrke et al., 2008).

Consequently, we can present a tentative model for the mechanism of organismal death in *C. elegans*. Cellular homeostasis supports membrane integrity, and as cellular homeostasis declines with age, membrane integrity also begins to fail, especially in the int1 cells. In particular, loss of lysosomal membrane integrity (perhaps driven by increased Ca^{2+} leakage) leads to proton leakage, cytosolic acidosis and, eventually, cellular necrosis. This then initiates an intercellular cascade of necrotic cell death, propagated by Ca^{2+} signalling, leading to organismal death. In this view, lysosomal membrane integrity represents the breaking point in the cell, and int1 intestinal cells the breaking point in the organism.

3.3.3. The evolution of cellular and systemic necrosis

As discussed in section 1.3, evolutionary theories seek to explain ageing as a negative product arising from other beneficial mechanisms. One theory suggests ageing results from a quasi-programme of hyper-function (Blagosklonny, 2007, 2008). Another theory hypothesizes that ageing may arise as a result of antagonistic pleiotropy. Here genes which confer a youthful selective advantage will be selected for irrespective of any deleterious effects, such as ageing, experienced when older. It is possible that cellular necrosis may also have arisen as a non-adaptive product of antagonist pleiotropy, or a quasi-programme (Blagosklonny, 2007; Williams, 1957). By this view, elements of the necrosis pathway contribute to early life fitness, while cellular necrosis is an unselected, deleterious consequence of their action under lethal stress or as a result of aging.

The existence of the mechanism systemic necrosis, which brings about *organismal death* in *C. elegans* also raises the question of its evolutionary origin. Systemic necrosis could arise simply from uncontrolled cellular necrosis. Alternatively, given that death fluorescence is conserved in the related nematode species of *C. briggsae and P. pacificus*, it is possible that the existence of this systemic necrosis and generation of DF serves an evolutionary purpose. Systemic necrosis may also arise from pleiotropy or hyper-function, but it is possible that this organismal self destruct mechanism may also serve an evolutionary purpose. When food is limited, gravid hermaphrodites typically die with multiple embryos in their uterus, which hatch internally and consume their mother's corpse (matricidal

endotoky or “bagging”). Potentially, this improves the mother’s fitness by increasing survival of her genetically identical offspring, and it has been suggested that this frequently occurs in the wild (McCulloch and Gems, 2003). Thus, systemic necrosis may have evolved to enhance fitness by aiding efficient transfer of nutrients from mother to offspring during endotoky.

5. BIOCHEMICAL IDENTIFICATION OF DEATH FLUORESCENCE AS ANTHRANILIC ACID DERIVATIVES

5.1 Introduction to the kynurenine pathway

5.1.1. The biochemical composition of death fluorescence

As discussed in chapter 3, *C. elegans* intestinal LRO blue fluorescence increases with death, not with age. Moreover, we showed that, unlike mammalian lipofuscin, *C. elegans* blue fluorescence does not increase with increased oxidative damage. We thus concluded at the end of chapter 3 that *C. elegans* blue fluorescence was most probably not lipofuscin. Consequently, we were interested in trying to determine the biochemical composition of both gut granule and death fluorescence. Death fluorescence may well arise anew at death: however if both types of fluorescence are biochemically identical it would imply that death fluorescence is generated from gut granule fluorescence.

5.1.2. Flu mutants

One clue to the nature of death fluorescence came from a series of papers published in the 1970s – 1980s describing Flu mutants (Babu, 1974; Bhat and Babu, 1980; Siddiqui and Babu, 1980; Siddiqui and Von Ehrenstein, 1980). Flu mutants display altered colours of intestinal fluorescence (please see Table 5.1, details taken from Babu, 1974). The mutations have been provisionally mapped to different linkage groups but have not been cloned (Table 5.1). However enough work has been done on *flu-1* and *flu-2* to begin to unravel their functions. *flu-1* mutants demonstrate significantly reduced kynurenine-3-hydroxylase activity; most alleles have ~5% of wild type enzyme activity (Siddiqui and Babu, 1980). Kynurenine-3-hydroxylase catalyzes the conversion of kynurenine into 3-hydroxy kynurenine (Babu, 1974). FLU-2 also uses kynurenine as a substrate: *flu-2* mutants have less than 7% of the activity of wild type kynureninase (Bhat and Babu, 1980). Kynureninase catalyzes the conversion of kynurenine to anthranilic acid (Babu, 1974). Both genes have been identified through altered enzymatic activity rather than structural identification; the identification of both hinged on failure to metabolize their respective substrates *in situ* (Bhat and Babu, 1980; Siddiqui and Babu, 1980). However, the best BLAST homolog

matches for both genes lie on the same linkage groups that they have been provisionally mapped to.

Gene	Tentative gene identification	Putative gene product	Intestinal fluorescence colour	Provisional linkage group mapping
flu-1	R07B7.5	Kynurenine hydroxylase	Blue-purple	5
flu-2	C15H9.7	Kynureninease	Dull green	X
flu-3	?	?	Purple	2
flu-4	?	?	Bright blue	X
flu-1; flu-2	-	-	Green-blue	-

Table 5.1: Summary of known or proposed genotypes and phenotypes of Flu mutants.

The best BLAST match for mammalian kynurenine hydroxylase (R07B7.5) sits on chromosome 5, and the best BLAST match for mammalian kynureninase (C15H9.7) sits on the X chromosome (Altschul et al., 1990; Kanehisa, 2012). Taken with these probable homologs, and the fact that *flu-1; flu-2* double mutant contains much higher levels of kynurenine than either of the individual mutants (Babu, 1974), the identification of these genes as enzymes within the kynurenine pathway seems likely to be correct.

5.1.3. The kynurenine pathway

5.1.3.1. Tryptophan is catabolized by the kynurenine pathway

Tryptophan, the rarest essential amino acid, has two forms (Rongvaux et al., 2003). L-tryptophan is the most common and found in all proteins, whilst D-tryptophan is found in secreted peptides (Chung and Gadupudi, 2011). The structure of L-tryptophan is shown in Figure 5.1. There are three pathways that catabolize L-tryptophan (L-Trp): the 5-hydroxytryptamine (serotonin), indole and kynurenine pathways. L-Trp catabolism is required for the generation of multiple important compounds, including the ubiquitous enzyme co-factor nicotine adenine dinucleotide (NAD), the neurotransmitter serotonin and the vitamin niacin (Stone et al., 2012).

The mammalian kynurenine pathway, shown in Figure 5.2, catabolizes ~90% of L-Trp. In mammals, L-Trp catabolism by the kynurenine pathway is controlled by two rate limiting enzymes, tryptophan dioxygenase (TDO) and indoleamine-2,3 dioxygenase (IDO) (Chung and Gadupudi, 2011). Of these, IDO is ubiquitously expressed except for the liver, where only TDO is found. TDO is also found at low concentrations in the central nervous system (Chung and Gadupudi, 2011).

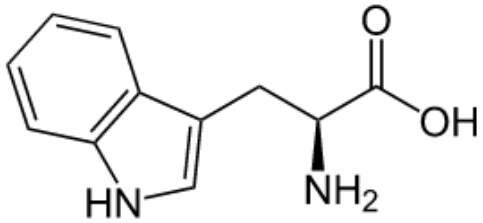

Figure 5.1: The structure of L-tryptophan.

Both IDO and TDO catalyze the same reactions, but TDO is highly substrate specific for L-Trp whereas IDO can also catalyze D-tryptophan (Chung and Gadupudi, 2011). Perhaps because of this, in mammals the primary site of L-Trp catabolism is the liver, catalyzed by TDO. TDO was discovered in 1951 to be induced by tryptophan ingestion: the first example of an inducible enzyme in mammals (Li et al., 2007; Rongvaux et al., 2003). By contrast, IDO synthesis responds not to L-Trp levels but instead to inflammatory stimuli, including bacterial and viral products (Rongvaux et al., 2003). Moreover, TDO activity decreases following IDO induction, suggesting a co-ordinated shift from L-Trp catabolism to non-hepatic tissues as an immune response (Rongvaux et al., 2003).

For many years after the discovery that the kynurenine pathway generated NAD, little attention was paid to the biological functions of kynurenine pathway intermediates ("kynurenines"). However recent investigations have shown that many kynurenines are both biologically active and significant, and seem to play important roles in both neurodegeneration and immunity.

5.1.3.2. Biological function of the kynurenine pathway

The first kynurenine discovered to have a major biological function was quinolinic acid (QA). QA was found to be a potent, direct stimulator of NMDA receptors (Stone and Perkins, 1981).

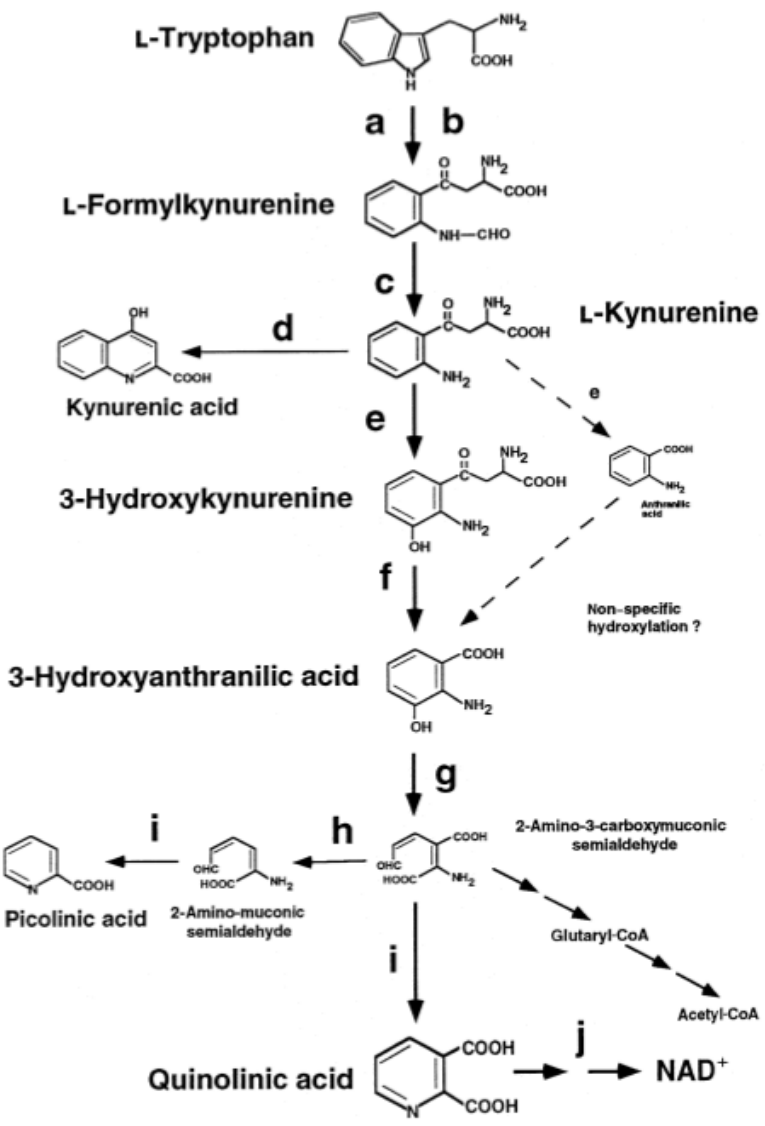

Figure 5.2: The kynurenine pathway. Conversion steps are labelled a-j, as follows:

(a) indoleamine2,3-dioxygenase, EC 1.13.11.17

(b) tryptophan2,3-dioxygenase, EC 1.13.11.11

(c) kynurenine formamidase, EC 3.5.1.9

(d) kynurenine aminotransferase (2- oxoglutarate aminotransferase), EC 2.6.1.7

(e) kynurenine 3-hydroxylase, EC 1.14.13.9

(f) kynureninase, EC 3.7.1.3

(g) 3-hydroxyanthranilate 3,4-dioxygenase (3-hydroxyanthranilic acid oxidase),EC 1.13.11.6

(h) picolinic carboxylase,EC4.1.1.45

(i) non-enzymic cyclization

(j) quinolinic acid phosphoribosyltransferase, EC 2.4.2.19.

Figure reproduced from Heyes et al., 1997.

Intra-cerebral injection of QA caused seizures in mice (Lapin, 1978), and subsequent research has shown that NMDA receptor activation is required for all neurobiological effects of QA (Schwarcz et al., 2012). Interestingly it was then discovered that kynurenic acid (KA) is a competitive *antagonist* of all excitatory amino acid receptors (Perkins and Stone, 1982; Schwarcz et al., 2012). Upon this discovery, Perkins and Stone suggested that the combination of endogenous agonist and antagonist arising from the same pathway implicated that pathway in control over neuronal control and modulation (1982).

Recent work is beginning to support this suggestion as multiple kynurenines are discovered to play roles in neurodegeneration. The best studied disease in which kynurenines has been shown to play an important role is Huntington's disease. Huntington's disease is a neurodegenerative disorder clinically characterized by personality alterations, movement disorders and eventual dementia (Zheng et al., 2012). It arises from a mutation in the huntington gene which causes increased numbers of CAG repeats, encoding a polyglutamine sequence at the N-terminus of the huntingtin protein. The severity of the disease increases in a dose dependent manner with the number of CAG repeats (Walker, 2007). In 1976 it was discovered that when rats' straitum were injected with the potent NMDA agonist kianic acid, the rats exhibited many of the same phenotypic traits as Huntington's patients (Coyle and Schwarcz, 1976). Huntington's disease was consequently established to be a disease of excitotoxic neuronal cell death (please see section 4.1.2. for discussion on excitotoxicity).

Further research has demonstrated that striatal injections of QA gives a Huntington's phenotype in many different species, characterized by specific cellular and neurochemical changes (Stone et al., 2012). These experimental data are reflected in endogenous changes found in post mortem brains of Huntington's patients: QA levels are substantially increased, and KA are reduced (Schwarcz et al., 2012). In the R6/2 mouse model of Huntington's, QA and its precursor 3-hydroxykynurenine (3-HK) was found at high levels (Guidetti et al., 2006). It was then shown that there was a substantial increase in the activity of the enzyme kynurenine 3-monooxygenase (KMO), which synthesizes 3-HK from kynurenine (Sathyasaikumar et al., 2010). These data confirm that the changes seen in Huntington's models arise from dysregulation of the kynurenine pathway.

Interesting data from *Drosophilia* further demonstrates this. *Drosophila* lack QA but otherwise have an intact kynurenine pathway. Campesan and colleagues showed that increasing the levels of KA relative to 3-HK levels through genetic and pharmacological manipulation ameliorated neurodegeneration in a fly model of Huntington's (Campesan et al., 2011). They also demonstrated that inhibition of TDO, the rate limiting enzyme in the kynurenine pathway, shifted the ratio towards production of KA, also leading to increased neuroprotection in the model. Strikingly, they found that these interventions did not have any effects in non-Huntington's controls, suggesting that the Huntington's model is especially vulnerable to kynurenine pathway dysregulation (Campesan et al., 2011).

Kynurenine dysregulation has also been implicated in neurodegeneration caused by acute neurological insults, such as stroke (Stone et al., 2012). As discussed in Chapter 4, neurones can die by excitotoxic cell death in response to ischemia and other insults. There is much data showing that high levels of glutamate are produced and released to induce excitotoxic death. However, the discovery that glutamate antagonists do not entirely ameliorate neurodegeneration in animal models and humans implies that other factors are also important. It has subsequently been shown that QA levels increase following ischemia, and that the levels of QA correlate with increased neurodegeneration (Saito et al., 1993a). Strikingly these changes in response to ischemia were shown to be associated with increased activity of kynurenine pathway enzymes within the brain, as well as with upregulated IDO activity (Saito et al., 1993b). Upregulation of IDO accompanied an immune response, with macrophages invading the ischemic tissue and the release of inflammatory cytokines. Thus, the kynurenine pathway appears to contribute to post-injury neurodegeneration through both active stimulation of excitotoxicity and through a damaging inflammatory response (Stone et al., 2012). Subsequent to this discovery, other examples of the kynurenine pathway have roles in immunity have come to light.

In 1998, it was demonstrated that IDO function was required to prevent maternal rejection of the allogenic foetal placenta in mice. When IDO function was inhibited, potent T cell stimulation and proliferation was observed (Munn et al., 1998). The mechanism by which kynurenine pathway activation and immunity interact is still unclear. One possibility is that activation of IDO deprives the local cellular environment of the rarest, and thus most important, amino acid L-Trp, thus inhibiting growth of invading viruses, bacteria and other pathogens (Grohmann et al.,

2003). However other work has demonstrated that kynurenines themselves have a role: for example, 3-HA and QA have been shown to induce apoptosis specifically in activated T-cells in mice (Fallarino et al., 2002; Piscianz et al., 2011).

Thus the kynurenines themselves have important roles within neurotoxicity and immunity: it is clear that the pathway does not exist simply to generate NAD. Recent work in model organisms has begun to examine the role of kynurenines in ageing. Age-related changes in kynurenine metabolism have been observed in rats (Braidy et al., 2011), and genetic and pharmacological inhibition of TDO has shown to extend longevity in *Drosophilia* (Oxenkrug, 2010; Oxenkrug et al., 2011). However, aside from the discovery of Flu mutants, very little work has been carried out in *C. elegans* on the kynurenine pathway. Based on Flu mutations and BLAST sequencing, the kynurenine pathway appears to be well-conserved between mammals and *C. elegans* (Babu, 1974). The NCBI has constructed a putative *C. elegans* kynurenine pathway based on sequence homology; however this has not been biologically verified (Kanehisa, 2012). Consequently very little is empirically known about the kynurenine pathway structure and function in *C. elegans* and so it presents an intriguing subject for investigation.

5.2 Results

5.2.1. *glo-1* animals do not show blue fluorescence or death fluorescence

As discussed in section 3.1.2., *C. elegans* Glo mutants do not contain lysosome related organelles (LROs) (Fig 3.2) (Hermann et al., 2005). The easiest way of determining the biochemical nature of gut granule and death fluorescence would be to compare the metabolites of a mutant lacking both with wild type. We therefore investigated both living and death fluorescence in age-related changes in *glo-1(zu437)* animals.

The *glo-1(zu437)* allele contains a Trp106 to stop mutation in the Rab GTPase required for lysosomal biogenesis, and results in 100% of embryos and adults possessing a Glo phenotype (Hermann et al., 2005). Intestinal fluorescence in individual *glo-1* animals was followed over age as previously described (see section 3.2.2). DF in *glo-1* cohorts were measured via plate reader as described in Section 2.1.6.

We found that *glo-1* animals did not accumulate any blue fluorescence over the course of their lives (Figure 5.3A). We also found that *glo-1* animals did not show death fluorescence, either when they died of age or when young animals were killed (Figure 5.3B). These data confirm that *glo-1(zu437)* animals do not show any intestinal fluorescence, either increasing with age or rising at death. This finding has three implications. Firstly, it adds to the body of evidence against equating *C. elegans* intestinal fluorescence with lipofuscin: given that lipofuscin accumulates by oxidative damage, it would be expected that some increases or change would be seen over life, even if the fluorescence was mislocalized. Secondly, the discovery that *glo-1(zu437)* mutants show neither living nor death fluorescence strongly implies that both types of fluorescence have a common origin. Finally, these data confirm that *glo-1(zu437)* animals can serve as a negative control for chemical identification of the blue fluorescence.

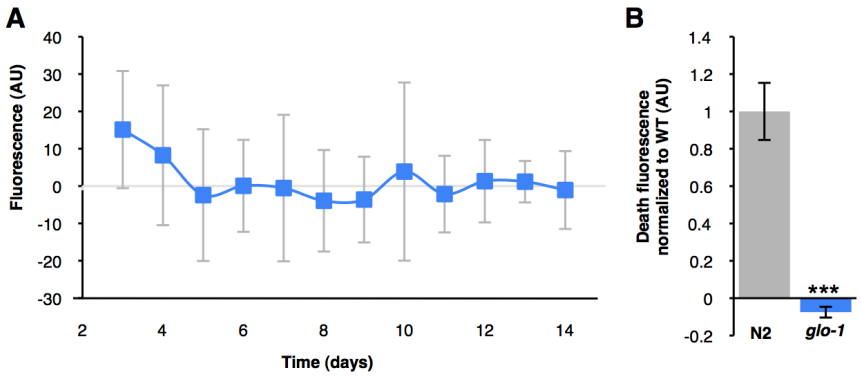

Figure 5.3: *glo-1(zu437)* animals do not show any increases in fluorescence. (A) Animals were monitored daily for fluorescence, as described in Section 2.2; here 29 animals were followed. (B) Animals were killed by heat, as described in Section 2.1.6, data is mean of 3 biological replicates. All error bars ± SD, Student's t test. Negative fluorescence arises from background subtraction.

5.2.2. Extraction of *C. elegans* blue fluorescence

The first step in trying to biochemically analyze the blue fluorescent substance was to isolate it in a sample. To this end, an aqueous extraction protocol was developed based on protocol details in Davis et al (1982). For full protocol see Section 2.4.1.2. Briefly, large number of animals were washed off plates using distilled water, lysed by sonication, and the resulting homogenate was centrifuged to obtain a pellet and a supernatant. The resulting pellet and supernatant were then analyzed. The sample supernatant was aspirated off, and the pellet was re-suspended

in distilled water. The re-suspended pellet and supernatant were measured for death fluorescence ($\lambda_{ex}/\lambda_{em}$ 340/430nm) in a plate reader, along with a water control. The supernatant was found to contain significantly more fluorescence (Figure 5.4A).

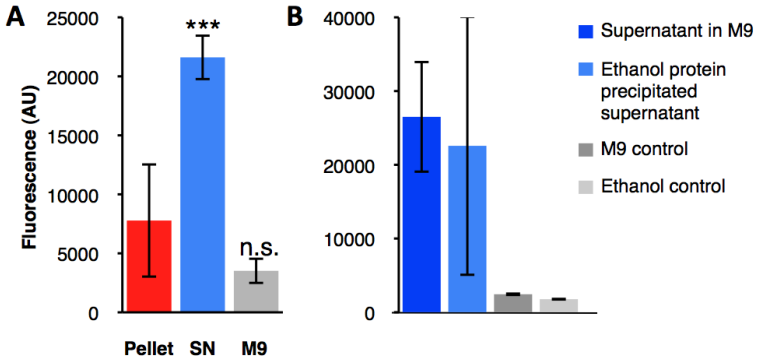

Figure 5.4: Blue fluorescence is unlikely to be proteinaceous. (A) Fluorescence can be isolated to the supernatant of a homogenate and remains even after removal of protein (B). Data is mean of three (A) or two (B) biological replicates, error bars ± SD.

Once the fluorescence had been isolated to the sample supernatant, cold ethanol was added in a 1:9 ratio to precipitate out protein from the sample. The sample was incubated overnight, centrifuged down again and the supernatant re-measured for fluorescence (Figure 5.4B). Given that the fluorescence isolated initially to the supernatant and remained after protein had been precipitated out of the sample, this data implied that the fluorescent substance was non-proteinaceous.

5.2.3. DF can be isolated via HPLC and is not protein

In order to try and biochemically identify the nature of blue fluorescence, we used high performance liquid chromatography (HPLC). HPLC is used to isolate substances from a homogenous compound; please see section 2.4.1. for more details. Using the protein-purified supernatant described above (5.2.2), we attempted to devise an HPLC protocol to extract and separate blue fluorescence peaks. After some trial and error, a protocol was devised which gave clearly separated compound peaks with blue fluorescence spectral characteristics ($\lambda_{ex}/\lambda_{em}$ 340/430nm) (see Section 2.4.1).

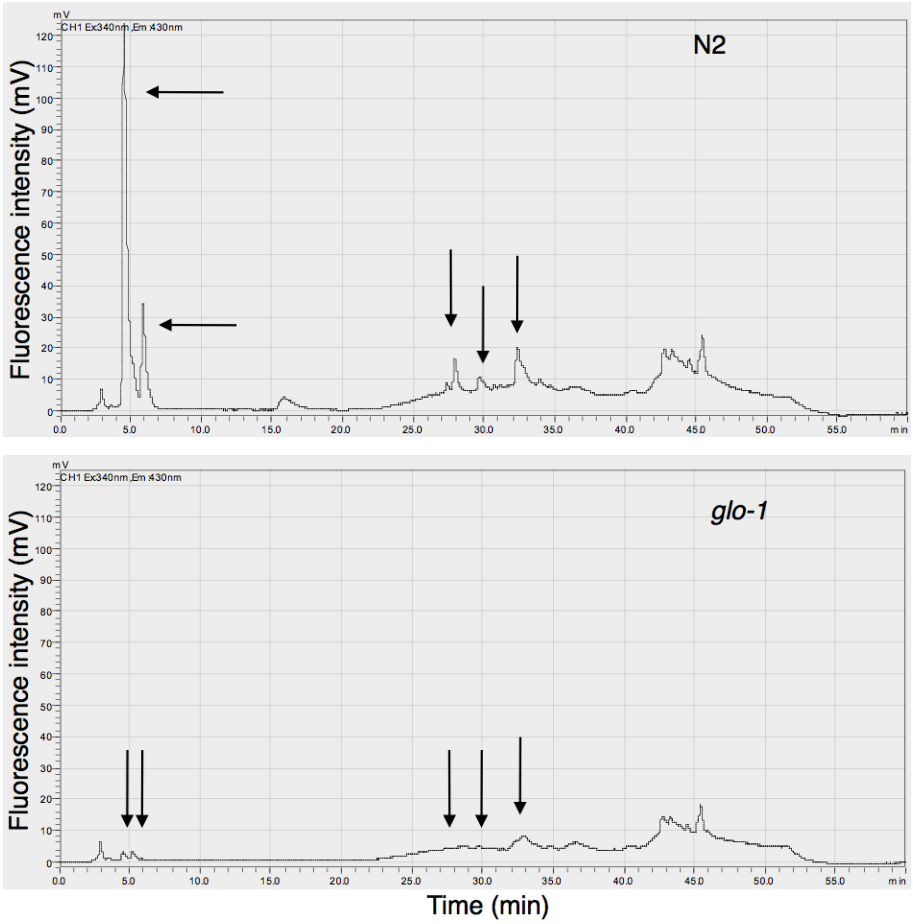

Figure 5.5: HPLC chromatograms showing differentially expressed metabolites (indicated by arrows) in N2 and *glo-1* backgrounds.

This protocol shows five clear peaks, implying five distinct compounds, in a wild-type background which were not visible in a *glo-1(zu437)* background (Figure 5.5). Of the five peaks, two are much greater, with one peak at ~4 minutes' elution being particularly high (Figure 5.5). These findings confirm that *glo-1(zu437)* animals are biochemically distinct from wild-type, and lack several blue fluorescent compounds.

We also examined the UV absorbance of these compounds. The peptide bonds present in proteins absorb UV light of different wavelengths depending on the forces of interaction within the protein (Goldfarb et al., 1951). Consequently, it is possible to identify different protein structures by measuring their UV absorbance. We measured the UV absorbance at 215, 254 and 280nm. However, we found no UV absorbance in the eluted mobile phase at the time which corresponded with the appearance of the differentially expressed fluorescent peaks (Figure 5.6). This, taken with the finding

that protein precipitation did not abrogate fluorescence, as discussed above, strongly suggested that the blue fluorescent substance was not comprised of protein.

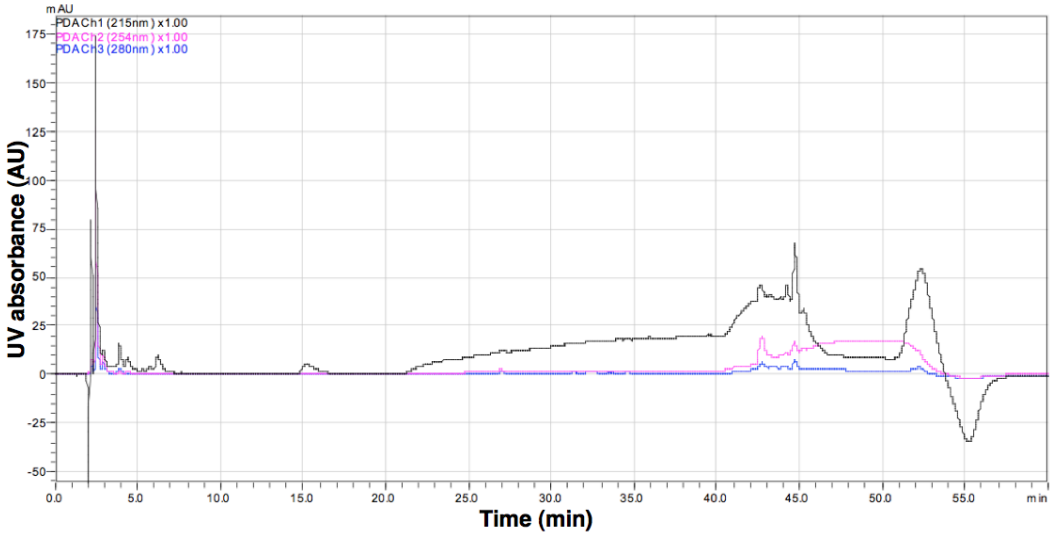

Figure 5.6: No UV absorption at 215, 254 or 280nm was detected at the time of the differentially eluted peaks.

5.2.4. NMR and DANS identification of DF as anthranilic acid derivatives

Once we had determined that *glo-1(zu437)* was biochemically distinct from N2, we used these samples as a negative control for NMR and DANS (**D**ifferential **A**nalysis of 2D **N**MR **S**pectra). This work was carried out in coloration with Parag Mahanti and Frank Schroeder, in Cornell University. DANS is used isolate unique signals from different metabolomes by graphically comparing their 2D NMR spectra; for further details please see section 2.4.2. Again we used the protein-purified supernatant samples derived from N2 and *glo-1* animals, as described above. When the 2D NMR spectra were analyzed, there were multiple differentially expressed signals between the two metabolomes. Detailed analysis of the fine structures of the differential signals indicated that the compounds absent in *glo-1* mutants include three anthranilic acid moieties, an N-substituted indole, as well as four β-glucosyl units (Figure 5.7). The chemical shift values of the protons in the four β-glucosyl moieties suggested that two of these are attached to anthranilic acid moieties forming two glucosyl esters, whereas the two remaining glucose units appeared to be part of N-glucosyl indoles. Furthermore, a characteristic downfield shift and additional J-splitting of the protons in position 3 of two of the four glucose moieties indicated that anthranilic acid glucosyl ester (angl#1) and N-glucosyl indole (iglu#1) were both

accompanied by the corresponding 3'-phosphorylated compounds (angl#2 and iglu#2) (Figure 5.8).

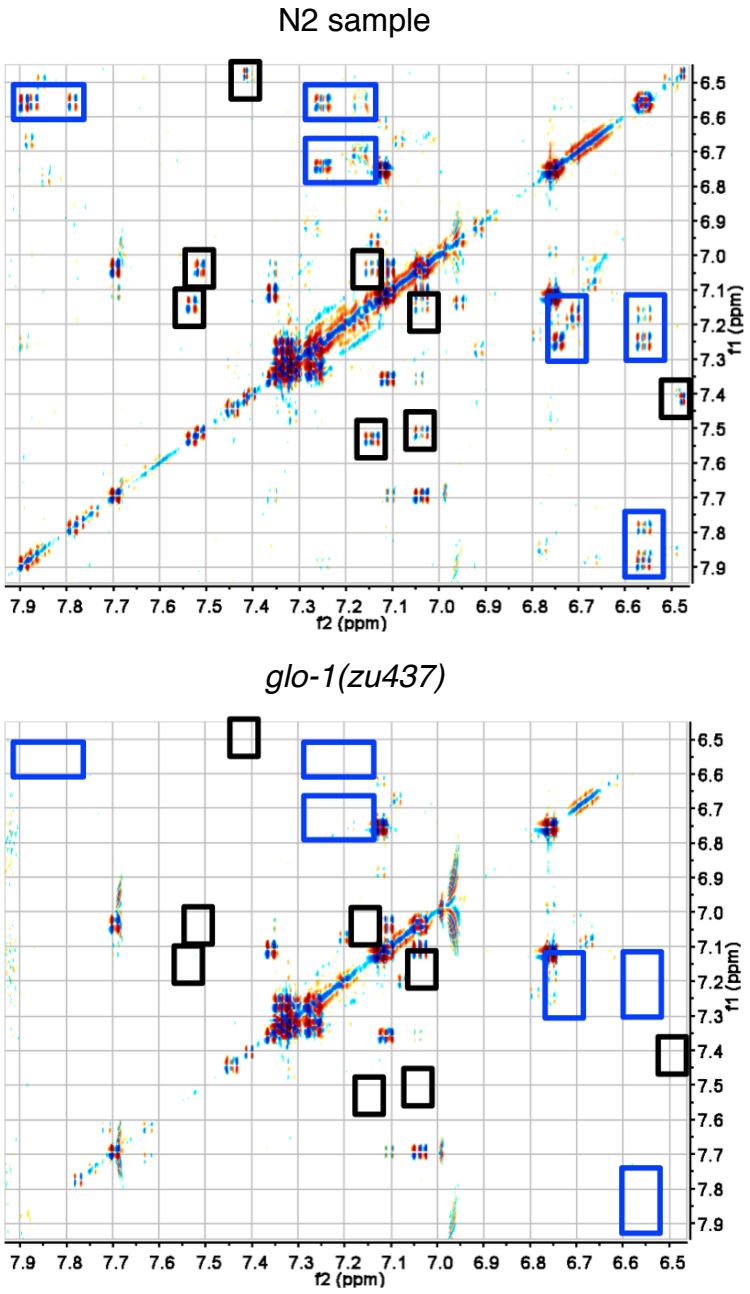

Figure 5.7: DANS analysis shows differentially expressed metabolites between N2 and *glo-1* backgrounds. The figure is comprised of graphically overlaying multiple 2D NMR spectra. Signals highlighted in blue boxes are those which contribute significantly to blue fluorescence signal; signals in black boxes are significantly differentially expressed metabolites which do not contribute to fluorescence.

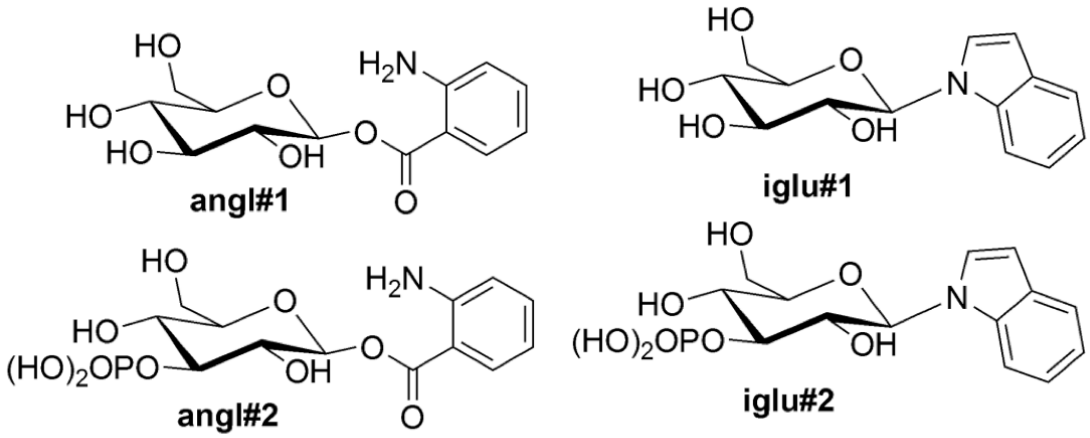

Figure 5.8: Blue fluorescence is comprised of glycosylated anthranillic acid derivates. Differentially expressed metabolites between glo-1 and N2 backgrounds are derivatives of anthranilic acid. angl1 and angl2 form blue fluorescence.

These structural assignments were confirmed via high-resolution mass spectrometry and synthesis of authentic samples of anthranilic acid glucosyl ester and N-glucosylindole (Please see Appendices 2 - 4). In addition, wild-type but not *glo-1* extracts contained smaller quantities of free anthranilic acid.

Anthranilic acid (AA) is derived from L-tryptophan (Trp) via the kynurenine pathway and its presence has previously been noted in *C. elegans* (Figure 3G) (Babu, 1974; Rongvaux et al., 2003); however neither angl#1 nor angl#2 have previously been identified in animals. AA derivatives show characteristic fluorescence at $\lambda_{ex}/\lambda_{em}$ 340/430 nm (Nakken, 1963), and their absence from *glo-1* extracts strongly suggests that these compounds are responsible for the blue fluorescence observed in the wild type. Furthermore, the HPLC retention times of the identified AA derivatives match those of the fluorescent peaks detected in the initial HPLC analysis of the wild-type extract (Figure 5.5 and Appendix 4). The two indole glucosides iglu#1 and iglu#2, also previously unreported from animals, do not contribute to the blue fluorescence.

5.2.5. DF arises from tryptophan

The absence of angl#1, angl#2, iglu#1, and iglu#2 in *glo-1* extracts indicates altered Trp metabolism in this mutant, which, strikingly, appears to affect both the tryptophanase and kynurenine pathways (Figure 5.9).

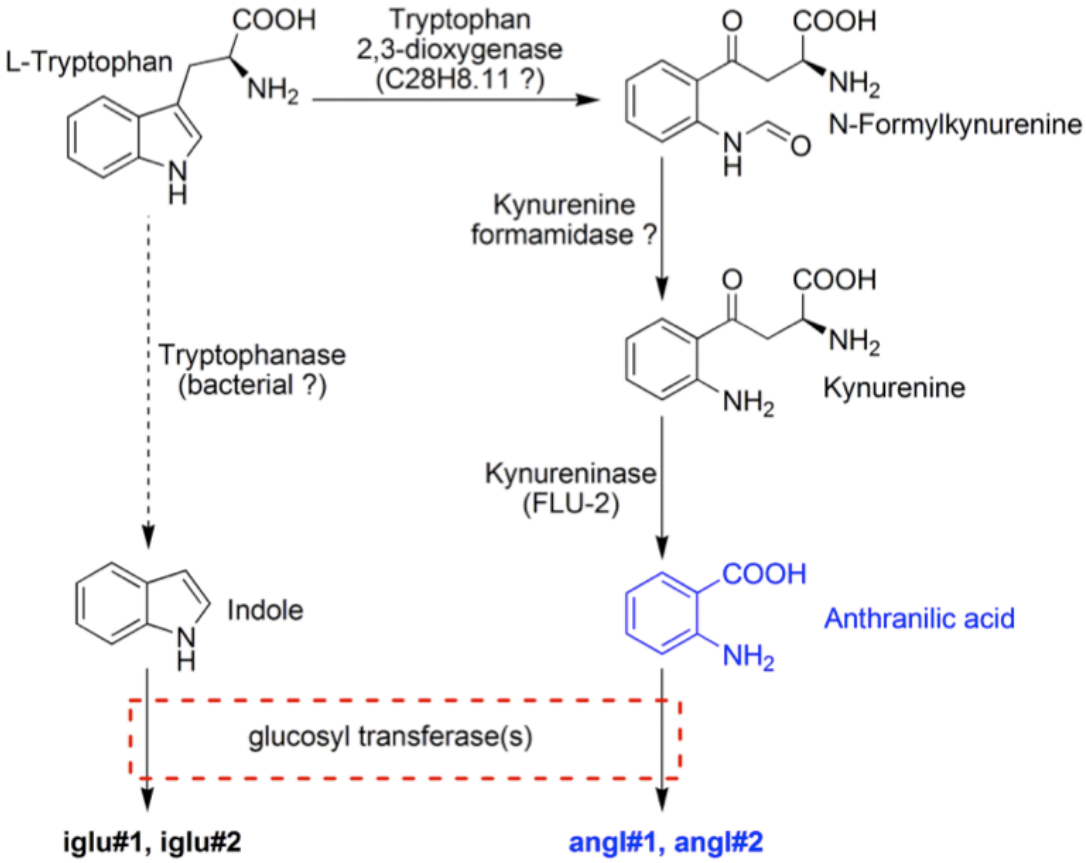

Figure 5.9: *glo-1* metabolites are differentially expressed. *glo-1* differentially expresses metabolites via both the tryptophanase and kynurenine pathway.

Differences in Trp metabolism between *glo-1* and N2 worms were also revealed by fluorescence spectroscopy, carried out in collaboration with Filip Matthijssens and Bart Braeckman in the University of Ghent. Live animals of both genotypes showed a fluorescence peak at $\lambda_{ex}/\lambda_{em}$ 290/~340nm (Figure 5.10), which has been previously observed, and is believed to correspond to Trp (Davis et al., 1982). After killing, a large peak at $\lambda_{ex}/\lambda_{em}$ 340/430nm, corresponding to DF, appeared in N2 but not *glo-1* animals (Figure 5.10). Notably, in N2 there was a marked reduction (~35%) in the size of the Trp peak, compared to a reduction of only ~20% in *glo-1*. These data are consistent with conversion of Trp to AA derivatives during death.

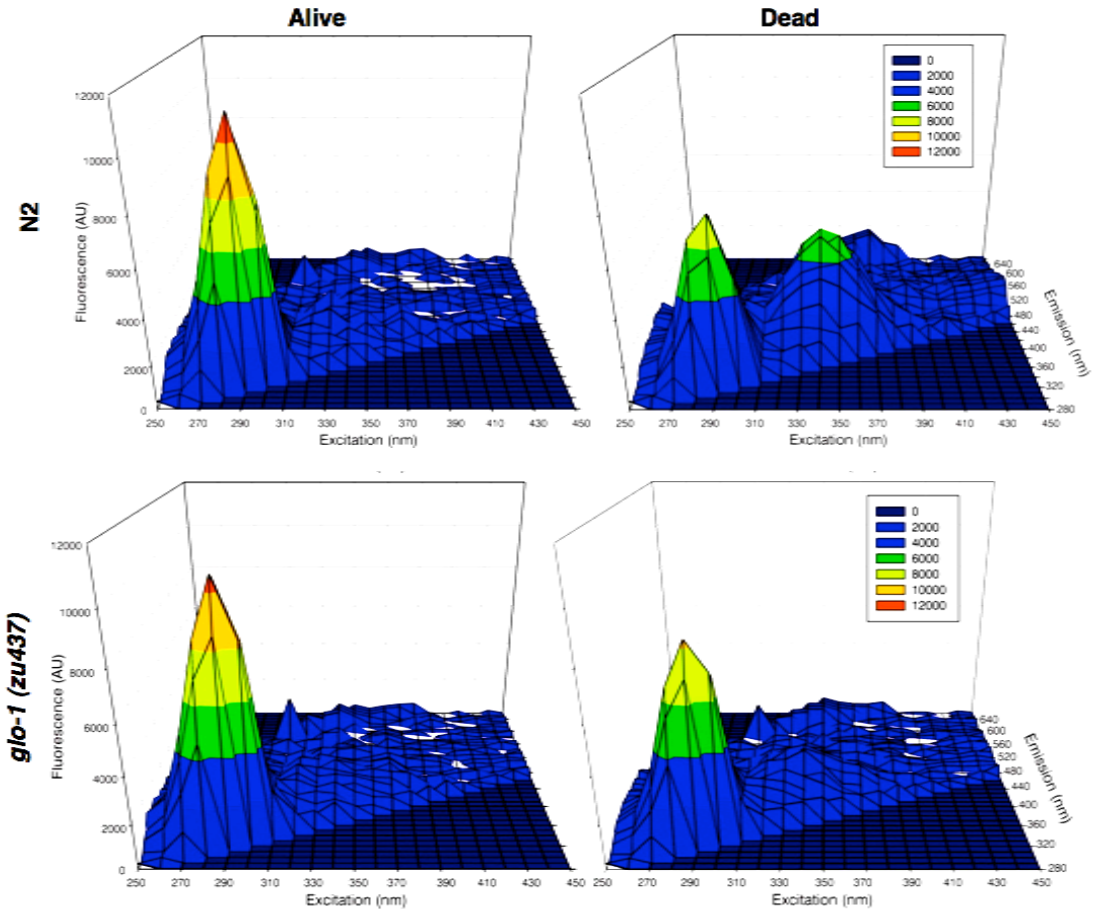

Figure 5.10: L-Trp is converted to DF in an N2 background, but not in a *glo-1* background. At death there is a 35% loss of L-Trp in N2, compared to a 20% loss in *glo-1*.

5.2.6. TDO RNAi abrogates DF and LRO fluorescence

As discussed in the introduction, the anthranilic acid generating kynurenine pathway catabolizes L-Tryptophan (L-Trp) via the two rate limiting enzymes TDO and IDO. We therefore sought to genetically confirm that DF is generated by AA. The *C. elegans* gene C28H8.11 encodes a putative TDO: the *C. elegans* homolog of IDO is unknown or not present (Rongvaux et al., 2003). We obtained an RNAi feeding clone of C28H8.11 from the Ahringer library (see Section 2.3), this work was done by Abbie Mandel. Reduction of expression of C28H8.11 by RNAi suppressed both living gut granule blue fluorescence and death fluorescence (Figure 5.11). The finding that TDO RNAi abrogates both gut granule and death fluorescence is striking as it implies that both types of fluorescence arise from the same pathway and are the same substance.

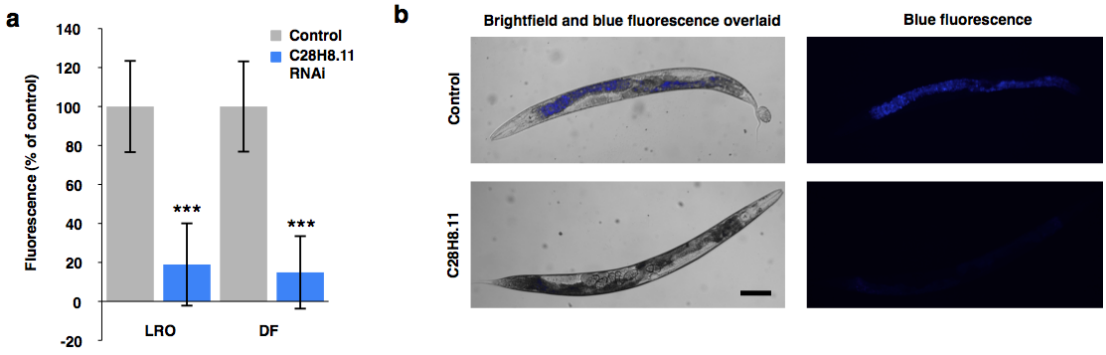

Figure 5.11: RNAi of TDO abrogates both gut granule fluorescence and DF in N2 animals. (a) Both gut granule and death fluorescence are reduced by TDO RNAi. Both types of fluorescence were measured using a plate reader; DF generated by freeze-thaw killing. Data is mean of three biological replicates, error bars are ± SD. (b) Representative images of TDO RNAi knockdown of DF.

5.2.7. TDO RNAi extends longevity but Flu mutants are not long lived

Once we had positively confirmed the identity of the blue fluorescent substance as AA derivates, we were interested in seeing what, if any, biological function they had. Work in *Drosphila* showed that genetic and biochemical inhibition of their TDO homolog extended lifespan (Oxenkrug, 2010; Oxenkrug et al., 2011). Consequently we wondered if manipulating the kynurenine pathway altered lifespan in *C. elegans*.

Lifespan was measured in TDO RNAi animals by Abbie Mandel, as described in Materials and Methods (lifespan assay, section 2.1.3., RNAi, section 2.3.1). TDO RNAi caused a 12% increase in lifespan relative to the L4440 control (Figure 5.12, Table 5.2).

We also measured the lifespan of two Flu mutants, *flu-1(e1002)* and *flu-2(e1003)*. These mutations have been shown to decrease the activity of kynurenine-3-hydroxylase and kynurenine respectively (Babu, 1974). Both of these enzymes lie downstream of TDO in the kynurenine pathway (Figure 5.2). However, unlike TDO RNAi, both *flu-1* and *flu-2* mutants were significantly short lived, with only 58.7% and 67.2% of wild type lifespan respectively (Figure 5.12, Table 5.3).

However, it is unknown if either Flu strain is backcrossed. Flu mutants were generated by exposure to the mutagenic compound ethylmethane sulfonate (EMS), selecting for progeny with altered intestinal fluorescence (Babu, 1974). Thus this mutagenesis may have induced secondary or background mutations elsewhere in the

genome which may affect lifespan (Partridge and Gems, 2007). To avoid these unwanted background effects, it is standard procedure to extensively backcross mutant progeny to a wildtype background. Babu does not state whether these strains were backcrossed, nor is there any record of them being so (Babu, 1974). Thus it is possible that Flu mutants' reduced longevity can be attributed to a background mutation.

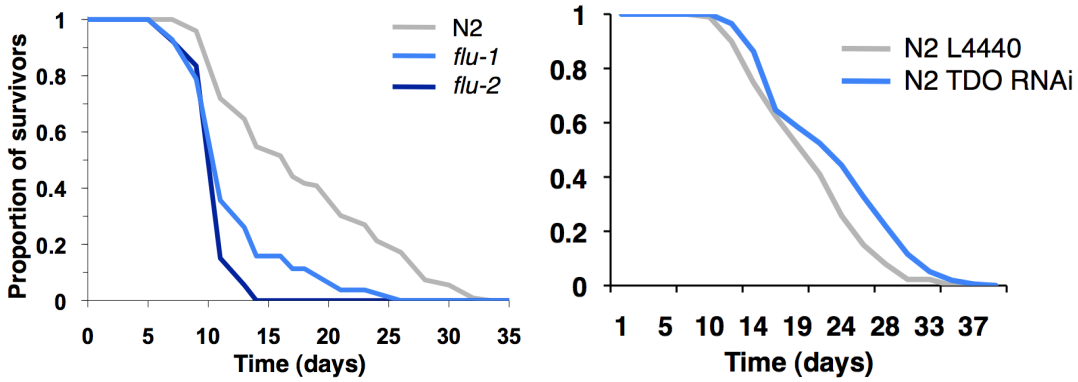

Figure 5.12 Inhibition of kynurenine pathway components affects longevity. (a) *flu-1* and *flu-2* mutants have significantly reduced lifespans compared to N2. Data mean of two repeats. (b) TDO RNAi significantly extends lifespan compared to empty vector control. Data mean of three repeats. All assays were carried out at 20°C, with 10μM FUDR applied topically, n = 100 animal per strain in each trial.

Strain	Mean lifespan (days)	% of N2 mean lifespan	p vs N2
N2 (control)	18.5	-	-
TDO RNAi	23.0	124	<0.0001

Table 5.2: TDO RNAi significantly extends lifespans compared to L4440 control, long-rank test.

Strain	Mean lifespan (days)	% of N2 mean lifespan	p vs N2
N2 (control)	18.5	-	-
flu-1	10.9	59	<0.0001
flu-2	12.4	67	<0.0001

Table 5.3: Flu mutants have significantly shortened lifespans compared to wild-type, log-rank test.

These data imply that alteration in kynurenine pathway activity can affect lifespan, depending on which pathway component is inhibited. RNAi-mediated TDO knockdown probably decreases whole pathway activity whereas *flu-1* and *flu-2*

mutations most likely alter the ratio of kynurenine metabolites generated. Thus TDO knockdown may reduce the production of other potentially toxic kynurenine metabolites, such as quinolinic acid, leading to increased longevity. By contrast, if an excess of any one metabolites is generated, as would be expected in the Flu mutants (Siddiqui and Babu, 1980), this could have potentially toxic and lifespan shortening effects. These data also rather argues against the idea that DF accelerates death. If it did, then *flu-2* mutants, which are predicted to generate lower levels of AA via kynurenine inhibition (and consequently have green intestinal fluorescence) should be long lived too. As they are not, generation of AA derivatives specifically most probably correlate with death, rather than cause it.

5.2.7. Kynurenine pathway mutants confer stress resistance

Given that necrosis mutants do not show extended lifespan but are stress resistant, we wondered whether or not kynurenine pathway mutants might show the same property. As discussed in Section 4.2.5, death from ageing is most likely determined by many pathologies acting in parallel, and consequently suppressing a single cause may not markedly increase lifespan (Olshansky et al., 1990). We therefore exposed Flu mutants and wildtype animals on TDO RNAi to heat stress (35°C) in order to test for thermotolerance.

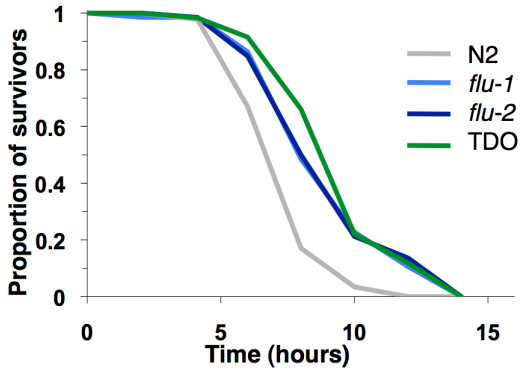

Figure 5.13: Preliminary data shows that inhibiting kynurenine pathway activity increases thermal stress resitance relative to WT. Flu mutants and N2 on TDO RNAi are significantly more resistant to thermal stress than N2. Data from one biological repeat, n = 40 animals. Please note that *flu-1* and *flu-2* share almost identical survival curves and so it is difficult to distinguish them on this figure.

Strain	Mean survival time (hours)	% N2 mean survival time	*p* vs N2
N2 (control)	7.1		
flu-1	8.6	121	<0.0001
flu-2	8.9	125	<0.0001
TDO	9.7	136	<0.0001

Table 5.4: Kynurenine pathway inhibition increases more thermal stress resistance.

Inhibiting the kynurenine pathway through mutation and RNAi strongly and significantly extended thermotolerance (Table 5.4). However, it is important to note that this data is preliminary as only one biological replicate has been done. Moreover, only N2 was used as a control; an appropriate control for TDO RNAi would be an N2 animals grown on empty vector L4440 containing HT115 bacteria.

Assuming this data is replicable, given Flu mutants' reduction of lifespan this data might suggest that thermotolerance resulting from TDO RNAi is not the cause of life extension. Alternatively, *flu-1* and *flu-2* mutants may be more pleiotropic, other traits shortening lifespan. There is a growing body of data which shows that kynurenines have been shown to stimulate necrotic mammalian neuronal death (Schwarcz et al., 2012). Given that we have now shown that a mechanism similar to this occurs during *C. elegans* organismal death, it is possible that kynurenine pathway mutations protect against this type of cell death by reducing the formation of necrosis-stimulating metabolites. Another possibility is suggested by the fact that both AA and other kynurenine pathway metabolites are highly redox active (Schwarcz et al., 2012). Again, lowering the concentration of these metabolites may be insufficient to extend lifespan but may protect oxidative damage leading to cell death. It is possible that TDO RNAi increases the L-Trp:kynurenine ratio thus reducing the levels of damage redox active metabolites. However, this data needs to be replicated, and further work will be required to fully test these hypotheses.

Discussion

5.3.1 Biochemical identification of blue fluorescence as anthranilic acid derivatives

Through the use of the mutant *glo-1*, HPLC and NMR, we biochemically identified DF as the glycosylated anthranilic acid derivatives angl#1 and angl#2. We confirmed this identification by genetically manipulating AA generation through

TDO (C28H8.11) RNAi. C28H8.11 RNAi led to loss of both gut granule and death fluorescence, presumably due to inhibition of kynurenine pathway. These results are valuable for several reasons. Firstly, we have clearly demonstrated the biochemical source of gut granule and death fluorescence, and thus shown it not to be lipofuscin. Secondly, we have shown that the kynurenine pathway is, at least partially, functionally conserved in *C. elegans*. Finally, as we have shown that both gut granule and death fluorescence is generated by this AA pathway. These findings provoke many interesting new questions about the biological function of the kynurenine pathway in *C. elegans*.

5.3.2. How is DF generated at death?

Both gut granule and death fluorescence issue from AA derivatives. An unanswered question is how the fluorescent burst arises at death. There are several possibilities. The enzymes of the kynurenine pathway are required for AA generation. Consequently the change in intensity and distribution of blue fluorescence at death may arise from a change in enzyme distribution. If the enzymes are localized to the gut granules then presumably they would act upon L-Trp freed by proteolytic enzymes within the gut granules. We have shown that necrosis leads to lysosomal lysis during *C. elegans* organismal death (section 4.2.4). Lysosomal lysis causes acidosis and releases the lysosomal contents into the cystol, including low-pH activated non-specific proteases. These proteases may degrade cytosolic proteins, releasing large amounts of free L-Trp as substrate for the newly released kynurenine pathway enzymes. Consequently, DF could arise from high concentrations of cytosolic free L-Trp being converted to AA derivatives within the cytosol, thus explaining both the increase in fluorescence (greater substrate concentration) and the alteration in distribution at death.

Alternatively in a slightly different scenario, low-pH dependent kynurenine enzymes could be ubiquitously distributed throughout the cell. Only active in low pH gut granules, AA derivative generation would be localized to gut granules until lysosomal lysis and cytosolic acidosis. At this point, activated kynurenine enzymes would again generate DF as outlined above. Neither the mammalian or *C. elegans* sub-cellular location of the kynurenine enzymes are known. However, we are currently in the process of cloning the *flu-1* and *flu-2* genes. Once cloned, we hope to

tag them with a fluorescent marker and observe their sub-cellular distribution pattern which will begin to answer this question.

5.3.3. The role of kynurenines in *C. elegans*

Our data identifies glycosylated anthranilic acids as the differentially expressed compounds responsible for death fluorescence. However despite their identification, the reasons underlying the presence of AA derivatives in gut granules and their large and rapid increase at death are unknown. There are several possibilities to explore.

Firstly, it is possible that AA derivatives may have a protective function. There is evidence that the kynurenine pathway is involved in immunity, as described above. AA can inhibit growth of bacterial pathogens, e.g. *Legionella pneumophila* (Sasaki et al., 2012), and 3-hydroxyanthranilic acid can induce cell death in lymphocytes (Piscianz et al., 2011) and neurons (Smith et al., 2009). Thus perhaps gut granules act as a store of anti-bacterial agents in the event of pathogen attack. This may also explain why the gut granules are unique to the intestine, the site most likely to experience pathogenic invasion in *C. elegans* (Hodgkin and Partridge, 2008).

Alternatively, the kynurenines may contribute to organismal death in some fashion. angl#1 and angl#2 have not previously been biologically identified, but AA in its non glycosolated form has been shown to have, like other kynurenines, a role in disease. It was found that a greatly increased AA to 3-HA ratio in patients suffering from stroke, Huntington's, chronic brain injury and depression, amongst other diseases (Darlington et al., 2010). Especially interesting from our point of view is the discovery that stroke patients who eventually died of their neuronal injuries had significantly lower levels of 3-HA to AA than those who survived, and there was a significant negative correlation between the size of their infarct and the levels of 3-HA (Darlington et al., 2007).Thus, at least in stroke victims, there appears to be an increase in AA generation at death, as seen in *C. elegans.* The authors hypothesized that increased production of AA may be acting to protect already damaged tissues from the production of the cytotoxic QA, a 3-HA metabolite (Darlington et al., 2010). However, they do not comment on the fact that AA can be metabolized into 3-HA and subsequently into QA, which would not be predicted to be protective.

Given that we have shown organismal death in *C. elegans* is dependent on necrosis and spreads in an excitotoxic-like manner, it is intriguing to note that

kynurenines have also been shown to be heavily involved in excitotoxic neuronal death. It may be possible that somehow AA derivatives are involved in stimulating necrotic cell death, perhaps through conversion to QA and subsequent over-stimulation of endogenous NMDA receptors in the *C. elegans* CNS (Brockie and Maricq, 2003). Thus it could be that necrosis triggers hyper-activation of the kynurenine pathway which eventually contributes to organismal death in some manner. Moreover, we have shown that as with *Drosophilia*, inhibition of TDO expression by RNAi extends lifespan (Oxenkrug, 2010; Oxenkrug et al., 2011). We have also shown that kynurenine pathway manipulation confers resistance to thermal and osmotic stressors. TDO RNAi has been shown to reduce the toxicity of α-synuclein formation in a *C. elegans* Parkinson's disease model (van Ham et al., 2008). Clearly the kynurenine pathway does play a biological role in *C. elegans* other than simple NAD generation and its manipulation does appear to act in a protective manner. Thus the kynurenine pathway may contribute to *C. elegans* organismal death, although the mechanisms remain unclear.

5.3.4. The biological function of gut granules

Despite the biochemical identification of the blue fluorescence contained within *C. elegans* gut granules, the nature of these lysosome related organelles remains unknown. One possibility, touched on above is that gut granules could act as a store of angl#1 and angl#2. The glycosylation of anthranillic acid may promote its accumulation in gut granules. For example, in *Arabidopsis*, glycosylation by UDP-glucosyltransferases promotes AA accumulation due to increased compound stability (Quiel and Bender, 2003).

Another possibility is that gut granules could protect against UV damage. Being pigmented lysosome-related organelles, gut granules resemble mammalian melanosomes, which confer UV resistance (Raposo and Marks, 2007). However, some preliminary trials performed by Abraham Mandel showed that, against expectations, *glo-1* animals showed the highest survival rates when exposed to UV radiation (data not shown). Consequently it seems unlikely that gut granules have evolved to confer UV protection.

glo-1 mutants appear to develop and age normally, implying that gut granules are not necessary for survival (Hermann et al., 2005). However, preliminary work done by Michele Riesen, a postdoctoral researcher in the Gems lab, suggests that *glo-*

1 RNAi abrogates the increased longevity of *daf-2* mutants. Taken together these data could imply that Glo-1 may play an important role in regulating stress resistance, and consequently suggest a functional role for gut granules.

6. CONCLUSIONS

The initial aim of this project was to verify a biomarker of ageing; instead we discovered a biomarker of death. Consequently, to *C. elegans*' multiple advantages as a model organism, we can add another useful trait. Using death fluorescence (DF) as a biomarker, we have already discovered that organismal death in *C. elegans* involves a cascade of systemic necrosis. DF is already being investigated as a potential means of automating lifespan trials. Continued characterization of *C. elegans* DF could provide insights into this new biology of death.

In our discovery of DF, we have removed a key piece of evidence for the oxidative damage theory in *C. elegans* ageing: the age accumulation of the molecular damage product lipofuscin. Whether *C. elegans* possess lipofuscin remains an open question.

Our results demonstrate that blue fluorescence is not lipofuscin but rather anthranlic acid glucosyl esters. They also reveal the issue of the use of fluorescence as a biomarker of ageing to be a complex one. In worms observed *in situ* in culture, blue fluorescence does not increase with age but with death. However, for unknown reasons, when mounted on microscope slides worms do show an age increase in blue fluorescence, perhaps due an age-related increase in frailty. By contrast, red fluorescence showed a non-condition dependent age increase and so could be a useful biomarker of ageing in *C. elegans*, assuming its death-dependent increase is accounted for.

The mechanisms which underpin the systemic necrotic cascade are homologous to calcium-dependent necrotic propagation in mammals during excitotoxic neurodegeneration. Consequently, the study of organismal death in *C. elegans* may prove to be a useful model for studying mammalian neurodegeneration.

The kynurenine pathway has been implicated in excitotoxic mammalian neuronal death; our findings suggest it also has a role in *C. elegans* organismal death. Is the burst of AA derivatives or other kynurenine metabolites peculiar to *C. elegans* and other soil dwelling nematodes? Increases in blue fluorescence associated with death have been reported, e.g. in budding yeast (Liang 2007) and porcine hepatocytes (Anderson 2004). Anecdotal data suggest that some kind of fluorescence arises from the necrotic interior of human cancers (personal communication, Ralph DaCosta,

University of Toronto). Further investigation may reveal conserved mechanisms which link the kynurenine pathway to necrotic death.

To the best of our knowledge, this is the first account of the mechanisms of organismal death in *C. elegans*. As ageing once was, the process of death is considered to be a catastrophic processes of a sort that is not amenable to scientific analysis. However, as discussed in Chapter 4, there is no reason why this necrotic cascade of death itself cannot be viewed through the prism of evolution as the result of a quasi-programme or antagonistic pleiotropy. Death, as all other biological processes, can and should be studied.

Appendix 1: *C. elegans* intestinal fluorescence has been used a biomarker of ageing in many different research papers. *C. elegans* autofluorescence has also been equated with lipofuscin in some cases. Many papers have used this as a way of distinguishing between progeria and life-shortening genetic or environmental interventions.

Paper reference	Example of usage
Apfeld et al., 2004	While preliminary evidence suggests that *aak-1* does not appear to be required for the control of lifespan (data not shown), *aak-2(ok524)* mutants have a 12% shorter lifespan than wild-type animals. Moreover, a lipofuscin-like fluorescent pigment that accumulates in an age-dependent manner in the intestine accumulates at a faster rate in *aak-2* mutants than in wild-type animals.
Baeriswyl et al., 2009	As age-dependent accumulation of autofluorescent compounds is a universal biomarker of aging, we also measured this in C. elegans fed different bacterial strains. … . The autofluorescence was 17% stronger in nematodes fed on IAI1 than on OP50 ($N = 40$ and $N = 41$, respectively, Mann–Whitney U test: $P < 0.05$). Therefore, faster accumulation of the autofluorescence in nematodes exposed to bacteria causing higher mortality may result from self-injury inflicted by the innate immune response.
Boehm and Slack, 2005	To determine whether the short life span of lin-4(lf) mutants is due to accelerated aging or to an unrelated, pleiotropic cause, we monitored the accumulation of intestinal autofluorescence in adult animals. Intestinal autofluorescence, which is caused by lysosomal deposits of lipofuscin, accumulates over time in the aging animal and is an established marker for aging. In agreement with its short life span, the lin-4(lf) mutant accumulated intestinal autofluorescence more rapidly than the wild type.
Chavez et al., 2007	The presence of the NADPH oxidase inhibitor DPI in the plates significantly reduces lipofuscin accumulation in wild-type worms.
Clokey and Jacobson, 1986	The nematode Caenorhabditis elegans contains autofluorescent lipofuscin granules, located exclusively in the 32-34 intestinal cells.
Fisher and Lithgow, 2006	Accumulation of autofluorescent material in the gut of the worm has been associated with aging, and mutations that alter organismal aging have been shown to speed or slow the rate of development of autofluorescence consistent with the effects on lifespan. We find that in comparison to N2 and daf-12(rh273), the shorter-lived daf-12(rh61rh411) accumulates autofluorescent material earlier in adulthood.

Fujii et al., 2009	Caenorhabditis elegans shows increasing fluorescence signals in intestinal cells with advancing age. These fluorescent materials contain lipofuscin consisting of oxidized and cross-linked macromolecules such as lipids and. In the oxygen-sensitive mutant mev-1, the fluorescent materials accumulate at a greater rate than in N2, and the accumulation rate depends on the concentration of oxygen. We then examined the fluorescence signals in N2 and oxy-4 at day 10 with fluorescence microscopy, and found that a significant portion of oxy-4 worms (ca. 30%–50%) showed increased fluorescence signals, compared with N2 worms.
Gardner et al., 2004	Most significantly, S. ratti exhibits an acceleration in age-specific mortality rate, one which is more rapid than that seen in C. elegans. Several characteristics of organismal aging previously documented in C. elegans also occur in S. ratti, but at a faster rate. For example, with increasing age, levels of autofluorescence (lipofuscin) increase.
Garigan et al., 2002	Several short-lived mutants that accumulate lipofuscin granules more rapidly than normal have been postulated to age rapidly, on the basis of this one age-related phenotype.
Gerstbrein et al., 2005	That age pigments might reflect physiological aging state has been suggested based on other work that correlated metabolic rate with lipofuscin levels (Sohal, 1981; Sohal & Brunk, 1989). Our observations sug- gest that screening for genetic or pharmacological interventions that block or delay age pigment accumulation might identify genetic manipulations that extend middle age healthspan, a goal of considerable importance. Evaluating healthspan by age pigment scores is far more rapid than other indicators that have been carefully quantitated, such as locomotory or cellular decline.
Gill, 2006	The accumulation of fluorescent pigment is also associated with increased age in C. elegans and correlates with lifespan in a variety of mutants. This raises the possibility that automated fluorescence detection could be used to screen for compounds that delay the age-related rise in auto-fluorescence signal.
Hartman and Ishii, 2007	To distinguish between these, we measured three biomarkers (body movement, pharyngeal pumping and intestinal lipofusin autofluorescence) that others have shown to correlate strongly with normal aging in both wild-type and long-lived mutants of C. elegans. Cessation of fast body movement, decreases in pharyngeal pumping and increases in lipofusin autofluorescence all occurred precociously in the “dosage compensation” Dpy's relatively to the “non-dosage compensation” Dpy's, consistent with the suggestion that the former age through normal mechanisms, albeit at accelerated rates.

Hosokawa et al., 1994	Fluorescent material accumulated in both wild type and mev-1 animals with increasing age. The mev-I mutant accumulated more fluorescent ma- terial at a greater rate than dose wild type. Furthermore, the accumulation rates depended on concentration of oxygen. Since this phenotype has been widely used as an aging marker, these results validate mev-l's use as a model to study aging.
Ishii et al., 1998	Strains bearing this mutation accumulate markers of ageing (such as fluorescent materials and protein carbonyls) faster than the wild type.
Ishii et al., 2006	Fluorescent materials (lipofuscin) and protein carbonyl derivatives are formed in vivo as a result of metal-catalyzed oxidation and accumulate during aging in disparate model. The presence of fluorescent materials and protein carbonyl modifications can be a specific indicator of oxidized lipid and protein. The mev-1 mutants accumulated fluorescent materials and protein-carbonyl derivatives at significantly higher rates than did their wild-type cohorts. Thus, the aging process in mev-1 animals approximates that of wild type except for its precocious nature.
Jain et al., 2009	Worms also produce lipofuscin, a marker of oxidative stress, in intestinal cells as they age, and lipofuscin is produced earlier in development when young worms are infected with a pathogen that elicits ROS production.
Joeng et al., 2004	Lipofuscin accumulation, a typical aging marker, began 2−3 d later in F25−2 worms than in N2 controls, indicating that telomere length has an effect not only on the mean lifespan but also on the rate of aging.
Kampkotter et al., 2007a	Lipofuscin is generated by oxidative degeneration and autophagy of cellular components and its accumulation only in the intestinal cells of the worm correlates with the life span making it an established marker for ageing in C. elegans. The treatment of wild type worms with kaempferol resulted in a significant reduction of lipofuscin autofluorescence of 25% whereas after the fisetin treatment a non-significant decrease (12%) was measured The effect of kaempferol and fisetin on lipofuscin accumulation.
Kampkotter et al., 2007b	The higher antioxidative activity of quercetin may explain the protection against lethal thermal stress and the reduction in accumulation of the ageing marker lipofuscin exerted by quercetin but not by rutin.

Kim et al., 2008	Lipofuscin accumulation in the nematode intestine. Shown are Nomarski images (A–C) and intestinal autofluorescence from lipofuscin (a–c) of age-synchronized N2 animals of Day 10: (A and a) Control; (B and b) 0.5 mM nano-Pt; (C and c) 0.5 mM EUK-8.
Kimura et al., 2007	Therefore, the reduced motility and life span found in hsp-6(RNAi) in the present study were thought to be premature aging or progeria-like phenotypes. To examine this hypothesis, we assayed autofluorescence in hsp-6(RNAi) because lipofuscin-like fluorescent pigment is reported to accumulate with age and can be used as a general marker for aging in C. elegans … The level of autofluorescence gradually increased in both mock- and RNAi-treated worms (D2 and D4) during aging, but the level of autofluorescence remained significantly higher in RNAi-treated worms up to 4th day of the RNAi treatment (D4, about 18%). This is consistent with progeria-like phenotypes in adult hsp-6(RNAi) similar to those found in daf-16 and mev-1 mutants.
Lee et al., 2004	To determine whether the reduced life span of *wrn-1*(RNAi) worms was due to progeria or to sickness, symptoms of normal aging, such as lipofuscin accumulation and tissue deterioration in the head.
Masse et al., 2008	We next tested whether the previously isolated *smg-1(r861)* null allele also shows a lifespan phenotype. The average lifespan of *smg-1(r861)* mutant animals was not increased compared to wild-type animals (data not shown). Nonetheless, despite the fact that these mutants did not live longer than wild-type, we observed a delayed accumulation of the aging marker lipofuscin during the first week of life of *smg-1(r861)* mutants, as observed in *smg-1* RNAi treated animals.
Mehta et al., 2009	Consistent with the observed longevity effects, the accumulation of autofluorescent age pigments, which has been proposed as a biomarker of aging and health span in C. elegans, was reduced in vhl-1(ok161) animals. This reduction was also fully suppressed by deletion of hif-1.
Minniti et al., 2009	We found that msra-1 mutants also show increased accumulation of lipofuscin autofluorescence in the intestine compared to the WT (Supporting Data S1). Premature lipofuscin accumulation is indicative of tissue aging.

Neumann-Haefelin et al., 2008	To further support the hypothesis that the short life span of *shc-1(ok198)* mutants is due to accelerated aging rather than due to a more general pathology, we monitored the accumulation of intestinal autofluorescence in adult animals. Intestinal autofluorescence, which is caused by lysosomal deposits of lipofuscin, accumulates over time in the aging animal and is an established marker for aging. Consistently with its short life span, the *shc-1* mutant accumulated intestinal autofluorescence more rapidly than the wild type.
Ookuma et al., 2003	Thus, we observed the accumulation of lipofuscin-like intestinal fluorescence, which is one of the major markers of ageing in C. elegans. At 5 days after L4, no autofluorescence was observed in daf-2(e1370) or daf-2; scl-1(RNAi), and only a slight fluorescence could be observed in N2. At 10 days after L4, marked accumulation of intestinal fluorescence was observed both in daf-2; scl-1(RNAi) and N2, but not in daf-2(e1370). Additionally, in 12-day-old daf-2; scl-1(RNAi), N2-like tissue deterioration occurred in the intestine. These data indicate that daf-2; scl-1(RNAi) animals age faster than daf-2 animals.
Pluskota et al., 2010	In order to validate the life span results formation of lipofuscin was analysed in untreated WT worms and C. elegans fed on different NPs. Fluorescence quantification revealed that control worms accumulated nearly identical amounts of lipofuscin over time compared with C. elegans which were fed on PS-NPs (YO, carboxy) or plain silica-NPs. These results confirm the life span assays suggesting that nematodes fed with NPs that differ in composition, labelling and functional groups on the particle surface, do not differ from untreated control worms with respect to age-related oxidative processes.
Aubert et al., 2005	The accumulation of lipofuscin as a cause of cell death in ageing is receiving fresh attention. Its contribution to cell death in NCL, and the role of PPT-1 and saposins in this, could be readily addressed in an enhanced worm model of INCL.
Samuelson et al., 2007	Aging C. elegans show intestinal autofluorescence partially as a result of lysosomal deposits of the pigment lipofuscin. Aging tissues accumulate this pigment in secondary lysosomes due to the oxidative degradation and autophagocytosis of cellular components…We tested whether gene inactivations that shortened life span also led to a pre- mature accumulation of age pigment. Out of 39 strictly daf-2 pathway-specific clones, 17 gene inactivations caused strong or moderate acceleration in age pigment accumulation.

Shibamura et al., 2009	Nematodes were examined for lipofuscin, the so-called "age pigment" that accumulates with aging, at 5, 7, 10, and 15 days of age. In addition, 7-day-old worms were fed salmonella instead of OP50 for studies of the effects of chemicals on host defense. Liposome-mediated oral supplementation with antioxidants or the anticonvulsant trimethadione neither clearly altered the lipofuscin accumulation nor enhanced the host defense to salmonella.
Taub et al., 1999	Another measure of ageing in C. elegans is the accumulation of fluorescent material. ctl-1 mutants contain much more fluorescent material at 15 days after hatching than do wild-type animals. These observations suggest that ctl-1 is an important determinant of normal ageing in C. elegans.
Toth et al., 2008	An important question is whether short-lived mutant nematodes deficient in autophagy age more rapidly than normal animals or become simply sick and die earlier for reasons unrelated to aging. To address this issue, we assayed the levels of lipofuscin granules in adults at different ages. Lipofuscin is a pigment that accumulates progressively, in particular during the postreproductive period, in aging tissues as a result of the oxidative degradation of cellular components. We found that bec-1, unc-51 and atg-18 mutants accumulated lipofuscin more rapidly during the course of life than wild-type animals.
Uccelletti et al., 2008	In agreement with short life span, the apy-1(RNAi) animals accumulated intestinal autofluorescence more rapidly than the control worms.
Vanfleteren and Braeckman, 1999	Next, they enter the postreproductive phase of the life cycle, in which symptoms of senescence accumulate, including …and the accumulation of …. lipofuscin-like granules.
Willett et al., 2010	Lipofuscin and other age-related compounds have been shown to accumulate with age in CE (58,59). Axenic Cohort A (adult) epifluorescence values (intensity per pixel per individual-pixels/nematode) ranged from 1,051 to 3,450 (with a mean of 2,512) in 25 live CE and 912 to 2,116 (with a mean of 1,414) in 22 live monoxenic adult CE Cohort A.
Wilson et al., 2006	One marker for cellular damage during aging is the intracellular level of lipofuscin, autofluorescent material that accumulates in aging cells. Lipofuscin levels increase with aging in many organisms, including C. elegans. We examined lipofuscin levels in the intestines of control and BB-treated adult day 16 animals. Consistent with the expectation that BB polyphenols could slow aging, intestinal lipofuscin levels were reduced 20% in BB-treated animals, compared with controls.

Yasuda et al., 2006	or example, both carbonylated protein and lipofusucin accumulate with advancing age, but there is little straightforward evidence to suggest that they strongly act to limit life span. However, accumulation is more rapid in short-lived mutants and slower in long-lived mutants, thus making these molecules excellent biomarkers of aging if nothing else.
Zheng et al., 2010	…in C. elegans, lower levels of lipofuscin in age-matched worms correlated with greater motility, suggesting that lipofuscin accumulation reflects biological versus chronological age.

Appendix 2: NMR spectroscopic data for angl#1

Position	*angl#1 $\delta^{13}C$ [ppm]*	*angl#1 $\delta^{1}H$ [ppm]*	*angl#2[1] $\delta^{1}H$ [ppm]*	*angl#1 ^{1}H-^{1}H-coupling constants [Hz]*	*angl#1 HMBC correlations*
1	*95.2*	*5.70*	*5.77*	$J_{1,2''}$ = *7.8*	*C-2, C-3, C-4, C-5, C-1'-COO*
2	*73.8*	*3.50*	*3.67*		*C-1, C-3*
3	*77.8*	*3.47*	*4.11 ($J_{H,P}$ = 8Hz)*		*C-2, C-4*
4	*70.8*	*3.40*	*3.59*		*C-5*
5	*78.5*	*3.44*			*C-1, C-4*
6a	*62.1*	*3.86*		$J_{6a,6b}$ = *12.1*, $J_{5,6a}$ = *5.2*	*C-4, C-5*
6b		*3.70*		$J_{5,6b}$ = *2.1*	*C-4, C-5*
1'-COO	*167.8*				
1'	*109.8*				
2'	*153.1*				
3'	*117.5*	*6.75*		$J_{3,4}$ = *8.5*, $J_{3,5}$ = *1.1*	*C-1', C-5', C-1'-COO*
4'	*135.5*	*7.26*		$J_{4,5}$ = *7.1*, $J_{4,6}$ = *1.7*	*C-2', C-6'*
5'	*116.1*	*6.57*		$J_{5,6}$ = *8.2*	*C-1', C-3'*
6'	*132.1*	*7.89*			*C-2', C-4', C-1'-COO*

[1]Characteristic ^{1}H NMR signals of angl#2.

^{1}H (600 MHz), ^{13}C (151 MHz), and HMBC NMR spectroscopic data for angl #1 in methanol-d_4. Chemical shifts were referenced to ($CD_2\underline{H}OD$) = 3.31 ppm and ($\underline{C}D_2HOD$) = 49.05 ppm.

Appendix 3: Spectroscopic data for iglu #1

Position	*iglu#1 δ ^{13}C [ppm]*	*iglu#1 δ ^{1}H [ppm]*	*iglu#2[1] δ ^{1}H [ppm]*	*iglu#1 ^{1}H-^{1}H-coupling constants [Hz]*	*iglu#1 HMBC correlations*
1	*86.5*	*5.46*	*5.55*	$J_{1,2}$ = *9.0*	*C-2, C-3, C-5, C-2', C-7a'*
2	*73.4*	*3.94*	*4.12*	$J_{2,3}$ = *9.0,*	*C-1, C-3*
3	*78.9*	*3.60*	*4.24 ($J_{H,P}$ = 8Hz)*	$J_{3,4}$ = *9.0*	*C-2, C-4*
4	*71.2*	*3.50*	*3.68*	$J_{4,5}$ = *9.0*	*C-3, C-5, C-6*
5	*80.4*	*3.58*		$J_{5,6a}$ = *5.8*	*C-1, C-3, C-6*
6a	*62.5*	*3.70*		$J_{6a,6b}$ = *12.1*	*C-4, C-5*
6b		*3.88*		$J_{5,6b}$ = *2.2*	*C-4, C-5*
2'	*126.2*	*7.40*		$J_{2',3'}$ = *3.3*	*C-1 (weak), C-3', C-3a', C-7' (weak), C-7a'*
3'	*103.2*	*6.49*			*C-2', C-3a', C-4' (weak), C-7a' (weak)*
3a'	*130.3*				
4'	*121.3*	*7.52*		$J_{4',5'}$ = *8.0,*	*C-3', C-6', C-7a'*
5'	*120.7*	*7.05*		$J_{5',6'}$ = *7.4,* $J_{3,5}$ = *1.1,*	*C-3a', C-7'*
6'	*122.4*	*7.15*		$J_{6',7'}$ = *8.0,* $J_{4',6'}$ = *1.0*	*C-4', C-7a'*
7'	*111.2*	*7.54*			*C-3a', C-5'*
7a'	*137.8*				

[1]Characteristic ^{1}H NMR signals of iglu#2. ^{1}H (600 MHz), ^{13}C (151 MHz), and HMBC NMR spectroscopic data for iglu #1 in methanol-d_4. Chemical shifts were referenced to ($CD_2\underline{H}OD$) = 3.31 ppm and ($\underline{C}D_2HOD$) = 49.05 ppm.

Appendix 4: High-resolution MS data angl#1, angl#2, iglu#1, and iglu#2

Compound	Ion	Ion formula	Calculated m/z	Observed m/z
angl#1	$[M-H]^-$	$C_{13}H_{16}NO_7^-$	298.0932	298.0910
angl#2	$[M-H]^-$	$C_{13}H_{17}NO_{10}P^-$	378.0596	378.0600
iglu#1	$[M-H]^-$	$C_{14}H_{16}NO_5^-$	278.1034	278.1071
iglu#2	$[M-H]^-$	$C_{14}H_{17}NO_8P^-$	358.0697	358.0701

High-resolution MS data for previously unreported *C. elegans* metabolites angl#1, angl#2, iglu#1, and iglu#2, acquired using negative-ion electrospray ionization (ESI^-).

BIBLIOGRAPHY

Aarts, M., Iihara, K., Wei, W.L., Xiong, Z.G., Arundine, M., Cerwinski, W., MacDonald, J.F., and Tymianski, M. (2003). A key role for TRPM7 channels in anoxic neuronal death. Cell *115*, 863-877.

Adachi, H., Fujiwara, Y., and Ishii, N. (1998). Effects of oxygen on protein carbonyl and aging in Caenorhabditis elegans mutants with long (age-1) and short (mev-1) life spans. J Gerontol A Biol Sci Med Sci *53*, B240-244.

Adams, C.M., Snyder, P.M., Price, M.P., and Welsh, M.J. (1998). Protons activate brain Na+ channel 1 by inducing a conformational change that exposes a residue associated with neurodegeneration. J Biol Chem *273*, 30204-30207.

Altschul, S.F., Gish, W., Miller, W., Myers, E.W., and Lipman, D.J. (1990). Basic local alignment search tool. J Mol Biol *215*, 403-410.

Apfeld, J., O'Connor, G., McDonagh, T., DiStefano, P.S., and Curtis, R. (2004). The AMP-activated protein kinase AAK-2 links energy levels and insulin-like signals to lifespan in C. elegans. Genes Dev *18*, 3004-3009.

Arking, R. (1987). Successful selection for increased longevity in Drosophila: analysis of the survival data and presentation of a hypothesis on the genetic regulation of longevity. Experimental gerontology *22*, 199-220.

Aubert, B., Barate, R., Boutigny, D., Couderc, F., Karyotakis, Y., Lees, J.P., Poireau, V., Tisserand, V., Zghiche, A., Grauges, E.*, et al.* (2005). Evidence for B+ --> K0K+ and B0 --> K0K0, and measurement of the branching fraction and search for direct CP violation in B+ --> K0pi+. Phys Rev Lett *95*, 221801.

Babu, P. (1974). Biochemical Genetics of Caenorhabditis elegans. Molec gen Genet *135*, 39-44.

Baeriswyl, S., Diard, M., Mosser, T., Leroy, M., Maniere, X., Taddei, F., and Matic, I. (2009). Modulation of aging profiles in isogenic populations of Caenorhabditis elegans by bacteria causing different extrinsic mortality rates. Biogerontology *11*, 53-65.

Baker, G.T., 3rd, and Sprott, R.L. (1988). Biomarkers of aging. Experimental gerontology *23*, 223-239.

Bennett, M.V., and Zukin, R.S. (2004). Electrical coupling and neuronal synchronization in the Mammalian brain. Neuron *41*, 495-511.

Bhat, S.G., and Babu, P. (1980). Mutagen sensitivity of kynureninase mutants of the nematode Caenorhabditis elegans. Mol Gen Genet *180*, 635-638.

Biswas, S., Ray, M., Misra, S., Dutta, D.P., and Ray, S. (1997). Selective inhibition of mitochondrial respiration and glycolysis in human leukaemic leucocytes by methylglyoxal. The Biochemical journal *323 (Pt 2)*, 343-348.

Bivik, C., Rosdahl, I., and Ollinger, K. (2007). Hsp70 protects against UVB induced apoptosis by preventing release of cathepsins and cytochrome c in human melanocytes. Carcinogenesis *28*, 537-544.

Blagosklonny, M.V. (2006). Aging and immortality: quasi-programmed senescence and its pharmacologic inhibition. Cell Cycle *5*, 2087-2102.

Blagosklonny, M.V. (2007). Paradoxes of aging. Cell Cycle *6*, 2997-3003.

Blagosklonny, M.V. (2008). Aging: ROS or TOR. Cell Cycle *7*, 3344-3354.

Bluher, M., Kahn, B.B., and Kahn, C.R. (2003). Extended longevity in mice lacking the insulin receptor in adipose tissue. Science *299*, 572-574.

Boehm, M., and Slack, F. (2005). A developmental timing microRNA and its target regulate life span in C. elegans. Science *310*, 1954-1957.

Bokov, A., Chaudhuri, A., and Richardson, A. (2004). The role of oxidative damage and stress in aging. Mechanisms of ageing and development *125*, 811-826.

Braidy, N., Guillemin, G.J., Mansour, H., Chan-Ling, T., and Grant, R. (2011). Changes in kynurenine pathway metabolism in the brain, liver and kidney of aged female Wistar rats. Febs J *278*, 4425-4434.

Brenner, S. (1974). The genetics of Caenorhabditis elegans. Genetics *77*, 71-94.

Brockie, P.J., and Maricq, A.V. (2003). Ionotropic glutamate receptors in Caenorhabditis elegans. Neurosignals *12*, 108-125.

Brunk, U.T., Jones, C.B., and Sohal, R.S. (1992). A novel hypothesis of lipofuscinogenesis and cellular aging based on interactions between oxidative stress and autophagocytosis. Mutat Res *275*, 395-403.

Brunk, U.T., and Terman, A. (2002a). Lipofuscin: mechanisms of age-related accumulation and influence on cell function. Free Radic Biol Med *33*, 611-619.

Brunk, U.T., and Terman, A. (2002b). The mitochondrial-lysosomal axis theory of aging: accumulation of damaged mitochondria as a result of imperfect autophagocytosis. Eur J Biochem *269*, 1996-2002.

C.S.C., *elegans, C.*, Sequencing, and Consortium (1998). Genome sequence of the nematode C. elegans: a platform for investigating biology. Science *282*, 2012-2018.

Campesan, S., Green, E.W., Breda, C., Sathyasaikumar, K.V., Muchowski, P.J., Schwarcz, R., Kyriacou, C.P., and Giorgini, F. (2011). The kynurenine pathway modulates neurodegeneration in a Drosophila model of Huntington's disease. Curr Biol *21*, 961-966.

Carter, C.S., Ramsey, M.M., and Sonntag, W.E. (2002). A critical analysis of the role of growth hormone and IGF-1 in aging and lifespan. Trends Genet *18*, 295-301.

Cassada, R.C., and Russell, R.L. (1975). The dauerlarva, a post-embryonic developmental variant of the nematode Caenorhabditis elegans. Dev Biol *46*, 326-342.

CGC (2012). Caenorhabditis Genetics Center

Chalfie, M., and Wolinsky, E. (1990). The identification and suppression of inherited neurodegeneration in Caenorhabditis elegans. Nature *345*, 410-416.

Chautan, M., Chazal, G., Cecconi, F., Gruss, P., and Golstein, P. (1999). Interdigital cell death can occur through a necrotic and caspase-independent pathway. Curr Biol *9*, 967-970.

Chavez, V., Mohri-Shiomi, A., Maadani, A., Vega, L.A., and Garsin, D.A. (2007). Oxidative stress enzymes are required for DAF-16-mediated immunity due to generation of reactive oxygen species by Caenorhabditis elegans. Genetics *176*, 1567-1577.

Chio, K.S., and Tappel, A.L. (1969). Synthesis and characterization of the fluorescent products derived from malonaldehyde and amino acids. Biochemistry *8*, 2821-2826.

Chitwood, B.G., and Chitwood, M.B. (1950). An Introduction to Nematology (Baltimore, University Park Press).

Chung, K.T., and Gadupudi, G.S. (2011). Possible roles of excess tryptophan metabolites in cancer. Environ Mol Mutagen *52*, 81-104.

Chung, S., Gumienny, T.L., Hengartner, M.O., and Driscoll, M. (2000). A common set of engulfment genes mediates removal of both apoptotic and necrotic cell corpses in C. elegans. Nature cell biology *2*, 931-937.

CKC (2012). *C. elegans* Knockout Consortium.

Clancy, D.J., Gems, D., Harshman, L.G., Oldham, S., Stocker, H., Hafen, E., Leevers, S.J., and Partridge, L. (2001). Extension of life-span by loss of CHICO, a Drosophila insulin receptor substrate protein. Science *292*, 104-106.

Clokey, G.V., and Jacobson, L.A. (1986). The autofluorescent "lipofuscin granules" in the intestinal cells of Caenorhabditis elegans are secondary lysosomes. Mech Ageing Dev *35*, 79-94.

Commoner, B., Townsend, J., and Pake, G.E. (1954). Free radicals in biological materials. Nature *174*, 689-691.

Coux, O., Tanaka, K., and Goldberg, A.L. (1996). Structure and functions of the 20S and 26S proteasomes. Annu Rev Biochem *65*, 801-847.

Coyle, J.T., and Schwarcz, R. (1976). Lesion of striatal neurones with kainic acid provides a model for Huntington's chorea. Nature *263*, 244-246.

Dang, W., Steffen, K.K., Perry, R., Dorsey, J.A., Johnson, F.B., Shilatifard, A., Kaeberlein, M., Kennedy, B.K., and Berger, S.L. (2009). Histone H4 lysine 16 acetylation regulates cellular lifespan. Nature *459*, 802-807.

Darlington, L.G., Forrest, C.M., Mackay, G.M., Smith, R.A., Smith, A.J., Stoy, N., and Stone, T.W. (2010). On the Biological Importance of the 3-hydroxyanthranilic Acid: Anthranilic Acid Ratio. Int J Tryptophan Res *3*, 51-59.

Darlington, L.G., Mackay, G.M., Forrest, C.M., Stoy, N., George, C., and Stone, T.W. (2007). Altered kynurenine metabolism correlates with infarct volume in stroke. The European journal of neuroscience *26*, 2211-2221.

Davis, B.O., Jr., Anderson, G.L., and Dusenbery, D.B. (1982). Total luminescence spectroscopy of fluorescence changes during aging in Caenorhabditis elegans. Biochemistry *21*, 4089-4095.

de Castro, E., Hegi de Castro, S., and Johnson, T.E. (2004). Isolation of long-lived mutants in Caenorhabditis elegans using selection for resistance to juglone. Free radical biology & medicine *37*, 139-145.

Doonan, R., McElwee, J.J., Matthijssens, F., Walker, G.A., Houthoofd, K., Back, P., Matscheski, A., Vanfleteren, J.R., and Gems, D. (2008). Against the oxidative damage theory of aging: superoxide dismutases protect against oxidative stress but have little or no effect on life span in Caenorhabditis elegans. Genes & development *22*, 3236-3241.

Driscoll, M., and Chalfie, M. (1991). The mec-4 gene is a member of a family of Caenorhabditis elegans genes that can mutate to induce neuronal degeneration. Nature *349*, 588-593.

Durrell, G. (2004). Birds, Beasts and Relatives (Penguin Books).

Eldred, G.E., Miller, G.V., Stark, W.S., and Feeney-Burns, L. (1982). Lipofuscin: resolution of discrepant fluorescence data. Science *216*, 757-759.

Ellis, R.E., Yuan, J.Y., and Horvitz, H.R. (1991). Mechanisms and functions of cell death. Annu Rev Cell Biol *7*, 663-698.

Evans, J. (1995). Biomolecular NMR Spectroscopy (Oxford, Oxford University Press).

Evans, T. (2005). Transformation and microinjection. In WormBook, T.*C.e.*R. Community, ed.

Fallarino, F., Grohmann, U., Vacca, C., Bianchi, R., Orabona, C., Spreca, A., Fioretti, M.C., and Puccetti, P. (2002). T cell apoptosis by tryptophan catabolism. Cell Death Differ *9*, 1069-1077.

Felix, M.A., and Braendle, C. (2010). The natural history of Caenorhabditis elegans. Curr Biol *20*, R965-969.

Fisher, A.L., and Lithgow, G.J. (2006). The nuclear hormone receptor DAF-12 has opposing effects on Caenorhabditis elegans lifespan and regulates genes repressed in multiple long-lived worms. Aging Cell *5*, 127-138.

Fletcher, B.L., Dillard, C.J., and Tappel, A.L. (1973). Measurement of fluorescent lipid peroxidation products in biological systems and tissues. Anal Biochem *52*, 1-9.

Forseth, R.R., and Schroeder, F.C. (2011a). NMR-spectroscopic analysis of mixtures: from structure to function. Current opinion in chemical biology *15*, 38-47.

Forseth, R.R., and Schroeder, F.C. (2011b). NMR-spectroscopic analysis of mixtures: from structure to function. Curr Opin Chem Biol *15*, 38-47.

Friedman, D.B., and Johnson, T.E. (1988). A mutation in the age-1 gene in Caenorhabditis elegans lengthens life and reduces hermaphrodite fertility. Genetics *118*, 75-86.

Friguet, B., and Szweda, L.I. (1997). Inhibition of the multicatalytic proteinase (proteasome) by 4-hydroxy-2-nonenal cross-linked protein. FEBS Lett *405*, 21-25.

Fryer, H.J., Knox, R.J., Strittmatter, S.M., and Kalb, R.G. (1999). Excitotoxic death of a subset of embryonic rat motor neurons in vitro. J Neurochem *72*, 500-513.

Fujii, M., Adachi, N., Shikatani, K., and Ayusawa, D. (2009). [FeFe]-hydrogenase-like gene is involved in the regulation of sensitivity to oxygen in yeast and nematode. Genes Cells *14*, 457-468.

Fujii, M., Ishii, N., Joguchi, A., Yasuda, K., and Ayusawa, D. (1998). A novel superoxide dismutase gene encoding membrane-bound and extracellular isoforms by alternative splicing in Caenorhabditis elegans. DNA Res *5*, 25-30.

Gandhi, S., Santelli, J., Mitchell, D.H., Stiles, J.W., and Sanadi, D.R. (1980). A simple method for maintaining large, aging populations of Caenorhabditis elegans. Mech Ageing Dev *12*, 137-150.

Gardner, M.P., Gems, D., and Viney, M.E. (2004). Aging in a very short-lived nematode. Experimental gerontology *39*, 1267-1276.

Garigan, D., Hsu, A.L., Fraser, A.G., Kamath, R.S., Ahringer, J., and Kenyon, C. (2002). Genetic analysis of tissue aging in Caenorhabditis elegans: a role for heat-shock factor and bacterial proliferation. Genetics *161*, 1101-1112.

Gems, D., and Doonan, R. (2009). Antioxidant defense and aging in C. elegans: is the oxidative damage theory of aging wrong? Cell Cycle *8*, 1681-1687.

Gems, D.H., and de la Guardia, Y.I. (2012). Alternative Perspectives on Aging in C. elegans: Reactive Oxygen Species or Hyperfunction? Antioxid Redox Signal.

Gerstbrein, B., Stamatas, G., Kollias, N., and Driscoll, M. (2005). In vivo spectrofluorimetry reveals endogenous biomarkers that report healthspan and dietary restriction in Caenorhabditis elegans. Aging Cell *4*, 127-137.

Gill, M.S. (2006). Endocrine targets for pharmacological intervention in aging in Caenorhabditis elegans. Aging Cell *5*, 23-30.

Gill, M.S., Olsen, A., Sampayo, J.N., and Lithgow, G.J. (2003). An automated high-throughput assay for survival of the nematode Caenorhabditis elegans. Free Radic Biol Med *35*, 558-565.

Goldfarb, A.R., Saidel, L.J., and Mosovich, E. (1951). The ultraviolet absorption spectra of proteins. J Biol Chem *193*, 397-404.

Golstein, P., and Kroemer, G. (2007). Cell death by necrosis: towards a molecular definition. Trends Biochem Sci *32*, 37-43.

Grohmann, U., Fallarino, F., Bianchi, R., Orabona, C., Vacca, C., Fioretti, M.C., and Puccetti, P. (2003). A defect in tryptophan catabolism impairs tolerance in nonobese diabetic mice. J Exp Med *198*, 153-160.

Guidetti, P., Bates, G.P., Graham, R.K., Hayden, M.R., Leavitt, B.R., MacDonald, M.E., Slow, E.J., Wheeler, V.C., Woodman, B., and Schwarcz, R. (2006). Elevated brain 3-hydroxykynurenine and quinolinate levels in Huntington disease mice. Neurobiol Dis *23*, 190-197.

Hamilton, M.L., Guo, Z., Fuller, C.D., Van Remmen, H., Ward, W.F., Austad, S.N., Troyer, D.A., Thompson, I., and Richardson, A. (2001). A reliable assessment of 8-oxo-2-deoxyguanosine levels in nuclear and mitochondrial DNA using the sodium iodide method to isolate DNA. Nucleic Acids Res *29*, 2117-2126.

Harman, D. (1956). Aging: a theory based on free radical and radiation chemistry. J Gerontol *11*, 298-300.

Hartman, P.S., and Ishii, N. (2007). Chromosome dosage as a life span determinant in Caenorhabiditis elegans. Mech Ageing Dev *128*, 437-443.

Heidler, T., Hartwig, K., Daniel, H., and Wenzel, U. (2010). Caenorhabditis elegans lifespan extension caused by treatment with an orally active ROS-generator is dependent on DAF-16 and SIR-2.1. Biogerontology *11*, 183-195.

Henzi, V., and MacDermott, A.B. (1992). Characteristics and function of Ca(2+)- and inositol 1,4,5-trisphosphate-releasable stores of Ca2+ in neurons. Neuroscience *46*, 251-273.

Herman, R.K. (2005). Introduction to sex determination. In WormBook, B. Meyer, ed.

Hermann, G.J., Schroeder, L.K., Hieb, C.A., Kershner, A.M., Rabbitts, B.M., Fonarev, P., Grant, B.D., and Priess, J.R. (2005). Genetic analysis of lysosomal trafficking in Caenorhabditis elegans. Mol Biol Cell *16*, 3273-3288.

Herndon, L.A., Schmeissner, P.J., Dudaronek, J.M., Brown, P.A., Listner, K.M., Sakano, Y., Paupard, M.C., Hall, D.H., and Driscoll, M. (2002). Stochastic and genetic factors influence tissue-specific decline in ageing C. elegans. Nature *419*, 808-814.

Heyes, M.P., Chen, C.Y., Major, E.O., and Saito, K. (1997). Different kynurenine pathway enzymes limit quinolinic acid formation by various human cell types. The Biochemical journal *326 (Pt 2)*, 351-356.

Hodgkin, J. (2005). Introduction to genetics and genomics. In WormBook, T.*C.e.*R. Community, ed.

Hodgkin, J., and Partridge, F.A. (2008). Caenorhabditis elegans meets microsporidia: the nematode killers from Paris. PLoS Biol *6*, 2634-2637.

Holzenberger, M., Dupont, J., Ducos, B., Leneuve, P., Geloen, A., Even, P.C., Cervera, P., and Le Bouc, Y. (2003). IGF-1 receptor regulates lifespan and resistance to oxidative stress in mice. Nature *421*, 182-187.

Honda, S., Ishii, N., Suzuki, K., and Matsuo, M. (1993). Oxygen-dependent perturbation of life span and aging rate in the nematode. J Gerontol *48*, B57-61.

Hong, K., and Driscoll, M. (1994). A transmembrane domain of the putative channel subunit MEC-4 influences mechanotransduction and neurodegeneration in C. elegans. Nature *367*, 470-473.

Hosokawa, H., Ishii, N., Ishida, H., Ichimori, K., Nakazawa, H., and Suzuki, K. (1994). Rapid accumulation of fluorescent material with aging in an oxygen-sensitive mutant mev-1 of Caenorhabditis elegans. Mech Ageing Dev *74*, 161-170.

Houthoofd, K., Braeckman, B.P., Lenaerts, I., Brys, K., De Vreese, A., Van Eygen, S., and Vanfleteren, J.R. (2002). Ageing is reversed, and metabolism is reset to young levels in recovering dauer larvae of C. elegans. Experimental gerontology *37*, 1015-1021.

Hu, P.J., and Sherman, D.H. (2009). DANSing with Caenorhabditis elegans. Proceedings of the National Academy of Sciences of the United States of America *106*, 7685-7686.

Hwang, J.J., Lee, S.J., Kim, T.Y., Cho, J.H., and Koh, J.Y. (2008). Zinc and 4-hydroxy-2-nonenal mediate lysosomal membrane permeabilization induced by H2O2 in cultured hippocampal neurons. J Neurosci *28*, 3114-3122.

Ishida, A., Shimazaki, K., and Kawai, N. (1992). Ischemia-induced changes in PIP2 levels of gerbil hippocampus. Neurosci Res *15*, 305-309.

Ishii, N., Fujii, M., Hartman, P.S., Tsuda, M., Yasuda, K., Senoo-Matsuda, N., Yanase, S., Ayusawa, D., and Suzuki, K. (1998). A mutation in succinate dehydrogenase cytochrome b causes oxidative stress and ageing in nematodes. Nature *394*, 694-697.

Ishii, N., Ishii, T., and Hartman, P.S. (2006). The role of the electron transport gene SDHC on lifespan and cancer. Experimental gerontology *41*, 952-956.

Jacobson, L.A., Jen-Jacobson, L., Hawdon, J.M., Owens, G.P., Bolanowski, M.A., Emmons, S.W., Shah, M.V., Pollock, R.A., and Conklin, D.S. (1988). Identification of a putative structural gene for cathepsin D in Caenorhabditis elegans. Genetics *119*, 355-363.

Jain, C., Yun, M., Politz, S.M., and Rao, R.P. (2009). A pathogenesis assay using Saccharomyces cerevisiae and Caenorhabditis elegans reveals novel roles for

yeast AP-1, Yap1, and host dual oxidase BLI-3 in fungal pathogenesis. Eukaryot Cell *8*, 1218-1227.

Joeng, K.S., Song, E.J., Lee, K.J., and Lee, J. (2004). Long lifespan in worms with long telomeric DNA. Nat Genet *36*, 607-611.

Johansson, A.C., Steen, H., Ollinger, K., and Roberg, K. (2003). Cathepsin D mediates cytochrome c release and caspase activation in human fibroblast apoptosis induced by staurosporine. Cell Death Differ *10*, 1253-1259.

Jung, T., Bader, N., and Grune, T. (2007). Lipofuscin: formation, distribution, and metabolic consequences. Ann N Y Acad Sci *1119*, 97-111.

Kamath, R.S., and Ahringer, J. (2003). Genome-wide RNAi screening in Caenorhabditis elegans. Methods *30*, 313-321.

Kampkotter, A., Gombitang Nkwonkam, C., Zurawski, R.F., Timpel, C., Chovolou, Y., Watjen, W., and Kahl, R. (2007a). Effects of the flavonoids kaempferol and fisetin on thermotolerance, oxidative stress and FoxO transcription factor DAF-16 in the model organism Caenorhabditis elegans. Arch Toxicol *81*, 849-858.

Kampkotter, A., Nkwonkam, C.G., Zurawski, R.F., Timpel, C., Chovolou, Y., Watjen, W., and Kahl, R. (2007b). Investigations of protective effects of the flavonoids quercetin and rutin on stress resistance in the model organism Caenorhabditis elegans. Toxicology *234*, 113-123.

Kanehisa, L. (2012). Kyoto Encyclopedia of Genes and Genomes, C. elegans Tryptophn.

Keaney, M., and Gems, D. (2003). No increase in lifespan in Caenorhabditis elegans upon treatment with the superoxide dismutase mimetic EUK-8. Free radical biology & medicine *34*, 277-282.

Keaney, M., Matthijssens, F., Sharpe, M., Vanfleteren, J., and Gems, D. (2004). Superoxide dismutase mimetics elevate superoxide dismutase activity in vivo but do not retard aging in the nematode Caenorhabditis elegans. Free radical biology & medicine *37*, 239-250.

Kenyon, C. (2005). The plasticity of aging: insights from long-lived mutants. Cell *120*, 449-460.

Kenyon, C., Chang, J., Gensch, E., Rudner, A., and Tabtiang, R. (1993). A C. elegans mutant that lives twice as long as wild type. Nature *366*, 461-464.

Kenyon, C.J. (2010). The genetics of ageing. Nature *464*, 504-512.

Kerr, J.F., Wyllie, A.H., and Currie, A.R. (1972). Apoptosis: a basic biological phenomenon with wide-ranging implications in tissue kinetics. Br J Cancer *26*, 239-257.

Ketting, R.F., Haverkamp, T.H., van Luenen, H.G., and Plasterk, R.H. (1999). Mut-7 of C. elegans, required for transposon silencing and RNA interference, is a homolog of Werner syndrome helicase and RNaseD. Cell *99*, 133-141.

Kim, J., Takahashi, M., Shimizu, T., Shirasawa, T., Kajita, M., Kanayama, A., and Miyamoto, Y. (2008). Effects of a potent antioxidant, platinum nanoparticle, on the lifespan of Caenorhabditis elegans. Mechanisms of ageing and development *129*, 322-331.

Kimura, K., Tanaka, N., Nakamura, N., Takano, S., and Ohkuma, S. (2007). Knockdown of mitochondrial heat shock protein 70 promotes progeria-like phenotypes in caenorhabditis elegans. J Biol Chem *282*, 5910-5918.

Kirino, T., and Sano, K. (1984). Selective vulnerability in the gerbil hippocampus following transient ischemia. Acta Neuropathol *62*, 201-208.

Kirkwood, T.B. (1977). Evolution of ageing. Nature *270*, 301-304.

Kirkwood, T.B., and Holliday, R. (1979). The evolution of ageing and longevity. Proc R Soc Lond B Biol Sci *205*, 531-546.

Klass, M., and Hirsh, D. (1976). Non-ageing developmental variant of Caenorhabditis elegans. Nature *260*, 523-525.

Klass, M.R. (1977). Aging in the nematode Caenorhabditis elegans: major biological and environmental factors influencing life span. Mech Ageing Dev *6*, 413-429.

Klass, M.R. (1983). A method for the isolation of longevity mutants in the nematode Caenorhabditis elegans and initial results. Mechanisms of ageing and development *22*, 279-286.

Kostich, M., Fire, A., and Fambrough, D.M. (2000). Identification and molecular-genetic characterization of a LAMP/CD68-like protein from Caenorhabditis elegans. J Cell Sci *113 (Pt 14)*, 2595-2606.

Kroemer, G., Galluzzi, L., Vandenabeele, P., Abrams, J., Alnemri, E.S., Baehrecke, E.H., Blagosklonny, M.V., El-Deiry, W.S., Golstein, P., Green, D.R.*, et al.* (2009). Classification of cell death: recommendations of the Nomenclature Committee on Cell Death 2009. Cell Death Differ *16*, 3-11.

Kurz, T., Terman, A., and Brunk, U.T. (2007). Autophagy, ageing and apoptosis: the role of oxidative stress and lysosomal iron. Arch Biochem Biophys *462*, 220-230.

Lapin, I.P. (1978). Stimulant and convulsive effects of kynurenines injected into brain ventricles in mice. Journal of neural transmission *42*, 37-43.

Larsen, P.L. (1993). Aging and resistance to oxidative damage in Caenorhabditis elegans. Proceedings of the National Academy of Sciences of the United States of America *90*, 8905-8909.

Laufer, J.S., Bazzicalupo, P., and Wood, W.B. (1980). Segregation of developmental potential in early embryos of Caenorhabditis elegans. Cell *19*, 569-577.

Lee, R.Y., Hench, J., and Ruvkun, G. (2001). Regulation of C. elegans DAF-16 and its human ortholog FKHRL1 by the daf-2 insulin-like signaling pathway. Curr Biol *11*, 1950-1957.

Lee, S.J., Yook, J.S., Han, S.M., and Koo, H.S. (2004). A Werner syndrome protein homolog affects C. elegans development, growth rate, life span and sensitivity to DNA damage by acting at a DNA damage checkpoint. Development *131*, 2565-2575.

Li, J.S., Han, Q., Fang, J., Rizzi, M., James, A.A., and Li, J. (2007). Biochemical mechanisms leading to tryptophan 2,3-dioxygenase activation. Arch Insect Biochem Physiol *64*, 74-87.

Lin, K., Dorman, J.B., Rodan, A., and Kenyon, C. (1997). daf-16: An HNF-3/forkhead family member that can function to double the life-span of Caenorhabditis elegans. Science *278*, 1319-1322.

Lithgow, G.J., Gill, M.S., Olsen, A., and Sampayo, J.N. (2005). Pharmacological intervention in invertebrate aging. Age *27*, 213-223.

Liu, B., Larsson, L., Caballero, A., Hao, X., Oling, D., Grantham, J., and Nystrom, T. (2010). The polarisome is required for segregation and retrograde transport of protein aggregates. Cell *140*, 257-267.

Lough, W.J., and Wainer, I.W. (1996). High performance liquid chromatography: Fundamental Principles and Practice (Glasgow, Blackie Academic & Professional).

Luke, C.J., Pak, S.C., Askew, Y.S., Naviglia, T.L., Askew, D.J., Nobar, S.M., Vetica, A.C., Long, O.S., Watkins, S.C., Stolz, D.B.*, et al.* (2007). An intracellular serpin regulates necrosis by inhibiting the induction and sequelae of lysosomal injury. Cell *130*, 1108-1119.

Luke, C.J., and Silverman, G.A. (2011). Necrotic cell death: harnessing the Dark side of the Force in mammary gland involution. Nat Cell Biol *13*, 197-199.

Mair, W., Goymer, P., Pletcher, S.D., and Partridge, L. (2003). Demography of dietary restriction and death in Drosophila. Science *301*, 1731-1733.

Martinez, D.E. (1998). Mortality patterns suggest lack of senescence in hydra. Experimental gerontology *33*, 217-225.

Masse, I., Molin, L., Mouchiroud, L., Vanhems, P., Palladino, F., Billaud, M., and Solari, F. (2008). A novel role for the SMG-1 kinase in lifespan and oxidative stress resistance in Caenorhabditis elegans. PLoS One *3*, e3354.

Mattson, M.P. (2007). Calcium and neurodegeneration. Aging Cell *6*, 337-350.

Mattson, M.P., and Magnus, T. (2006). Ageing and neuronal vulnerability. Nat Rev Neurosci *7*, 278-294.

McCall, K. (2010). Genetic control of necrosis - another type of programmed cell death. Curr Opin Cell Biol *22*, 882-888.

McCulloch, D., and Gems, D. (2003). Evolution of male longevity bias in nematodes. Aging Cell *2*, 165-173.

Mehta, R., Steinkraus, K.A., Sutphin, G.L., Ramos, F.J., Shamieh, L.S., Huh, A., Davis, C., Chandler-Brown, D., and Kaeberlein, M. (2009). Proteasomal regulation of the hypoxic response modulates aging in C. elegans. Science *324*, 1196-1198.

Melov, S., Ravenscroft, J., Malik, S., Gill, M.S., Walker, D.W., Clayton, P.E., Wallace, D.C., Malfroy, B., Doctrow, S.R., and Lithgow, G.J. (2000). Extension of life-span with superoxide dismutase/catalase mimetics. Science *289*, 1567-1569.

Miesenbock, G., De Angelis, D.A., and Rothman, J.E. (1998). Visualizing secretion and synaptic transmission with pH-sensitive green fluorescent proteins. Nature *394*, 192-195.

Minniti, A.N., Cataldo, R., Trigo, C., Vasquez, L., Mujica, P., Leighton, F., Inestrosa, N.C., and Aldunate, R. (2009). Methionine sulfoxide reductase A expression is regulated by the DAF-16/FOXO pathway in Caenorhabditis elegans. Aging Cell *8*, 690-705.

Mockett, R.J., Orr, W.C., Rahmandar, J.J., Benes, J.J., Radyuk, S.N., Klichko, V.I., and Sohal, R.S. (1999). Overexpression of Mn-containing superoxide dismutase

in transgenic Drosophila melanogaster. Archives of biochemistry and biophysics *371*, 260-269.

Mole, S.E. (2011). The Neuronal Ceroid Lipofuscinoses (Batten Disease) (Oxford University Press).

Montgomery, M.K. (2006). RNA interference: unraveling a mystery. Nat Struct Mol Biol *13*, 1039-1041.

Moriyoshi, K., Masu, M., Ishii, T., Shigemoto, R., Mizuno, N., and Nakanishi, S. (1991). Molecular cloning and characterization of the rat NMDA receptor. Nature *354*, 31-37.

Muller, F.L., Lustgarten, M.S., Jang, Y., Richardson, A., and Van Remmen, H. (2007). Trends in oxidative aging theories. Free radical biology & medicine *43*, 477-503.

Munn, D.H., Zhou, M., Attwood, J.T., Bondarev, I., Conway, S.J., Marshall, B., Brown, C., and Mellor, A.L. (1998). Prevention of allogeneic fetal rejection by tryptophan catabolism. Science *281*, 1191-1193.

Murphy, C.T., McCarroll, S.A., Bargmann, C.I., Fraser, A., Kamath, R.S., Ahringer, J., Li, H., and Kenyon, C. (2003). Genes that act downstream of DAF-16 to influence the lifespan of Caenorhabditis elegans. Nature *424*, 277-283.

Nakken, K.F. (1963). Quantitative fluorometric determination of anthranilic acid, 3-hydroxy-5-hydroxyanthranilic acid in urine. Scand J Clin Lab Invest *15*, 78-79.

NBR (2012). National Bioresources Project.

Nehrke, K. (2003). A reduction in intestinal cell pHi due to loss of the Caenorhabditis elegans Na+/H+ exchanger NHX-2 increases life span. J Biol Chem *278*, 44657-44666.

Nehrke, K., Denton, J., and Mowrey, W. (2008). Intestinal Ca2+ wave dynamics in freely moving C. elegans coordinate execution of a rhythmic motor program. Am J Physiol Cell Physiol *294*, C333-344.

Neumann-Haefelin, E., Qi, W., Finkbeiner, E., Walz, G., Baumeister, R., and Hertweck, M. (2008). SHC-1/p52Shc targets the insulin/IGF-1 and JNK signaling pathways to modulate life span and stress response in C. elegans. Genes Dev *22*, 2721-2735.

Nill, K. (2006). Glossary of Biotechnology Terms, 4th edn (CRC Press).

Ogg, S., Paradis, S., Gottlieb, S., Patterson, G.I., Lee, L., Tissenbaum, H.A., and Ruvkun, G. (1997). The Fork head transcription factor DAF-16 transduces insulin-like metabolic and longevity signals in C. elegans. Nature *389*, 994-999.

Olshansky, S.J., Carnes, B.A., and Cassel, C. (1990). In search of Methuselah: estimating the upper limits to human longevity. Science *250*, 634-640.

Ookuma, S., Fukuda, M., and Nishida, E. (2003). Identification of a DAF-16 transcriptional target gene, scl-1, that regulates longevity and stress resistance in Caenorhabditis elegans. Curr Biol *13*, 427-431.

Oxenkrug, G.F. (2010). The extended life span of Drosophila melanogaster eye-color (white and vermilion) mutants with impaired formation of kynurenine. J Neural Transm *117*, 23-26.

Oxenkrug, G.F., Navrotskaya, V., Voroboyva, L., and Summergrad, P. (2011). Extension of life span of Drosophila melanogaster by the inhibitors of tryptophan-kynurenine metabolism. Fly (Austin) *5*.

Paradis, S., and Ruvkun, G. (1998). Caenorhabditis elegans Akt/PKB transduces insulin receptor-like signals from AGE-1 PI3 kinase to the DAF-16 transcription factor. Genes & development *12*, 2488-2498.

Partridge, L., and Gems, D. (2007). Benchmarks for ageing studies. Nature *450*, 165-167.

Perkins, M.N., and Stone, T.W. (1982). An iontophoretic investigation of the actions of convulsant kynurenines and their interaction with the endogenous excitant quinolinic acid. Brain Res *247*, 184-187.

Peters, M.A., Teramoto, T., White, J.Q., Iwasaki, K., and Jorgensen, E.M. (2007). A calcium wave mediated by gap junctions coordinates a rhythmic behavior in C. elegans. Curr Biol *17*, 1601-1608.

Pincus, Z., Smith-Vikos, T., and Slack, F.J. (2011a). MicroRNA Predictors of Longevity in Caenorhabditis elegans. PLoS Genet *7*, e1002306.

Pincus, Z., Smith-Vikos, T., and Slack, F.J. (2011b). MicroRNA predictors of longevity in Caenorhabditis elegans. PLoS genetics *7*, e1002306.

Piscianz, E., Cuzzoni, E., De Iudicibus, S., Valencic, E., Decorti, G., and Tommasini, A. (2011). Differential action of 3-hydroxyanthranilic acid on viability and activation of stimulated lymphocytes. Int Immunopharmacol.

Pluskota, A., Horzowski, E., Bossinger, O., and von Mikecz, A. (2010). In Caenorhabditis elegans nanoparticle-bio-interactions become transparent: silica-nanoparticles induce reproductive senescence. PLoS One *4*, e6622.

Pungaliya, C., Srinivasan, J., Fox, B.W., Malik, R.U., Ludewig, A.H., Sternberg, P.W., and Schroeder, F.C. (2009). A shortcut to identifying small molecule signals that regulate behavior and development in Caenorhabditis elegans. Proc Natl Acad Sci U S A *106*, 7708-7713.

Quiel, J.A., and Bender, J. (2003). Glucose conjugation of anthranilate by the Arabidopsis UGT74F2 glucosyltransferase is required for tryptophan mutant blue fluorescence. J Biol Chem *278*, 6275-6281.

Raposo, G., and Marks, M.S. (2007). Melanosomes--dark organelles enlighten endosomal membrane transport. Nat Rev Mol Cell Biol *8*, 786-797.

Repnik, U., Stoka, V., Turk, V., and Turk, B. (2012). Lysosomes and lysosomal cathepsins in cell death. Biochim Biophys Acta *1824*, 22-33.

Reveillaud, I., Phillips, J., Duyf, B., Hilliker, A., Kongpachith, A., and Fleming, J.E. (1994). Phenotypic rescue by a bovine transgene in a Cu/Zn superoxide dismutase-null mutant of Drosophila melanogaster. Mol Cell Biol *14*, 1302-1307.

Riddle, D.L., Blumenthal, T., and Meyer, B. (1997). The Biological Model. In *C elegans* II (Cold Spring Harbor, Cold Spring Harbor Laboratory Press).

Rohde, C.B., Zeng, F., Gonzalez-Rubio, R., Angel, M., and Yanik, M.F. (2007). Microfluidic system for on-chip high-throughput whole-animal sorting and screening at subcellular resolution. Proceedings of the National Academy of Sciences of the United States of America *104*, 13891-13895.

Rongvaux, A., Andris, F., Van Gool, F., and Leo, O. (2003). Reconstructing eukaryotic NAD metabolism. Bioessays *25*, 683-690.

Saido, T.C., Sorimachi, H., and Suzuki, K. (1994). Calpain: new perspectives in molecular diversity and physiological-pathological involvement. Faseb J *8*, 814-822.

Saito, K., Nowak, T.S., Jr., Markey, S.P., and Heyes, M.P. (1993a). Mechanism of delayed increases in kynurenine pathway metabolism in damaged brain regions following transient cerebral ischemia. J Neurochem *60*, 180-192.

Saito, K., Nowak, T.S., Jr., Suyama, K., Quearry, B.J., Saito, M., Crowley, J.S., Markey, S.P., and Heyes, M.P. (1993b). Kynurenine pathway enzymes in brain: responses to ischemic brain injury versus systemic immune activation. J Neurochem *61*, 2061-2070.

Samuelson, A.V., Carr, C.E., and Ruvkun, G. (2007). Gene activities that mediate increased life span of C. elegans insulin-like signaling mutants. Genes Dev *21*, 2976-2994.

Sasaki, T., Mizuguchi, S., and Honda, K. (2012). Growth inhibitory effects of anthranilic acid and its derivatives against Legionella pneumophila. J Biosci Bioeng *113*, 726-729.

Sathyasaikumar, K.V., Stachowski, E.K., Amori, L., Guidetti, P., Muchowski, P.J., and Schwarcz, R. (2010). Dysfunctional kynurenine pathway metabolism in the R6/2 mouse model of Huntington's disease. J Neurochem *113*, 1416-1425.

Sattler, R., and Tymianski, M. (2000). Molecular mechanisms of calcium-dependent excitotoxicity. J Mol Med (Berl) *78*, 3-13.

Schmich, J., Kraus, Y., De Vito, D., Graziussi, D., Boero, F., and Piraino, S. (2007). Induction of reverse development in two marine Hydrozoans. Int J Dev Biol *51*, 45-56.

Schroeder, F.C., Gibson, D.M., Churchill, A.C., Sojikul, P., Wursthorn, E.J., Krasnoff, S.B., and Clardy, J. (2007). Differential analysis of 2D NMR spectra: new natural products from a pilot-scale fungal extract library. Angew Chem Int Ed Engl *46*, 901-904.

Schulz, T.J., Zarse, K., Voigt, A., Urban, N., Birringer, M., and Ristow, M. (2007). Glucose restriction extends Caenorhabditis elegans life span by inducing mitochondrial respiration and increasing oxidative stress. Cell Metab *6*, 280-293.

Schuster, E., McElwee, J.J., Tullet, J.M., Doonan, R., Matthijssens, F., Reece-Hoyes, J.S., Hope, I.A., Vanfleteren, J.R., Thornton, J.M., and Gems, D. (2010). DamID in C. elegans reveals longevity-associated targets of DAF-16/FoxO. Molecular systems biology *6*, 399.

Schwarcz, R., Bruno, J.P., Muchowski, P.J., and Wu, H.Q. (2012). Kynurenines in the mammalian brain: when physiology meets pathology. Nature reviews Neuroscience *13*, 465-477.

Seto, N.O., Hayashi, S., and Tener, G.M. (1990). Overexpression of Cu-Zn superoxide dismutase in Drosophila does not affect life-span. Proceedings of the National Academy of Sciences of the United States of America *87*, 4270-4274.

Shibamura, A., Ikeda, T., and Nishikawa, Y. (2009). A method for oral administration of hydrophilic substances to Caenorhabditis elegans: Effects of oral supplementation with antioxidants on the nematode lifespan. Mech Ageing Dev *130*, 652-655.

Shringarpure, R., Grune, T., Sitte, N., and Davies, K.J. (2000). 4-Hydroxynonenal-modified amyloid-beta peptide inhibits the proteasome: possible importance in Alzheimer's disease. Cell Mol Life Sci *57*, 1802-1809.

Siddiqui, S.S., and Babu, P. (1980). Kynurenine hydroxylase mutants of the nematode Caenorhabditis elegans. Mol Gen Genet *179*, 21-24.

Siddiqui, S.S., and Von Ehrenstein, G. (1980). Biochemical Genetics of Caenorhabditis elegans. Nematodes as Biological Models *1*, 285 - 304.

Sitte, N., Huber, M., Grune, T., Ladhoff, A., Doecke, W.D., Von Zglinicki, T., and Davies, K.J. (2000). Proteasome inhibition by lipofuscin/ceroid during postmitotic aging of fibroblasts. Faseb J *14*, 1490-1498.

Smith, A.J., Smith, R.A., and Stone, T.W. (2009). 5-Hydroxyanthranilic acid, a tryptophan metabolite, generates oxidative stress and neuronal death via p38 activation in cultured cerebellar granule neurones. Neurotox Res *15*, 303-310.

Sohal, R.S., Agarwal, A., Agarwal, S., and Orr, W.C. (1995). Simultaneous overexpression of copper- and zinc-containing superoxide dismutase and catalase retards age-related oxidative damage and increases metabolic potential in Drosophila melanogaster. J Biol Chem *270*, 15671-15674.

Stone, T.W., Forrest, C.M., Stoy, N., and Darlington, L.G. (2012). Involvement of kynurenines in Huntington's disease and stroke-induced brain damage. Journal of neural transmission *119*, 261-274.

Stone, T.W., and Perkins, M.N. (1981). Quinolinic acid: a potent endogenous excitant at amino acid receptors in CNS. Eur J Pharmacol *72*, 411-412.

Suh, Y., Atzmon, G., Cho, M.O., Hwang, D., Liu, B., Leahy, D.J., Barzilai, N., and Cohen, P. (2008). Functionally significant insulin-like growth factor I receptor mutations in centenarians. Proceedings of the National Academy of Sciences of the United States of America *105*, 3438-3442.

Sulston, J.E., Schierenberg, E., White, J.G., and Thomson, J.N. (1983). The embryonic cell lineage of the nematode Caenorhabditis elegans. Dev Biol *100*, 64-119.

Syntichaki, P., Samara, C., and Tavernarakis, N. (2005). The vacuolar H+ -ATPase mediates intracellular acidification required for neurodegeneration in C. elegans. Curr Biol *15*, 1249-1254.

Syntichaki, P., and Tavernarakis, N. (2002). Death by necrosis. Uncontrollable catastrophe, or is there order behind the chaos? EMBO Rep *3*, 604-609.

Syntichaki, P., Xu, K., Driscoll, M., and Tavernarakis, N. (2002). Specific aspartyl and calpain proteases are required for neurodegeneration in C. elegans. Nature *419*, 939-944.

Tatar, M., Kopelman, A., Epstein, D., Tu, M.P., Yin, C.M., and Garofalo, R.S. (2001). A mutant Drosophila insulin receptor homolog that extends life-span and impairs neuroendocrine function. Science *292*, 107-110.

Taub, J., Lau, J.F., Ma, C., Hahn, J.H., Hoque, R., Rothblatt, J., and Chalfie, M. (1999). A cytosolic catalase is needed to extend adult lifespan in C. elegans daf-C and clk-1 mutants. Nature *399*, 162-166.

Taylor, A., and Davies, K.J. (1987). Protein oxidation and loss of protease activity may lead to cataract formation in the aged lens. Free Radic Biol Med *3*, 371-377.

Terman, A., and Brunk, U.T. (1998). Ceroid/lipofuscin formation in cultured human fibroblasts: the role of oxidative stress and lysosomal proteolysis. Mech Ageing Dev *104*, 277-291.

Toth, M.L., Sigmond, T., Borsos, E., Barna, J., Erdelyi, P., Takacs-Vellai, K., Orosz, L., Kovacs, A.L., Csikos, G., Sass, M.*, et al.* (2008). Longevity pathways converge on autophagy genes to regulate life span in Caenorhabditis elegans. Autophagy *4*, 330-338.

Troyano, A., Sancho, P., Fernandez, C., de Blas, E., Bernardi, P., and Aller, P. (2003). The selection between apoptosis and necrosis is differentially regulated in hydrogen peroxide-treated and glutathione-depleted human promonocytic cells. Cell Death Differ *10*, 889-898.

Tymianski, M., Charlton, M.P., Carlen, P.L., and Tator, C.H. (1993). Source specificity of early calcium neurotoxicity in cultured embryonic spinal neurons. J Neurosci *13*, 2085-2104.

Uccelletti, D., Pascoli, A., Farina, F., Alberti, A., Mancini, P., Hirschberg, C.B., and Palleschi, C. (2008). APY-1, a novel Caenorhabditis elegans apyrase involved in unfolded protein response signalling and stress responses. Mol Biol Cell *19*, 1337-1345.

Uchiyama, S., Koike, H., Shimizu, T., and Shirasawa, T. (2005). A superoxide dismutase/catalase mimetic extends the lifespan of short-lived *mev-1* mutant but not the wild type strain in *Caenorhabditis elegans*. Anti-Aging Med Research *2*, 39-47.

Urano, F., Calfon, M., Yoneda, T., Yun, C., Kiraly, M., Clark, S.G., and Ron, D. (2002). A survival pathway for Caenorhabditis elegans with a blocked unfolded protein response. The Journal of cell biology *158*, 639-646.

Valentini, S., Cabreiro, F., Ackerman, D., Alam, M.M., Kunze, M.B., Kay, C.W., and Gems, D. (2012). Manipulation of in vivo iron levels can alter resistance to oxidative stress without affecting ageing in the nematode C. elegans. Mechanisms of ageing and development *133*, 282-290.

van Ham, T.J., Thijssen, K.L., Breitling, R., Hofstra, R.M., Plasterk, R.H., and Nollen, E.A. (2008). C. elegans model identifies genetic modifiers of alpha-synuclein inclusion formation during aging. PLoS genetics *4*, e1000027.

Van Raamsdonk, J.M., and Hekimi, S. (2010). Reactive Oxygen Species and Aging in Caenorhabditis elegans: Casual or Casual Relationship? Antioxidants and Redox *13*, 1911-1953.

Vanfleteren, J.R., and Braeckman, B.P. (1999). Mechanisms of life span determination in Caenorhabditis elegans. Neurobiol Aging *20*, 487-502.

Vina, J., Borras, C., and Miquel, J. (2007). Theories of ageing. IUBMB Life *59*, 249-254.

Walker, F.O. (2007). Huntington's disease. Lancet *369*, 218-228.

Wang, Y., Denisova, J.V., Kang, K.S., Fontes, J.D., Zhu, B.T., and Belousov, A.B. (2010). Neuronal gap junctions are required for NMDA receptor-mediated excitotoxicity: implications in ischemic stroke. J Neurophysiol *104*, 3551-3556.

Wang, Y., Song, J.H., Denisova, J.V., Park, W.M., Fontes, J.D., and Belousov, A.B. (2012). Neuronal gap junction coupling is regulated by glutamate and plays critical role in cell death during neuronal injury. J Neurosci *32*, 713-725.

Waters, P. (2012). HPLC - High Performance Liquid Chromatography (http://www.waters.com/waters/nav.htm?locale=en_US&cid=10048919).

Willett, J.D., Podugu, N., Sudama, G., Kopecky, J.J., and Isbister, J. (2010). Applications of cold temperature stress to age fractionate Caenorhabditis elegans: a simple inexpensive technique. J Gerontol A Biol Sci Med Sci *65*, 457-467.

Williams, G.C. (1957). Pleiotropy, Natural Selection and the Evolution of Senescence. Evolution *11*, 398-411.

Wilson, M.A., Shukitt-Hale, B., Kalt, W., Ingram, D.K., Joseph, J.A., and Wolkow, C.A. (2006). Blueberry polyphenols increase lifespan and thermotolerance in Caenorhabditis elegans. Aging Cell *5*, 59-68.

Wong, D., Bazopoulou, D., Pujol, N., Tavernarakis, N., and Ewbank, J.J. (2007). Genome-wide investigation reveals pathogen-specific and shared signatures in the response of Caenorhabditis elegans to infection. Genome Biol *8*, R194.

WormAtlas (2002-2012). *C. elegans* anatomy, Z.F. Altun, L.A. Herndon, C. Crocker, R. Lints, and D.H. Hall, eds.

WormBase (2012).

Xiong, Z.G., Zhu, X.M., Chu, X.P., Minami, M., Hey, J., Wei, W.L., MacDonald, J.F., Wemmie, J.A., Price, M.P., Welsh, M.J.*, et al.* (2004). Neuroprotection in ischemia: blocking calcium-permeable acid-sensing ion channels. Cell *118*, 687-698.

Xu, K., Tavernarakis, N., and Driscoll, M. (2001). Necrotic cell death in C. elegans requires the function of calreticulin and regulators of Ca(2+) release from the endoplasmic reticulum. Neuron *31*, 957-971.

Yamashima, T. (2004). Ca2+-dependent proteases in ischemic neuronal death: a conserved 'calpain-cathepsin cascade' from nematodes to primates. Cell Calcium *36*, 285-293.

Yamashima, T. (2012). Hsp70.1 and related lysosomal factors for necrotic neuronal death. J Neurochem *120*, 477-494.

Yamashima, T., and Oikawa, S. (2009). The role of lysosomal rupture in neuronal death. Prog Neurobiol *89*, 343-358.

Yamashima, T., Saido, T.C., Takita, M., Miyazawa, A., Yamano, J., Miyakawa, A., Nishijyo, H., Yamashita, J., Kawashima, S., Ono, T.*, et al.* (1996). Transient brain ischaemia provokes Ca2+, PIP2 and calpain responses prior to delayed neuronal death in monkeys. Eur J Neurosci *8*, 1932-1944.

Yang, W., Li, J., and Hekimi, S. (2007). A Measurable increase in oxidative damage due to reduction in superoxide detoxification fails to shorten the life span of long-lived mitochondrial mutants of Caenorhabditis elegans. Genetics *177*, 2063-2074.

Yasuda, K., Ishii, T., Suda, H., Akatsuka, A., Hartman, P.S., Goto, S., Miyazawa, M., and Ishii, N. (2006). Age-related changes of mitochondrial structure and function in Caenorhabditis elegans. Mech Ageing Dev *127*, 763-770.

Zheng, S., Clabough, E.B., Sarkar, S., Futter, M., Rubinsztein, D.C., and Zeitlin, S.O. (2010). Deletion of the huntingtin polyglutamine stretch enhances neuronal autophagy and longevity in mice. PLoS Genet *6*, e1000838.

Zheng, Z., Burgunder, J.M., Shang, H., and Guo, X. (2012). Huntington's like conditions in China, A review of published Chinese cases. PLoS Curr *4*, RRN1302.

Zong, W.X., and Thompson, C.B. (2006). Necrotic death as a cell fate. Genes Dev *20*, 1-15.